UNIVERSIDADE DE SÃO PAULO
FACULDADE DE ODONTOLOGIA DE BAURU

CLAUDIA CRISTINA BIGUETTI

Role of DAMPS on the modulation of macrophage response after classical biomaterial (Ti) implantation and its impact on the subsequent repair and osseointegration processes

Participação de DAMPs na modulação da resposta de macrófagos à implantação de um biomaterial clássico (Ti) e seu impacto no processo de reparo e osseointegração subsequentes

BAURU
2018

CLAUDIA CRISTINA BIGUETTI

Role of DAMPS in the modulation of macrophage response after classical biomaterial (Ti) implantation and its impact in the subsequent repair and osseointegration processes.

Participação de DAMPs na modulação da resposta de macrófagos à implantação de um biomaterial clássico (Ti) e seu impacto no processo de reparo e osseointegração subsequentes

Tese constituída por artigos apresentada a Faculdade de Odontologia de Bauru da Universidade de São Paulo para obtenção do título de Doutor em Ciências no Programa de Ciências Odontológicas Aplicadas, na área de concentração Biologia Oral.

Orientador: Prof. Dr. Gustavo Pompermaier Garlet

BAURU
2018

Biguetti, Claudia Cristina
B488r Role of DAMPS on the modulation of macrophage response after classical biomaterial (Ti) implantation and its impact in the subsequent repair and osseointegration processes. / Claudia Cristina Biguetti. – Bauru, 2018.
135 p. : il. ; 30 cm.

Tese (Doutorado) – Faculdade de Odontologia de Bauru. Universidade de São Paulo

Orientador: Prof. Dr. Gustavo Pompermaier Garlet

DEDICATÓRIA

Dedico este trabalho aos meus pais, Izildinha Rodrigues e Luiz Biguetti

AGRADECIMENTOS

Ao meu orientador *Prof. Dr. Gustavo Pompermaier Garle*t.

A minha família.

Aos meus *amigos*, *colegas* e pós-graduandos do Departamento de Ciências Biológicas da Faculdade de Odontologia de Bauru, Universidade de São Paulo.

Aos *professores*, *técnicos* e *funcionários* do Departamento de Histologia da Faculdade de Odontologia de Bauru Universidade de São Paulo.

Aos *Professores Dra.Renato Silva*, *Dr*. *Ariadne Letra* e *Dr.Walid Fakhouri* da School of Dentistry University of Texas Health Science Center at Houston.

À *Professora Dra. Mariza Akemi Matsumoto* da Faculdade de Odontologia de Araçatuba, Universidade Estadual Paulista.

À *Professora Dra. Danieli Rodrigues* da School of Bioengineering University of Texas at Dallas.

AGRADECIMENTOS INSTITUCIONAIS

Ao *Prof. Dr. Marco Antonio Zago*, digníssimo reitor da Universidade de São Paulo.

Ao *Prof. Dr. Ignacio Maria Poveda Velasco*, digníssimo Secretário Geral da Universidade de São Paulo.

Ao *Prof. Dr. Carlos Ferreira dos Santos*, digníssimo Diretor da Faculdade de Odontologia de Bauru da Universidade de São Paulo.

Ao *Prof*. *Dr. Guilherme dos Reis Pereira Janson*, digníssimo vice-diretor da Faculdade de Odontologia de Bauru da Universidade de São Paulo.

Ao *Prof. Dr. José Roberto Pereira Lauris*, digníssimo Prefeito do Campus da Faculdade de Odontologia de Bauru da Universidade de São Paulo.

A *Profa. Dra. Izabel Regina Fischer Rubira Bullen*, digníssima Coordenadora do Programa de Pós-Graduação em Ciências Odontológicas Aplicadas e Presidente da Comissão de Pós Graduação na área de Estomatologia e Biologia Oral, da Faculdade de Odontologia de Bauru da Universidade de São Paulo.

A agência de fomento *Coordenação de Aperfeiçoamento de Pessoal de Nível Superior* (CAPES), pela concessão da bolsa de doutorado no período de junho a julho de 2014, no âmbito do Programa de Demanda Social.

A agência de fomento *Fundação de Amparo à Pesquisa do Estado de São Paulo* (FAPESP), pela concessão da bolsa de doutorado regular no âmbito do Convênio FAPESP/CAPES e pela concessão da bolsa BEPE, processos nº2014/09590-8 e nº 2015/18162-2, Fundação de Amparo à Pesquisa do Estado de São Paulo (FAPESP).

“All we have to decide is what to do with the time that is given us.”

— J.R.R. Tolkien, The Fellowship of the Ring

ABSTRACT

Role of DAMPS on the modulation of macrophage response after classical biomaterial (Ti) implantation and its impact on the subsequent repair and osseointegration processes.

Despite the successful clinical application of titanium (Ti) as a biomaterial, the exact cellular and molecular mechanisms responsible for Ti osseointegration remain unclear. Indeed, specific knowledge still lacks on what elements are present at biomaterial/host interface and how these factors can trigger inflammatory pathways involved in the subsequent osseointegration process. In this context, we hypothesize that the surgical trauma inherent to the biomaterial grafting results in the release of DAMPs (damage-associated molecular patterns), endogenous proteins that act as triggers of immune inflammatory response upon cellular/tissue stress and/or damage. HMGB1 comprises the prototypic DAMP, which triggers host response via its cognate receptor RAGE, present at leucocytes and somatic cells surfaces. In this context, the aim of this thesis is to study the influence of DAMPs on the biomaterial/host interface and its role in mediating a 'constructive' inflammatory process along tissue repair and osseointegration outcome. Methods and Results: In the article 1, we first characterized an oral osseointegration model in C57Bl/6 mice. This model of oral osseointegration was performed by using Ti screws (6AL-4V, Ø0.6mm, length of 1.5 mm) implanted in the edentulous alveolar crest of mice maxilla. The peri-implant sites were evaluated by microCT, as well histological and molecular assessments. In the article 2, we confirm the presence of DAMPs (HMGB1, HSP60, HSP70, S100A, Byglican, and Fibronectin) at Ti/host interface, analyzing Ti discs (6AL-4V, Ø6mm, 2mm of thick) implanted in the subcutaneous tissue of C57Bl/6 mice. Subsequently, the impact of HMGB1 and RAGE on the tissue repair around Ti discs was investigated by using HMGB1 (GZA 200mg/Kg) or RAGE (RAP, 4m/Kg/day) pharmacological inhibitors. The HMGB1/RAGE axis actively influences the inflammatory response post biomaterial implantation and the blocking of both molecules can negatively affect the subcutaneous tissue repair surrounding Ti disc in mice. In the article 3, Ti screws were implanted in the maxillary edentulous alveolar crest of C57Bl/6 mice, treated or untreated with GZA and RAP and the osseointegration process was evaluated by microscopic and molecular analysis (such as characterized in the article 1). The failure of osseointegration process was observed in mice treated with RAP or GZA, which present a disruption of the inflammatory process followed by foreign body reaction. In conclusion, HMGB1 and RAGE actively influence the tissue repair and osseointegration process in response to Ti-devices grafting, influencing the genesis and regulation of inflammatory immune response, which include the modulation of macrophages polarization state, MSC migration and differentiation in bone cells and consequent bone deposition.

Keywords: DAMP. Macrophages. Osseointegration. Host/Biomaterial. HMGB1.

RESUMO

Apesar do sucesso clínico do Titânio (Ti) como biomaterial, os exatos mecanismos celulares e moleculares que levam à sua osseointegração permanecem incertos. De fato, ainda há uma lacuna de conhecimento sobre quais elementos estão presentes na interface hospedeiro/biomaterial e como esses fatores poder deflagrar as vias inflamatórias envolvidas no subseqüente processo de osseointegração. Neste contexto, sugere-se que o trauma cirúrgico inerente à implantação do biomaterial resulta na liberação de DAMPs (do inglês *damage-associated molecular patterns*), os quais são proteínas endógenas que agem como ativadoras da resposta imune/inflamatória sob um estresse ou dano celular e tecidual. HMGB1 constitui um DAMP prototípico, o qual ativa a resposta do hospedeiro via seu receptor cognato RAGE, que por sua vez está presente na superfície de leucócitos e células somáticas. Neste contexto, o objetivo da presente tese é estudar a influencia de DAMPs na interface hospedeiro/biomaterial e seu papel na modulação de um processo inflamatório construtivo ao longo do reparo tecidual e da osseointegração. Material e Métodos: No artigo 1, caracterizou-se um modelo de osseointegração oral em camundongos C57Bl/6 . Tal modelo foi desenvolvido utilizando parafusos de Ti (6AL-4V, Ø0,6mm, 1.5 de comprimento) implantados no rebordo alveolar edentulo da maxila de camundongos, cujos tecidos peri-implatares foram avaliados por meio de microCT, bem como análises histológicas e moleculares. No artigo 2, inicialmente confirmou-se a presença de DAMPs (HMGB1, HSP60, HSP70, S100A, Biglicana e Fibronectina) na interface Ti/hospedeiro, analisando amostras com discos de Ti (6AL-4V, Ø6mm x 2mm de espessura) implantados no tecido subcutâneo de camundongos C57Bl/6. Posteriormente, o impacto de HMGB1 e RAGE no reparo tecidual ao redor dos discos de Ti foi analisado por meio de uso de inibidores farmacológicos de HMGB1 (GZA 200mg/Kg/dia) e RAGE (RAP, 4m/Kg/dia). O eixo HMGB1/RAGE influencia ativamente a resposta inflamatória pós implantação do biomaterial, e o bloqueio de ambas as moléculas pode afetar negativamente o reparo tecidual subcutâneo ao redor de discos de Ti em camundongos. No artigo 3, parafuso de Ti foram implantados no rebordo edentulo da maxila de camundongos C57Bl/6, tratados e não tratados com GZA e RAP; e o processo de osseointegração foi avaliado por meio de análises microscópicas e moleculares (tal como caracterizado no artigo 1). A falha da osseointegração foi observada em camundongos tratados com RAP ou GZA, os quais apresentaram alterações importantes no processo inflamatório seguidas por uma reação de corpo estranho nos perídos mais tardios. Em suma, conclui-se que HMGB1 e RAGE influenciam ativamente o processo de reparo tecidual e de osseointegração frente à implantação de dispositivos de Ti, influenciando a geração e a regulação da resposta imune inflamatória, a qual inclui a modulação da polarização de macrófagos, a migração de MSCs e a diferenciação de células ósseas para subsequente deposição óssea.

Palavras-chave: DAMP. Macrofágos. Osseointegração. Hospedeiro/Biomaterial. HMGB1.

TABLE OF CONTENTS

1 INTRODUCTION

1 INTRODUCTION

The influence of immunological cells and their molecules on the bone system has been widely investigated in the osteoimmunology field, especially concerning bone loss in chronic inflammatory diseases (GARLET et al.,2006; GRAVES et al., 2011; ARAUJO-PIRESa et al., 2014). In this context, chronic and exacerbated host responses, mediated by multiple pro-inflammatory and certain Th cytokines, have been associated with a destructive inflammatory response, whose molecules are directly associated with osteoclastogenic and bone resorption pathways (GRAVES et al., 2011; ARAUJO-PIRESb et al., 2014). By contrast, in a suitable environment for bone formation and maturation, the balance of pro- and anti-inflammatory molecules release is highly coordinated and is important to induce a transient and low magnitude response after bone injury, termed here as "constructive inflammation" (MOUNTZIARIS; MIKOS, 2008; VIEIRA et al., 2015).

The knowledge generated from these studies also has highlighted the importance of immune system components on the bone regenerative therapies using biomaterials (PARK; BARBUL, 2004; Al-AQL et al., 2008; MOUNTZIARIS;MIKOS, 2008). In particular, there is an increasing interest in the development of superior bone biomaterials, with immunomodulatory properties that could improve the outcome of reparative/regenerative treatments (CHEN et al., 2015; SRIDHARAN et al., 2015). In this sense, the current understanding of key immune cells and their regulatory molecules on bone healing in the presence of a biomaterial, has increasingly encouraged studies in the biomaterial science for developing future immune-engineering approaches with more clinical predictability (ALBREKTSSON et al., 2014).

Among the biomaterials used for development of long-term implantable devices in bone, Titanium (Ti) is the gold standard biomaterial in oral implantology (DAVIES 2003; GITTENS et al., 2014), especially due to its high biocompatibility and osseointegration capacity (WILLIAMS 2008, OGLE 2015), which lead to high rates of clinical success (OGLE 2015, TRINDADE et al., 2015). In this context, it is mandatory to consider that Ti-based devices are non-antigenic and non-immunogenic, and consequently, theoretically Ti-based devices would not be able to activate host inflammatory immune response per se. However, the Ti devices placement is

associated with a small degree of inflammation, which probably results of host cells and molecules interacting with the material surface (DAVIES 2003, TRINDADE et al., 2015). Interestingly, this low degree inflammation seems to be important to provide a proper chemoattraction, activation, and differentiation of mesenchymal stem cells (MSCs) into osteoblasts (DAVIES 2003). In other words, Ti-based devices seemingly allow a 'constructive inflammation' and the subsequent bone apposition towards its surface (COOPER et al., 1998; COLNOT et al., 2007; LIN et al., 2011; MOURARET et al., 2014, TRINDADE et al., 2016). For this reason, Ti is currently regarded as an immunomodulatory biomaterial rather than an inert metal (THALJIa et al., 2014; TRINDADE et al., 2016), although the immunological mechanisms that coordinate this 'constructive' host response at the Ti/host interface remain unclear, partly because of the limited methodological tools and animal models available in this field.

In general, current researches on Ti-mediated osseointegration are specially conducted in larger animal models (such as rabbits, minipigs, dogs and goats), and the vast majority of these studies are based in microtomographic and histological analysis, aiming the evaluation of biomechanical performance and osseointegration capacity of new Ti-devices, with different topographies, coatings and shapes (WILLIE et al. 2010; FERRAZ et al. 2015; ZHANG et al., 2015; THOMA et al., 2016; FABBRO et al., 2017). While useful for certain pre-clinical applications, the large size/weight of these animal models does not permit the use of specific experimental tools and molecular assays, which are essential for a detailed understanding of the biological basis of osseointegration. In this scenario, mice models present a number of advantages in molecular biology, including availability of efficient genetic/molecular tools, and reduced quantities of drugs due to the small animal size, making it a cost-efficient model (BECHER; HOLLAND 2006; VANDAMME, 2014). In fact, the use of mice allows valuable cause-and-effect experimentation to determine gene/cell functions in bioengineering and regenerative processes. Finally, there is a large inventory of wild-type strains with distinct host response features, as well numerous genetically engineered mice strains, particularly with the C57Bl/6 background (VANDAMME, 2014).

In our efforts to make available a suitable *in vivo* experimental model for studying the biological basis of osseointegration, we characterized the Ti-mediated osseointegration in the oral cavity of C57Bl/6 mice, as described in the article 1 (BIGUETTI et al., 2018). In brief, this article (accepted for publication) provided a

molecular view of oral osseointegration kinetics in C57Bl/6 mice, evidencing potential elements responsible for orchestrating the immune and healing responses at the bone-implant interface in parallel with a novel microscopic analysis. Considering all findings of this study and comparing it with previous descriptions of osseointegration in other animal models and humans (THALJI; COOPER, 2013; THALJIa et al., 2014), this mice model was considered applicable for assessment of biological events upon osseointegration process and was subsequently used in the article 3.

Currently, biomaterials concepts state that an ideal biomaterial, such as Ti, have surface properties (physicochemical and morphological) that direct and select an initial protein adsorption and a provisional matrix formation, resulting in the modulation of the future healing and consequently resulting in the biomaterial integration with a minimal or inexistent foreign body reaction (FBR) (ANDERSON et al., 2008; TRINDADE et al., 2015). In this way, the protein adsorption and the inflammatory reaction that takes place along the an ideal biomaterial osseointegration is supposed to involve the recruitment of a sufficient number of MSCs and inflammatory cells, such as macrophages (THALJI; COOPER, 2013, THALJIb et al. 2013, THALJIa et al. 2014, VISHWAKARMA et al., 2016). In other words, theoretically Ti surface can direct a favorable protein adsorption and consequently, this protein layer directs beneficial cell activation for tissue regeneration around the biomaterial. Definitively, the key aspect of osseointegration is related to the Ti surface capability to modulate the protein adsorption, establishing the first bone/biomaterial interface and provisional matrix (VARIOLA et al., 2008; SANG et al., 2011; MARTINEZ-IBANEZ et al., 2017). Despite of these recent theories, one of the key issues yet to be solved in biomaterial science refers to the understanding of biomaterial/host interface composition, considering the presence of host proteins, and how these proteins are recognized by host cells at a biomaterial surface.

In this context, it has been demonstrated by means of *in vitro* studies, some of which using plasma serum (ROMERO-GAVILAN et al., 2017) or bone powder (SUGIMOTO et al., 2016), that Ti surfaces are able to attract bone-like proteins, ECM proteins, growth factors, as well immunological mediators (cytokines and complement proteins), which contributes for cell adhesion, proliferation and differentiation, as well biomaterial recognition by macrophages (OTHMAN et al., 2018). In fact, these studies provide some explanations about Ti regenerative capacity, but it is important to remind that *in vivo* host/biomaterial interfaces are substantially more complex that

artificial environments generated for *in vitro* studies. Consequently, it is reasonable to hypothesize that molecules released from tissue damage during the aseptic surgical trauma, collectively known as DAMPs (Damage Associated Molecular Patterns), also might interact with a biomaterial surface and/or influence the inflammatory response in the site of biomaterial implantation, with or without the direct adsorption at the biomaterial surface (VISHWAKARMA et al., 2016).

DAMPs are a family of endogenous molecules released from damaged, stressed and necrotic cells, and/or from the extracellular matrix, which activate the innate immune response in aseptic conditions by binding to specific receptors, such as Toll-like receptors (TLR2 and TLR4), RAGE (receptor for advanced glycation endproducts) and NOD-like receptors (FUKATA et al., 2009; LAND, 2015). Once released into the extracellular space following injury, DAMPs might trigger an immune/inflammatory response involving several inflammatory pathways, mainly expressed in macrophages (KANG et al; 2014, LAND, 2015; YANG et al., 2015). Importantly, recent studies have demonstrated that DAMPs are able to trigger tissue repair in different conditions (SCHIRALDI et al., 2012; AOYAGI et al., 2018), despite the lack of specific information about their role on bone repair and osseointegration of biomaterials.

At this point, it important to consider that most of DAMP receptors are primarily expressed in macrophages, which constitute the sensors of danger in the organism and play a central role in biomaterial recognition and incorporation (KOKKOLA et al., 2005). Furthermore, macrophages can contribute directly or indirectly in tissue healing by playing a number of functions, such as removing debris and dead cells after injury, as well as producing a large range of growth factors, immunological molecules and proteolytic enzymes(MOSSER;EDWARDS, 2008; MURRAY et al., 2014). In this context, depending on the basis of environmental molecular mediators, macrophages can polarize to proinflammatory/classically activated (M1) or anti-inflammatory/pro-reparative (M2) phenotypes (MOSSER;EDWARDS, 2008; BRANCATO; ALBINA, 2011; BROWN et al., 2012; JAGUIN et al., 2013; ALVAREZ et al., 2016). While M1-type response is related to a high expression of pro-inflammatory cytokines (TNFα, IL-6, IL1β); the M2-type response is associated with an increased expression of the prototypical anti-inflammatory cytokine IL10 and different growth factors (TGFβ1, PDGF, VEGF) (MANTOVANI et al., 2004; MOSSER;EDWARDS 2008; MURRAY et al, 2014). Since the balance of all these

molecules are directly related to the bone formation and remodeling (TANG et al., 2009; GRAVES et al., 2011) it is possible to assume that the ratio of M1:M2 macrophages along different stages of bone healing, can potentially affect the final outcome of osseointegration.

The interaction of DAMPs with their receptors in macrophage surface, such as TLRs and NLRs, can drastically change the protein surface expression and pro-inflammatory cytokines production (e.g.TNFα, IL6), determining the polarization into a M1 phenotype, whose profile is also induced by PAMPs (Pathogens Associated Molecular Patterns) in infections conditions and destructive inflammatory response, such as the lipopolysaccharides (LPS) found in the outer membrane of gram-negative bacteria (MARTINEZ et al. 2008; MOSSER;EDWARDS, 2008). In this sense, it is well described that DAMPs and PAMPs use, at least partially, the same receptors and signaling pathways when both are presented in inflammation(TANG et al., 2012). However, recent studies have also demonstrated that immune system deals with DAMPs and PAMPs in a different way, discriminating molecules from damage and infection by means CD24-Siglec G/10 receptor, which provide an additional 'fine-tunning' to cellular activation process (LIU et al., 2009). Also confirming the potential contribution of DAMPs in repair processes after injury, a pilot study on alveolar bone repair post tooth extraction in CD24KO mice, has recently demonstrated the bone healing is drastically impaired in the absence of CD24, suggesting an indirect role of DAMPs in a constructive inflammation along regenerative conditions (AOYAGI et al., 2018).

In a similar context, the well-studied prototypical DAMP called HMBG1 has been highly associated with wound healing by stimulating MSC migration, proliferation and differentiation (DEGRYSE et al., 2001, SCHIRALDI et al., 2012), collagen synthesis (DEGRYSE et al., 2001) as well angiogenesis induction (BISCETTI et al., 2010) and bone healing post tooth extraction model in mice (AOYAGI et al., 2018), among others. Importantly, the most well-established receptor for HMGB1 is RAGE, which can be a receptor for other DAMPs (e.g. S100 family), but not for PAMPs (KOKKOLA et al., 2005; KANG et al., 2014; ROJAS et al., 2016). Despite very scarce information known about the functionality of RAGE in macrophage polarization, there is some *in vitro* evidence demonstrating the role of HMGB1 promoting angiogenesis by treated M2 macrophages by a RAGE-dependent mechanism (ROJAS et al., 2016).

In face of all these evidences about the link between the DAMPs and tissue regeneration, as well DAMPs and ratio of M1:M2 macrophage polarization, the article 2 and article 3 presented in this thesis explore the role of DAMPS in the modulation of inflammatory response after Ti implantation in subcutaneous tissue (article 2), as well their role in the subsequent osseointegration in oral cavity of C57Bl/6 mice (article 3). Indirectly, the effect of HMGB1/RAGE axis on M1:M2 ratio is also indirectly demonstrated by the molecular analysis of M1 and M2 phenotype markers in both *in vivo* models.

Specifically, the article 2 (in preparation) presents the results of a biocompatibility model using Ti-discs subcutaneous implantation in C57Bl/6 mice, considering the possible presence of DAMPs in the protein layer deposited on Ti surface or Ti/host interface after initial periods post-Ti implantation. Subsequently, the impact of DAMPs on the constructive inflammatory response and host tissue repair were evaluated by means of pharmacological inhibition of the HMGB1 or RAGE.

The article 3 (in preparation) demonstrates the role of HMGB1 and RAGE on the constructive inflammatory response along osseointegration in C57Bl/6 mice, also by using pharmacological inhibition of the HMGB1 or the antagonism of its cognate receptor (RAGE). As previously mentioned, in this study we applied the oral osseointegration model already standardized in the article 1 (BIGUETTI et al., 2018).

Thus, the general aim of this study is to determine the positive influence of DAMPs adsorption on the biomaterial surface or biomaterial/host interface and its role in mediating a ‘constructive’ inflammatory process along repair outcome. The body of work presented here serves as a complement to the understanding of possible beneficial interactions between the immune system and biomaterial surface, which drives a successful osseointegration. Finally, considering the scarce knowledge about the role of DAMPs at Ti/host interface, we believe that the findings provided by these studies could be useful for future development of immuno-based biomaterials.

2 ARTICLES

2 ARTICLES

The articles presented in this thesis were written according to the instructions and guidelines for article submission of the corresponding journals.

- ARTICLE 1 – Oral implant osseointegration model in C57Bl/6 mice: microtomographic, histological, histomorphometric and molecular characterization. Journal of Applied Oral Science. (Accepted)
- ARTICLE 2 – Evidences of HGMB1 and RAGE contributions in the regenerative host response to Ti-based biomaterials. Journal - ACS Biomaterials Science & Engineering. (In preparation)
- ARTICLE 3 – ARTICLE 3 – HGMB1 and RAGE mediates Ti oral osseointegration in C57Bl/6 mice. Acta biomaterialia. (In preparation)

2.1 ARTICLE 1 – Oral implant osseointegration model in C57Bl/6 mice: microtomographic, histological, histomorphometric and molecular characterization*.

ABSTRACT

Despite the successful clinical application of titanium (Ti) as a biomaterial, the exact cellular and molecular mechanisms responsible for Ti osseointegration remains unclear, especially because of the limited methodological tools available in this field. **Objective:** In this study, we present a microscopic and molecular characterization of oral implant osseointegration model using C57Bl/6 mice. **Material and Methods**: Forty-eight male wild-type mice received a Ti implant placement in the edentulous alveolar crest and the peri-implant sites were evaluated by means microscopic (μCT, histological and birefringence) and molecular (RealTimePCRarray) analysis in different time points post surgery (3, 7, 14 and 21 days). **Results**: Early stages of osseointegration were marked by an increased expression of growth factors and MSC markers. Subsequently, a provisional granulation tissue was formed, with high expression of VEGFb and earlier osteogenic markers (BMPs, ALP and Runx2). The immune/inflammatory phase was evidenced by an increased density of inflammatory cells, and high expression of cytokines (TNF, IL6, IL1) chemokines (CXCL3, CCL2, CCL5 and CXC3CL1) and chemokine receptors (CCR2 and CCR5). Also, iNOS expression remained low, while ARG1 was upregulated, indicating predominance of a M2-type response. At later time points, the bone matrix density and volume was increased, in agreement with a high expression of Col1a1 and Col21a2. Remodelling process was marked by a peak of MMPs, RANKL and OPG expression at 14 days, and an increased density of osteoclasts. At 21 days, intimate Ti/bone contact was observed, with expression of final osteoblast differentiation markers (PHEX, SOST), as well as red spectrum collagen fibers. **Conclusions:** This study demonstrated an unique molecular view of oral osseointegration kinetics in C57Bl/6 mice, evidencing potential elements responsible for orchestrating cell migration, proliferation, ECM deposition and maturation, angiogenesis, bone formation and remodeling at the bone-implant interface in parallel with a novel microscopic analysis.

Keywords: Osseointegration. Dental Implants. Peri-implant endosseous healing.

Bone implant interface.

* Biguetti CC, Cavalla F, Silveira E, Fonseca AC, Vieira AE, Tabanez AP, Rodrigues DC, Trombone AP, Garlert GP. Oral implant osseointegration model in C57Bl/6 mice: microtomographic, histological, histomorphometric and molecular characterization. Journal of Applied Oral Science (Accepted for publication)

INTRODUCTION

Titanium (Ti) is considered the gold standard biomaterial in oral implantology[1], due to the material high biocompatibility, adequate mechanical properties, and osseointegration capacity[1,2], which lead to long-term performance and high rates of clinical success[1,3]. Additionally, Ti is also currently regarded as an immunomodulatory biomaterial rather than an inert metal, since Ti implantation in bone is associated with a transitory small degree of inflammation, which seems to contribute to the activation of host pathways that leads to osseointegration[2,4]. However, despite the clinical success and widespread application of Ti-based devices in dentistry and medicine, the exact cellular and molecular mechanisms responsible for the osseointegration phenomenon remains unclear[4], especially considering the immunological pathways involved in this process.

The majority of studies in the field of osseointegration have focused on surface modifications of Ti and their possible impact in the bone apposition outcome[5]. Indeed, most *in vitro* studies have focused on Ti surface topography and surface chemical composition with different treatments and coatings, aiming at the improvement of bone cells differentiation and matrix apposition/mineralization[5]. While useful in several aspects, *in vitro* studies are limited by intrinsic characteristics of cell culture, which evidently does not simulate all the biomaterial-host tissue interactions that take place *in vivo*[6]. In addition, *in vivo* preclinical evaluation of bone formation and remodelling around Ti surfaces are usually performed in animals with robust skeletal bone, such as minipigs[7] and dogs[8], which can recapitulate the architecture of human craniofacial bones and allow the analysis of implant modification (i.e. shapes, coatings and/or surface topographies) on the osseointegration[9]. While such large animal-based models are useful for certain applications, inherent factors such as animal size/height, lack of specific experimental tools for cause-and-effect experiments, as well as absent or restricted molecular assays, limits the possibilities of understanding the biological basis of osseointegration. In this scenario, mice have been demonstrated as a suitable animal model to properly investigate cellular and molecular aspects of a series of biological processes due to a number of experimental tools available for dissecting biological mechanisms[9].

Mouse models present a number of advantages including: 99% similarity to the human genome; availability of a number of efficient genetic/molecular tools; the

animal small size facilitates the use of reduced quantities of drugs and reduced experimental periods, making it a cost-efficient model[11]. Additionally, there is a large inventory of wild-type strains with distinct host response features, as well numerous genetically engineered mice strains, particularly with the C57Bl/6 background[11]. Consequently, such model allows valuable cause-and-effect experimentation to determine gene/cell functions in bioengineering and regenerative processes[9,12].

Finally, the use of mice in the osteoimmunology field as an experimental model host results in additional advantages due to the extensive knowledge of mice inflammatory and immunological responses[9,13]. In this context, endochondral long bones osseointegration models have been developed in mice with different approaches, such as for investigation of molecular and cellular regulation of osseointegration under micromotion stimuli[15], implant stability and insertion torque,[16] and acceleration of osseointegration[17]. In this context, osseointegration in long/endochondral bones is achieved through the program of endochondral ossification, which differs from the osseointegration in the maxillary/mandibular bone. In addition, there is a large proportion of marrow cavity in the implantation sites of long bones, which exhibit the slowest reaction to implant placement compared to the periosteum region[16]. Therefore, while these studies are useful to better understand the osseointegration process in orthopaedics applications, they cannot be fully translated for dentistry (i.e. maxillary/mandibular implants) framework.

On the other hand, maxillary and mandibular intramembranous bones are characterized by distinctive functional, anatomical and embryological features when compared to long bones, which could result in different aspects in the outcome of bone repair during osseointegration[3]. Thus, two different mice strains have been used in oral osseointegration studies: CD1 and C57/Bl-6 mice. Using CD1 mice strain, oral osseointegration models have been developed in edentulous alveolar crest in front of the first maxillary molar[17] or by using healed alveolar socket after upper molars extraction[28]. However, despite the advantage of having a robust skeletal phenotype compared to other mice strains, CD1 is an outbreed strain, which add some genetic variability as a limitation to this model, and also limits its genetic manipulation[26]. Alternatively, the use of C57Bl/6 mice overcome some of these limitations, since this inbred strain presents a widely known genetic background[18], comprising the mostly used strain in immunological studies[19]. However, the C57Bl/6 mice oral osseointegration model has been used for studying microtomographic and

histological aspects of peri-implantitis[28], by focusing on late stages of osseointegration and not in the entire bone repair process by which osseointegration is achieved.

Therefore, in this present study we propose to combine the advantages of previously developed models, using the edentulous alveolar crest (avoiding the limitations and complications of tooth extraction requirements) of C57Bl/6 mice (supported by the extensive knowledge and additional experimental possibilities inherent to this strain) as the implant placement site, followed by a detailed microtomographic, histological, histomorphometric, and molecular characterization of the osseointegration process.

MATERIAL AND METHODS

Animals

Forty-eight male wild-type mice (C57Bl/6) (10 weeks old, 25 g of weight in average) were obtained from the bred in the animal facilities of FOB/USP. Thirty-six animals were used for microscopic analysis (microCT, histological, and birefringence analysis) and twelve animals were used for molecular assays, distributed along 4 experimental periods: 3, 7, 14 and 21 days post surgical procedure. Throughout all experimental periods of this study, mice were provided sterile water *ad libitum* and were fed with sterile standard solid mice chow (Nuvital, Curitiba, PR, Brazil), except during the first 72 hours after surgery, in which diet was crumbled. No antibiotics and anti-inflammatory drugs were administered to the animals after implantation surgery and there was no evidence of weight loss, infection and persistent inflammation in surgical sites. This study was carried out in strict accordance with the recommendations in the Guide for the Care and Use of Laboratory Animals of the National Institutes of Health[20], and the experimental protocol was approved by the local Institutional Committee for Animal Care and Use (#012/2014).

Titanium implant screws

In an attempt to employ a comparable titanium screw as clinically used in dentistry, a screw of Ø 0.6 mm, titanium-6 aluminum-4 vanadium alloy (NTI-Kahla GmbH Rotary Dental Instruments, Kahla, Thüringen, Germany) with machined titanium surface was used in this study, as previously described in oral

osseointegration model in CD1 mice[10]. The screws were cut at length of 1.5 mm and sterilized by autoclaving before surgical procedures. Subsequently, screws were analyzed by means of scanning electron microscopy (SEM) and energy dispersive X-ray (EDX) before Ti implantation, in order to demonstrate the surface topography and chemical composition of screws used in this study. Screws were fixed on SEM-stub-holders and imaged by means of an ultra-high resolution SEM (FEI Nova NanoSEM, Thermo Fisher Scientific, OR, USA) - at 8kV with a resolution of 127.8 eV. The chemical composition was analyzed in the same regions of interest for qualitative SEM images, by using the software TEAM™ EDS Analysis System (AMETEK Materials Analysis Division, Mahwah, NJ, USA) concerning the amount of 10 chemical elements present in the bulk structure of titanium implants used in the clinic, as previously described[21]: Titanium (Ti), Aluminum (Al), Vanadium (V), Calcium (Ca), Nitrogen (N), Niobium (Nb), Oxygen(O), Phosphorus (P), Sulfur (S) and Zinc (Zn).

Experimental protocol

Previous to the surgical procedure, three different mouse maxillae were carefully measured by microtomographic images considering thicker areas to install the titanium implants, which comprised a 300 µm of thickness, between the maxillary right first molar and the incisors (Figure 1AB). For the surgical procedure, mice were anesthetized by intramuscular administration of 80 mg/kg of ketamine chloride (Dopalen®, Agribrands Brasil LTDA, Paulínia, SP, Brazil) and 160 mg/kg of xylazine chloride (Anasedan®, Agribrands Brasil LTDA, Paulínia, SP, Brazil) in the proportion 1:1, which was determined according to animal weight. Subsequently, mice were placed on a surgical table with a mouth retractor, as previously described in other dentistry mice models[14,22]. Briefly, the animal was placed in dorsal decubitus position and the 4 limbs were affixed to a surgical table, under a stereomicroscope (DF Vasconcellos S.A., Sao Paulo, SP, Brazil), with 25x magnification. Oral titanium implant screws were placed in C57Bl/6 mice following a previous surgical protocol described for CD1 mice[10], and each mouse received one oral implant inserted in the left edentulous alveolar crest. Oral mucosa was cleaned using topical chlorhexidine solution for 1 min followed by an incision of 2 mm width parallel to the palatal crease and 1 mm in front of the left first maxillary molar, by using a 22.5° angled micro scalpel blade (n.10316-14, Fine Science Tools®, British Columbia, CA, USA). A small

detachment of the mucoperiosteum was made and the subjacent bone was drilled using a pilot drill of Ø 0.50 mm (NTI-Kahla GmbH Rotary Dental Instruments, Kahla, Thüringen, Germany). The pilot hole was performed using a surgical motor (NSK-Nakanishi International, Kanuma,Tochigi, Japan), with a speed of 600 rpm and 35 N to kilogram force, under continuous irrigation with cold saline solution, in order to avoid heating and subsequent bone necrosis. The Ti-implant was screwed down in the implant bed using a Castro Viejo Micro Needle Holder (Fine Science Tools®, British Columbia, CA, USA) (Figure 1C). All surgical procedures were performed by a single calibrated surgeon (FC). At the end of the experimental periods (days 3, 7, 14 and 21 post-Ti- screw implantation), mice were killed with an excessive dose of anesthetic and the maxillae were collected. Nine maxillae were used for microscopic [micro-computed tomography (µCT), histological and birefringence] analyses; and three samples containing only the region of the implant bed were used for RealTimePCRarray analysis. Samples designated for microscopic analysis were fixed in PBS-buffered formalin (10%) solution (pH 7.2) for 48h at room temperature, subsequently washed over-night in running water and maintained temporarily in alcohol fixative (70% hydrous ethanol) until the conclusion of the µCT analysis, and them decalcified in 4.13% EDTA (pH 7,2). After sample decalcification, the Ti screw was carefully unscrewed from the implant bed with a Micro Needle Holder for histological processing and paraffin inclusion. Samples for molecular analysis were stored in RNAlater (Ambion, Austin, TX, USA) solutions[9].

Micro-computed tomography (µCT) assessment

Thirty-six mouse maxillae containing the Ti-implants were scanned by Skyscan 1176 System (Bruker Microct, Kontich, Belgium) at 80 kV, 300 µA, 180 degrees of rotation and exposure range of 1 degree. Images were captured with resolution of 12.45µm pixel size. Projection images were reconstructed using NRecon software (Bruker Microct, Kontich, Belgium) using 35% of Beam Hardening Correction and subsequently aligned using Dataviewer 1.4.4.0 software (Bruker Microct, Kontich, Belgium) in order to standardize the position of all specimens for subsequent quantitative evaluation (Figure 3A-C). Three-dimensional images obtained by CT-Vox 2.3 software. Quantitative evaluation of bone to implant interface was assessed using CTAn 1.1.4.1 software (Bruker Microct, Kontich, Belgium) in accordance with

recommended guidelines[23]. Briefly, for measuring the proportion of bone volume (BV/TV, %) at the implant-bone interface area, the data set of images saved in axial position was opened in the software CTAn and the region of interest (ROI) was determined using a cylindrical segmentation with axis length of 500 µm and diameter of 700 µm (Figure 3C). The first 200 um from the first third of Ti screw was excluded from ROI in order to standardize the positioning for starting bone quantification in all specimens, as demonstrated in Figure 3B. The bone quantification was performed considering 100 µm from the implant surface in an axial view, into the bone (Figure 3C). After binarization and separation between titanium body and bone by the difference of hyperdensities, the BV/TV was acquired (Figure 3E).

Histomorphometry

The same mice maxillae used for microCT scanning were processed for histological analysis. Forty semi-serial sections were cut with 4 µm thickness, of which nine serial sections considering the central region of bone to implant contact were chosen for histomorphometry and stained for hematoxylin and eosin [H&E] staining. The analysis were performed by a single calibrated investigator with a binocular microscope (Olympus Optical Co., Tokyo, Honshu, Japan) using a 100x immersion objective. Six histological fields *per* HE section, comprising the region adjacent to thread spaces, were captured using a 100× immersion objective. A grid image was superimposed on each histological field, with 10 parallel lines and 100 points in a quadrangular area, by using Image J software (Version 1.51, National Institutes of Health, Bethesda, MD, USA). Briefly, points were counted coinciding with the following parameters of the osseointegration process: blood clot, inflammatory cells, other elements (empty spaces left by implant space), blood vessels, fibroblasts, collagen fibers, osteoblasts, osteoclasts, and new bone matrix. Results were presented as the mean area density for each structure considered in each examined group.

Picrosirius-polarization method and quantification of birefringent fibers

For birefringence analysis, 4 sections with 5 µm thickness histological slides considering the central region of bone to implant contact were used for picrosirius red

staining and birefringence analysis. As previously described[9], green birefringence color indicates thin fibers; yellow and red colors at birefringence analysis indicate thick collagen fibers. Three fields from each section were analyzed through polarizing lens coupled to a binocular inverted microscope (Leica DM IRB/E, Leica Microsystems Wetzlar GmbH, Wetzlar, Germany), by using 40x magnification immersion objective. All the images were captured with the same parameters (the same light intensity and angle of the polarizing lens at 90° to the light source) from Leica Imaging Software (LAX, Leica Microsystems Wetzlar GmbH, Wetzlar, Germany). Briefly, the quantification of birefringence brightness was performed using the software AxioVision 4.8 (Carl Zeiss Microscopy GmbH, Jena, Germany). Images were binarized for green, yellow and red spectra, and the quantity of each color pixels^2 corresponding to the total area of each histological field was measured[9]. Mean values of 4 sections from each animal were calculated in pixels^2.

RealTimePCR array reactions

Samples containing only the region of the implant bed were resected and storage in RNA Stabilization Solution (RNAlater®, Thermofisher, Waltham, MA, USA) until RealTime PCR array reactions. RealTimePCR array reactions were performed as previously described[9,24,25]. First, RealTimePCR array was performed from a pool of all experimental time-points (3 d, 7 d, 14 d and 21 d), providing targets in which expression variation presented a significant variation compared to the control side. Then, upregulated targets were analyzed regarding their kinetics of expression for specific time points of 3, 7, 14 and 21-days during osseointegration process. Briefly, the extraction of total RNA from implantation site was performed with RNeasyFFPE kit (Qiagen Inc, Valencia, CA, USA) according to manufacturers' instructions. The integrity of RNA samples was checked by analyzing 1 mg of total RNA on 2100Bioanalyzer (Agilent Technologies, Santa Clara, CA, USA) according to manufacturers' instructions, and the complementary DNA was synthesized using 3 µg of RNA through a reverse transcription reaction (Superscript III, Invitrogen Corporation, Carlsbad, CA, USA). The Real-time PCR array was performed in a Viia7 instrument (LifeTechnologies, Carlsbad, CA, USA) using custom panels for "wound healing" (PAMM-121), "inflammatory cytokines and receptors" (PAMM-011) and "Osteogenesis" (PAMM-026) (SABiosciences, Frederick, MD, USA) for gene

expression profiling. Data were analyzed by RT2 Profiler PCR Array Data Analysis online software (SABiosciences, Frederick, MD, USA) for normalizing the initial geometric mean of three constitutive genes (GAPDH, ACTB, Hprt1), following normalizing the control group. Data are expressed as heat map fold change relative to the control group.

Statistical analysis

Differences among data sets were statistically analyzed by One-Way Analysis of variance (ANOVA) followed by Bonferroni's multiple comparison *post-hoc* test or student's t-test where applicable; for data that did not fit in the distribution of normality Kruskal-Wallis test (followed by Dunn's test) and Mann-Whitney test were used The statistical significance of the experiment involving PCR Array was evaluated by the Mann-Whitney test, and the values tested for correction of Benjamini and Hochberg[26] (1995). Values of $p<0.05$ were considered statistically significant. All statistical tests were performed with GraphPad Prism 5.0 software (GraphPad Software Inc., San Diego, CA, USA).

RESULTS

Development of the surgical protocol

Our focus is this study was to address a pre-clinic murine model of oral osseointegration, previously developed in CD1 mice[10] for C57Bl/6 mice. We first analyzed the anatomy of three different maxillae from 10 weeks C57Bl/6 male mice, by microtomographic images, and then selected the most robust skeletal area as an implant bed, specifically in the edentulous space between the maxillary right first molar and the incisor, along the alveolar crest, comprising an average of 300 μm of thickness (Figure 1AB).

SEM micrographs demonstrated uniform unidirectional threads, with no deposits and no particular features or deformation and features of a clearly machined surface topography, such as small irregularities. In the composition characterization, Ti screw alloy presented a mass of 75.35% of Ti, 14.66 % of V, 5% of N and 4.20% of Al. Other evaluated chemical elements were found in minor concentration, less than 1% (Figure 2D).

For developing the surgical protocol, Ti-screw was implanted in the edentulous space between the maxillary right first molar and the incisor. After a day of surgery,

animals were able to eat crumbled chow and were acting normally, with no signs of distress. All animals presented complete oral mucosal healing by day 7, as clinically demonstrated in Figure 1D. Importantly, of the 36 implants placed and investigated with microscopy, 33 demonstrated primary stability immediately from screw insertion and 28 achieved osseointegration, observed by microCT and histologic assessment, and totaling a 77.78% success rate in terms of osseointegration. Additionally, the 5 implants which presented failure post 14 and 21 days, did not present signs of infection in histological and clinical examination.

µCT assessment

Subsequently, we evaluated sites of Ti-implantation by microtomographic qualitative and quantitative analyses of mineralized bone matrix (Figure 3A-C). The three-dimensional images of maxillae containing sites of Ti implants (Figure 3D), as well as the quantitative assessment (BV/TV) indicated a gradual and significant bone apposition (BV/TV, %) around implant threads throughout 7 d (23.19±2.014), 14 d (31.20±3.82) and 21 d (42.12±3.01) (Figure 3E). At 3 d, the bone detected by microCT (16.73±1.11) was predominantly comprised by native/remaining bone supporting the Ti-screw, as demonstrated by the representative three-dimensional image (Figure 3D). Newly formed bone matrix was detected at 7 days post-implantation, as evidenced by Figure 3E. The maximum amount of osseointegration was achieved by 21 days, when the interface of bone/Ti was covered with an average of 42.12±3.01% of BV/TV (Figure 3E).

Histology, histomorphometry and birefringence

Considering the histological analysis, the panoramic transversal image of mouse maxillae, demonstrated that the Ti-screw was projected through the palatal bone into the olfactory epithelium of maxillary sinus (histological section at 14 days, Figure 4A), as also described previously in CD1 mice[10]. The histological and histomorphometric analysis were performed in the spaces occupied by three initial Ti-screw threads, from coronal to apical, on each side of the Ti-screw, as indicated by arrows in Figure 4A. At 3 days, the bone-implant interface was filled mainly by a blood clot and inflammatory infiltrate, as demonstrated by histomorphometry (Figure 5A, B). The blood clot was evidenced by erythrocytes, surrounded by an eosinophilic and slight matrix of fibrin network, also permeated by an inflammatory infiltrate with

predominance of mononuclear cells (Figure 4B and B'). Importantly, there was no newly formed bone matrix at 3 days. Consequently, the bone matrix quantified at 3 days was merely native viable bone and bone debris observed around Ti threads.

At 7 days post-implantation, there was a significant decrease in blood clot (Figure 5A), while fibroblasts and blood vessels area density were significantly increased (Figure 5D, E), as a consequence of a transitory granulation tissue formation (Figure 4C and C'). Aligned robust and cuboids cells, with a typical morphology of osteoblasts, were also observed producing newly bone matrix between the implant surface and pre-existing bone. Also at 7 days, osteoclastic resorption lacunae and a few quantity of osteoclasts were found around bone debris and pre-existing bone. From 14 to 21 days, granulation tissue components significantly decreased surrounding Ti threads spaces (Figure 5D, E, F), while newly formed bone matrix increased in these regions (Figure 5I). Newly produced bone matrix was deposited immediately adjacent at the bone threads spaces (Figure 4D, D', E, E'), indicating a direct contact between the implant surface and bone by 14 and 21 days. Scattered areas surrounding Ti thread spaces and bone were left with soft tissue, including connective tissue and bone marrow at 21 days. Furthermore, by days 14 and 21 post-implantation, the peri-implant mucosa presented a well organized connective tissue attachment, composed mainly of fibroblasts and collagen fibers, with slight quantities of inflammatory cells.

For analyzing the dynamic of collagen fibers maturation, we quantified different birefringent collagen fibers (green, yellow and red) from the new bone matrix and initial granulation tissue. A negligible quantity of collagen fibers was found starting at 3 to 7 days around the Ti threads, emitting birefringence in the green spectrum (i.e. immature and thinner fibers) (Figure 6A). From 7 to 21 days, there was a significant increase in the quantity of total collagen fibers (Figure 6C), as well as in organic matrix maturation, as evidenced by the presence of red color spectrum fibers upon polarized light (Figure 6A) in parallel with sequential increase of red color intensity pixels area (Figure 6B).

Gene expression patterns in the osseointegration process

A pool of samples from all periods post-Ti implantation were initially analyzed by means of an exploratory RealTimePCR array (Figure 7), considering molecules involved in inflammatory response and bone healing (growth factors;

immunological/inflammatory markers; extracellular matrix, MSC and bone markers) in order to select targets with a significant expression in comparison with the control samples. Subsequently, those targets with a significant variation expression in pooled samples were analyzed according to their kinetics of expression during experimental periods (Figure 8). Among several growth factors, the molecules BMP2, BMP4, BMP7 and TGFβ1 expression were upregulated during osseointegration in comparison with the control (Figure 7) with a peak of mRNA levels at 7 and 14 days (Figure 8). Considering immunological markers analyzed (cytokines, chemokines, chemokine receptors and other inflammatory mediators) the IL1β, IL6, IL10, TNF, ARG2, CCR2, CCR5, CCL2, CCL5, CCL17, CXCL3, CXCL12, CX3CL1 were positively regulated in the osseointegration process in comparison with the control samples (Figure 7). The kinetics analysis demonstrated that some immunological markers (IL1β, IL6, IL10, TNF, CCR2, CCR5, CCL2, CXCL12, and CX3CL1) were upregulated from 3 days post-implantation, but all those markers peaked at the 7 day time point, followed by a gradual decrease in their expression in subsequent experimental periods (Figure 8). Among the extracellular matrix markers, Col1a1, Col21a1, Col2a1, MMP1a, MMP2 and MMP9 were upregulated through oral osseointegration process in comparison with the control samples (Figure 7). The kinetics analysis demonstrated that Col1a1 peaked at 7 and 14 days, with gradual decrease at 21 days; while Col21a1, Col2a1, MMP1a, MMP2 and MMP9 was upregulated from 7 days and peaked at 14 days with gradual decrease at 21 days. MSC markers CD106, OCT-4, NANOG, CD34, CD146 and CD105 were found positively upregulated in osseointegration sites, with a peak of expression for CD106 at 3 days, while OCT-4, NANOG, CD34, CD146 and CD105 peaked at 7 days (Figure 8). All these cited MSC markers present a significant upregulation at 3, 7 and 14 days, with a significant decrease at 21 days (Figure 8). Among bone markers, early bone formation markers Runx2 and Alpl, late bone formation markers Phex and Sost, as well as remodeling markers RANKL and OPG were found upregulated in osseointegration sites compared to control samples (Figure 7). The kinetic analysis demonstrated that Runx2 and OPG presented higher mRNA levels mainly at 7 and 14 days, while Alpl peaked at 7 days with a gradual decrease at 14 and 21 days. Also in the kinetics analysis, late bone formation markers Phex and Sost were upregulated at 14 and 21 days, and RANKL presented higher mRNA levels at 14 and 21 days.

DISCUSSION

Despite the successful clinical application of Ti-based devices, the exact cellular and molecular mechanisms responsible for the osseointegration phenomenon remains unclear, especially considering the immunological pathways involved in this process. In view of the multiple experimental advantages conferred by the use of mice as the experimental host for Ti implantation, in this study we describe the microtomographic, histological/histomorphometric and molecular characterization of an oral maxillary osseointegration model along early (3 and 7 days) to late experimental periods (14 and 21 days) in the oral cavity of C57Bl/6 mice (Figure 9).

While C57Bl/6 strain was used in a previous study as recipients/hosts of Ti devices in the oral cavity[28], implants were placed in the maxillary bone after extraction of 3 upper molars. Considering the complex anatomic feature of mice upper molars and the potential surgical complications/intercurrences due exodontic procedures, and the requirement for 2 surgical procedures, we initially performed measurements of palatal bone thickness in C57Bl/6 mice to verify the possible implant insertion in the palatal edentulous area. The thicker region of palatal bone in the edentulous alveolar ridge of C57Bl/6 corresponded to 300 µm, which was considered suitable to receive a miniature Ti implant screw cut at length of 1.5 mm. The implant placement in this area, without preceding multiple tooth extraction, was previously reported in CD1 mice, which due to its increased size was suitable for a 2 mm implant insertion[10]. Additionally, the Ti screw used in this present study was based on a conventional Ti6Al4V alloy, with a machined surface without any treatments and/or topography alterations, as demonstrated by SEM and X-ray analysis (Figure 2), in order to characterize the osseointegration process *per se,* as has been frequently used in experimental studies using craniofacial[10] and long bones[16,25] as osseointegration models.

The surgical procedures used in this study were performed following the same principles and procedures used in dentistry, in order to avoid lack of primary stability and overheating. Of all titanium implants with adequate primary stability, 77.78% achieved osseointegration, demonstrated by means of µCT and histological data (Figures 3 and 4), which is in agreement with success rates previously described in a similar model performed in CD1mice (74% of osseointegration at 21 day)[10]. Additionally, the 5 implants which presented failure post 14 and 21 days, exhibited a

fibrous connective tissue surrounding the Ti screw area with no signs of infection. Possibly, osseointegration failure in those specimens could be a result of loosening of the primary stability in the first periods post-Ti implantation.

Initially, our histological characterization demonstrated that blood is the first biological element in contact with Ti surface, evidenced by the formation of a highly organized clot in contact with Ti threads and native bone at 3 days (Figures 4B and B´) as also observed in larger models in rats[27], where blood components, such as the fibrin network, provide a structural support for initial cell adhesion and migration toward the implant surface[28]. Indeed, at early stages, a protein adsorption layer is created on Ti surfaces, constituted mainly by blood molecules, platelets and plasma fibronectin, as also demonstrated by *in vitro* studies[29] where the presence of plasma fibronectin at Ti surface supports the first events of osteogenesis. Of note, theoretically this first protein layer on Ti surfaces also contains molecules required for regulation of subsequent steps that will lead to osseointegration[30], such as growth factors and immunologic mediators, that orchestrates bone formation in the peri implant space[27]. In agreement, our molecular data demonstrated an up regulation of TGFb1 and CXCL12 in the early stages after Ti implantation (Figure 8), which were also observed in early times of oral osseointegration in rats [27]. In the osseointegration context, TGFb1 and CXCL12 have been shown to enable migration of mesenchymal osteoprogenitor cells at the implant surface and threads spaces[2,31]. Accordingly, MSC are among the first cells to migrate to the Ti surface[31], and in fact, several MSC markers (CD106, OCT-4, NANOG, CD34, CD146 and CD105) also presented an early up regulation post-Ti implantation (Figure 8).

Concurrently with the early upregulation of MSCs markers, a provisional extracellular matrix is formed and gradually evolves to a high vascularized granulation tissue (Figures 4 and 5), which will provide further support for cell migration and differentiation. A similar response was observed in peri-implant sites in mice[10,22] and rats[27], but the presence of biomaterials was associated with a delayed healing dynamic compared to alveolar intramembranous bone healing in the absence of biomaterials[9,10]. Indeed, the earlier granulation tissue formed in the space between Ti threads and remaining bone works as a preosteoblastic supportive connective tissue[10,22], as evidenced in this study by an increased area density of blood vessels (Figure 5D), fibroblasts (Figure 5E) and osteoblasts (Figure 5G) after 7 days in implantation sites, with an up regulation of angiogenic (VEGFb) and earlier

osteogenic markers (BMP2,4 and 7, ALP and Runx2) (Figure 8). Indeed, BMPs (BMP2, BMP4 and BMP7) are key factors related to the commitment of MSC into osteoblast fate during physiological osteogenesis[32], bone repair[10] and osseointegration[33], since BMPs can stimulate the transcription factor RUNX2[32]. Importantly, RUNX-2 directly binds to enhancer regions of osteoblast-specific genes, such as the earlier matrix mineralization ALP[34], which is also in agreement with our findings.

Also in these earlier stages of the osseointegration, the immune/inflammatory response is triggered at the Ti/host interface, which integrate the key molecular events for determining the success or failure of the osseointegration[3,35]. Indeed, in this study the area density of inflammatory cells peaked in the earlier periods of the osseointegration process, in parallel with an up-regulation of a variety of immunological factors involved in leukocyte migration, such as pro-inflammatory cytokines (TNF, IL6, IL1) and monocytes/macrophages chemoattractants (i.e. the chemokines CXCL3, CCL2, CCL5, CC17, CXCL12 and CXC3CL1) and the chemokine receptors (CCR2 and CCR5), were highly expressed in the sites of implantation (Figures 7 and 8). In agreement with these findings, an early molecular assessment of osseointegration process in humans revealed a similar pattern of chemokines and interleukins expression in the early periods post-Ti implantation[30], which was also observed in rats[27], reinforcing the validity of the mouse model in the view of the similar inflammatory response pattern. Of note, while TNF, IL6 and IL1 comprise part of a macrophage cytokine portfolio, CCR2 and CCR5 are involved mainly in monocytes/macrophages migration into wound healing, suggesting an important involvement of macrophages with the oral regenerative processes[35].

Indeed, in addition to the classical role of macrophages on debris clearance after injury, these cells are key regulators of inflammatory and regenerative processes, by releasing different mediators in response to the state of polarization towards M1 (inflammatory) or M2 (reparative) phenotype, and orchestrate the outcomes of inflammation and bone healing[36]. Interestingly, it has been proposed that activation of these cells into M1 and M2 macrophages is a crucial step for orchestrating a foreign body reaction (FBR) post biomaterial implantation and also to determine the equilibrium between osteogenic factors/cells and osteolytic factors/cells around the Ti implant after osseointegration[2,3]. In this study, while iNOS (a M1 marker) expression remained low at the osseointegration sites, ARG1 (a M2

marker) was up regulated after Ti implantation, indicating a predominance of a M2-type response. Indeed, in enhanced osseointegration models observed in long bones in rats, the upregulation of ARG1 and downregulation of iNOS is correlated with a high proportion of M2 macrophages and beneficial bone healing around Ti surfaces[37]. Accordingly, a marked up regulation of reparative/regulatory M2-type macrophages is also observed after Ti implant placement in humans[30]. Indeed, the M2-type response has been suggested to be critical to wound healing outcomes by expressing several pro-resolutive molecules, including ARG1, IL10 and TGFb1[38]. These data are also compatible with the transitory nature of the inflammatory infiltrate surrounding the Ti surface, which presented a gradual decrease over time in this study (Figure 4B, C, D and Figure 5).

Following the resolution of inflammation (Figure 4D), while the expression of inflammatory factors and density of inflammatory infiltrate tend to decrease over time post- implantation, the expression of osteogenic factors and ECM components were gradually increased, in agreement with previous findings in rats[27]. In line with the events of intramembranous bone repair, the granulation tissue is directly replaced by bone over time (Figures 3 and 4), as also previously reported in other oral osseointegration animal models[10,27], while Ti osseointegration in long bones is dependent on hypertrophic cartilage formation[15]. As density area of primary bone matrix significantly increased at 14 days, also followed by expression of Col1a1 and Col21a2 and a gradual maturation of collagen fibers detected by birefringence analysis (Figure 6), there was a remarkable remodeling process, evidenced by peaks corresponding to MMPs (MMP1, MMP2 and MMP9), RANKL and OPG, and also an increased area density of osteoclasts (Figure 5H). As also demonstrated in other models[28,30], all these events collectively will determine bone quality and influence the mechanical properties of osseointegration[37]. Indeed, the quality of osseointegration is dependent on a high organized bone matrix and its ECM components, in which collagen plays a crucial role[38].

Consequently, in late stages, there was intimate bone contact over the Ti threads, associated with the expression of several bone markers typical of final osteoblast differentiation (PHEX, SOST)[9]. Noteworthy, the maximum amount of osseointegration was achieved in C57Bl/6 mice at day 21, with an average of 42.12±3.01% mineralized bone matrix (BV/TV) detected around Ti threads by microCT analysis (Figure 3), and also 87% of red spectrum collagen fibers of total

collagen content detected by birefringence analysis (Figure 6), possibly as a indicative of a well organized collagen bundles fibers[9,10]. Interestingly, in the complementary histomorphometry analysis, the percentage of bone matrix around/and in contact with Ti threads represented a density area of 81.03±3.87% in average, which is in agreement with histological investigations of Ti dental implants placed in humans, where bone area in individual threads achieved an average of 81.8%[38]. However, even 60% of histological bone-to-implant contact is considered as enough osseointegration for successful implants in humans for up to 17 years[3].

CONCLUSIONS

In summary, this study originally demonstrated a unique molecular view of the kinetics of osseointegration, evidencing potential elements responsible for orchestrating cell migration, proliferation, ECM deposition and maturation, angiogenesis, bone formation and remodeling at the bone-implant interface in parallel with a novel histological, birefringence and µCT analysis. Considering all of these observations and comparing with previous descriptions of osseointegration, this C57Bl/6 mice oral osseointegration model would be a suitable tool for the assessment of biological events upon osseointegration process.

Acknowledgments

The authors would like to thank Daniele Ceolin, Patricia Germino and Tania Cestari for their excellent technical assistance. This study was supported by grants (#2015/24637-3) and scholarships (#2014/09590-8, #2015/18162-2) from FAPESP.

Financial funding sources

This work was supported by grants from Fundação de Amparo à Pesquisa do Estado de São Paulo – FAPESP #2014/09590-8, FAPESP # 2015/18162-2, FAPESP #2015/24637-3.

REFERENCES

1- Ogle OE. Implant surface material, design, and osseointegration. Dent Clin North Am. 2015;59(2):505-20.

2- Davies JE. Understanding peri-implant endosseous healing. J Dent Educ. 2003;67(8): 932-49.

3-Trindade R, Albrektsson T, Wennerberg A. Current concepts for the biological basis of dental implants: foreign body equilibrium and osseointegration dynamics. Oral Maxillofac Surg Clin North Am. 2015;27(2):175-83.

4- Trindade R, Albrektsson T, Tengvall P, Wennerberg A. Foreign body reaction to biomaterials: on mechanisms for buildup and breakdown of osseointegration. Clin Implant Dent Relat Res. 2016;18(1):192-203.

5- Martínez-Ibáñez M, Murthy NS, Mao Y, Suay J, Gurruchaga M, Goñi I, et al. Enhancement of plasma protein adsorption and osteogenesis of hMSCs by functionalized siloxane coatings for titanium implants. J Biomed Mater Res B Appl Biomater. 2017. doi: 10.1002/jbm.b.33889.

6-Cooper LF, Masuda T, Yliheikkilä PK, Felton DA. Generalizations regarding the process and phenomenon of osseointegration. Part II. *In vitro* studies. Int J Oral Maxillofac Implants. 1998;13(2):163-74.

7-Fabbro MD, Taschieri S, Canciani E, Addis A, Musto F, Weinstein R, et al. Osseointegration of titanium implants with different rough surfaces: a histologic and histomorphometric study in an adult minipig model. Implant Dent. 2017;26(3):357-66.

8 - Gotfredsen K, Berglundh T, Lindhe J. Bone reactions adjacent to titanium implants subjected to static load of different duration. A study in the dog (III). Clin Oral Implants Res. 2001;12(6):552-8.

9-Vieira AE, Repeke CE, Ferreira Junior SB, Colavite PM, Biguetti CC, Oliveira RC, et al. Intramembranous bone healing process subsequent to tooth extraction in mice: micro-computed tomography, histomorphometric and molecular characterization. PLoS One. 2015;10(5):e0128021.

10-Mouraret S, Hunter DJ, Bardet C, Brunski JB, Bouchard P, Helms JA. A pre-clinical murine model of oral implant osseointegration. Bone. 2014;58:177-84.

11-Vandamme TF. Use of rodents as models of human diseases. J Pharm Bioallied Sci. 2014;6(1):2-9.

12- Salgado G, Ng YZ, Ko LF, Goh CS, Common JE. Human reconstructed skin xenografts on mice to model skin physiology. Differentiation. 2017;98:14-24.

13- Ferreira SB Jr, Repeke CE, Raimundo FM, Nunes IS, Avila-Campos MJ, Ferreira BR, et al. CCR5 mediates pro-osteoclastic and osteoclastogenic leukocyte chemoattraction. J Dent Res. 2011;90(5):632-7.

14- Andrade I Jr, Taddei SR, Garlet GP, Garlet TP, Teixeira AL, Silva TA, et al. CCR5 down-regulates osteoclast function in orthodontic tooth movement. J Dent Res. 2009;88(11):1037-41.

15- Wazen RM, Currey JA, Guo H, Brunski JB, Helms JA, Nanci A. Micromotion-induced strain fields influence early stages of repair at bone-implant interfaces. Acta Biomater. 2013;9(5):6663-74.

16- Cha JY, Pereira MD, Smith AA, Houschyar KS, Yin X, Mouraret S, et al. Multiscale analyses of the bone-implant interface. J Dent Res. 2015;94(3):482-90.

17- Popelut A, Rooker SM, Leucht P, Medio M, Brunski JB, Helms JA. The acceleration of implant osseointegration by liposomal Wnt3a. Biomaterials. 2010;31(35):9173-81.

18- Song HK, Hwang DY. Use of C57BL/6N mice on the variety of immunological researches. Lab Anim Res. 2017;33(2):119-23.

19- Pirih FQ, Hiyari S, Leung HY, Barroso AD, Jorge AC, Perussolo J, et al. A murine model of lipopolysaccharide-induced peri-implant mucositis and peri-implantitis. J Oral Implantol. 2015;41(5):e158-64.

20- Kilkenny C, Browne W, Cuthill IC, Emerson M, Altman DG; National Centre for the Replacement, Refinement and Reduction of Animals in Research. Animal research: reporting *in vivo* experiments - the ARRIVE guidelines. J Cereb Blood Flow Metab. 2011;31(4):991-3.

21- Rodrigues DC, Valderrama P, Wilson TG, Palmer K, Thomas A, Sridhar S, et al. Titanium corrosion mechanisms in the oral environment: a retrieval study. Materials (Basel). 2013;6(11):5258-74.

22- Taddei SR, Moura AP, Andrade I Jr, Garlet GP, Garlet TP, Teixeira MM, et al. Experimental model of tooth movement in mice: a standardized protocol for studying bone remodeling under compression and tensile strains. J Biomech. 2012;45(16):2729-35.

23- Bouxsein ML, Boyd SK, Christiansen BA, Guldberg RE, Jepsen KJ, Müller R. Guidelines for assessment of bone microstructure in rodents using micro-computed tomography. J Bone Miner Res. 2010;25(7):1468-86.

24- Araujo-Pires AC, Biguetti CC, Repeke CE, Rodini CO, Campanelli AP, Trombone AP, et al. Mesenchymal stem cells as active prohealing and immunosuppressive agents in periapical environment: evidence from human and experimental periapical lesions. J Endod. 2014;40(10):1560-5.

25- Araujo-Pires AC, Francisconi CF, Biguetti CC, Cavalla F, Aranha AM, Letra A, et al. Simultaneous analysis of T helper subsets (Th1, Th2, Th9, Th17, Th22, Tfh, Tr1 and Tregs) markers expression in periapical lesions reveals multiple cytokine clusters accountable for lesions activity and inactivity status. J Appl Oral Sci. 2014;22(4):336-46.

26- Benjamini Y, Hochberg Y. Controlling the false discovery rate: a practical and powerful approach to multiple testing. J R Stat Soc Series B Stat Methodol. 1995;1(57):289-300.

27- Lin Z, Rios HF, Volk SL, Sugai JV, Jin Q, Giannobile WV. Gene expression dynamics during bone healing and osseointegration. J Periodontol. 2011;82(7):1007-17.

28- Thalji G, Cooper LF. Molecular assessment of osseointegration *in vivo*: a review of the current literature. Int J Oral Maxillofac Implants. 2013;28(6):e521-34.

29- Jimbo R, Ivarsson M, Koskela A, Sul Y, Johansson CB. Protein adsorption to surface chemistry and crystal structure modification of titanium surfaces. J Oral Maxillofac Res. 2010;1(3): e3.

30- Thalji GN, Nares S, Cooper LF. Early molecular assessment of osseointegration in humans. Clin Oral Implants Res. 2014;25(11):1273-85.

31- Zwingenberger S, Yao Z, Jacobi A, Vater C, Valladares RD, Li C, et al. Enhancement of BMP-2 induced bone regeneration by SDF-1alpha mediated stem cell recruitment. Tissue Eng Part A. 2014;20(3-4):810-8.

32- Bandyopadhyay A, Tsuji K, Cox K, Harfe BD, Rosen V, Tabin CJ. Genetic analysis of the roles of BMP2, BMP4, and BMP7 in limb patterning and skeletogenesis. PLoS Genet. 2006;2(12):e216.

33- Balloni S, Calvi EM, Damiani F, Bistoni G, Calvitti M, Locci P, et al. Effects of titanium surface roughness on mesenchymal stem cell commitment and differentiation signaling. Int J Oral Maxillofac Implants. 2009;24(4):627-35.

34- Jonason JH, Xiao G, Zhang M, Xing L, Chen D. Post-translational regulation of Runx2 in bone and cartilage. J Dent Res. 2009;88(8):693-703.

35- Loi F, Córdova LA, Pajarinen J, Lin TH, Yao Z, Goodman SB. Inflammation, fracture and bone repair. Bone. 2016;86:119-30.

36- Mantovani A, Sica A, Sozzani S, Allavena P, Vecchi A, Locati M. The chemokine system in diverse forms of macrophage activation and polarization. Trends Immunol. 2004;25(12):677-86.

37- Östman PO, Wennerberg A, Albrektsson T. Immediate occlusal loading of NanoTite™ tapered implants: a prospective 1-year clinical and radiographic study. Clin Implant Dent Relat Res. 2013;15(6):809-18.

38- Albrektsson T, Eriksson AR, Friberg B, Lekholm U, Lindahl L, Nevins M, et al. Histologic investigations on 33 retrieved Nobelpharma implants. Clin Mater. 1993;12(1):1-9.

FIGURES AND LEGENDS

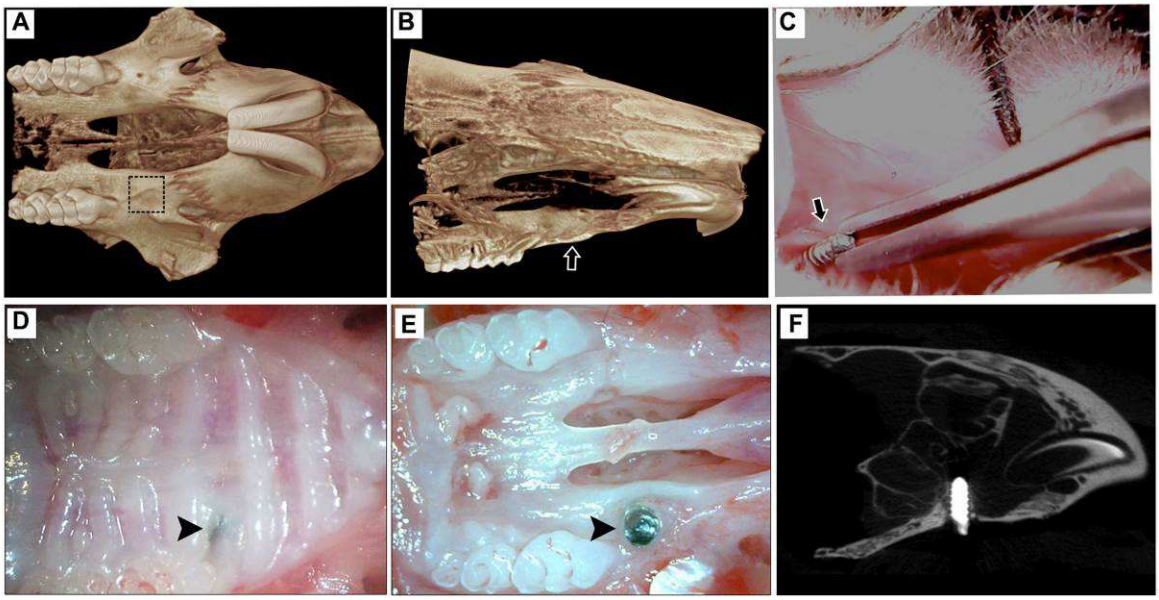

Figure 1- Experimental protocol for oral osseointegration in C57Bl/6 mice. A-B) Microtomographic tridimensional images from mouse maxilla bones showing the area of interest for screw implantation between the maxillary right first molar and the incisor (A-dotted square, B arrow); C) Ti-screw was screwed down in the implant bed (arrow), using a castroviejo Micro Needle Holder (Fine Science Tools®, British Columbia, CA); D) Macroscopic clinical view from oral mucosa covering the Ti-screw (arrow head) after day 7 post implantation and E) the same specimen without soft tissues post euthanasia; F) Representative microtomographic sagital slice from mouse maxilla at day 7 post Ti screw implantation

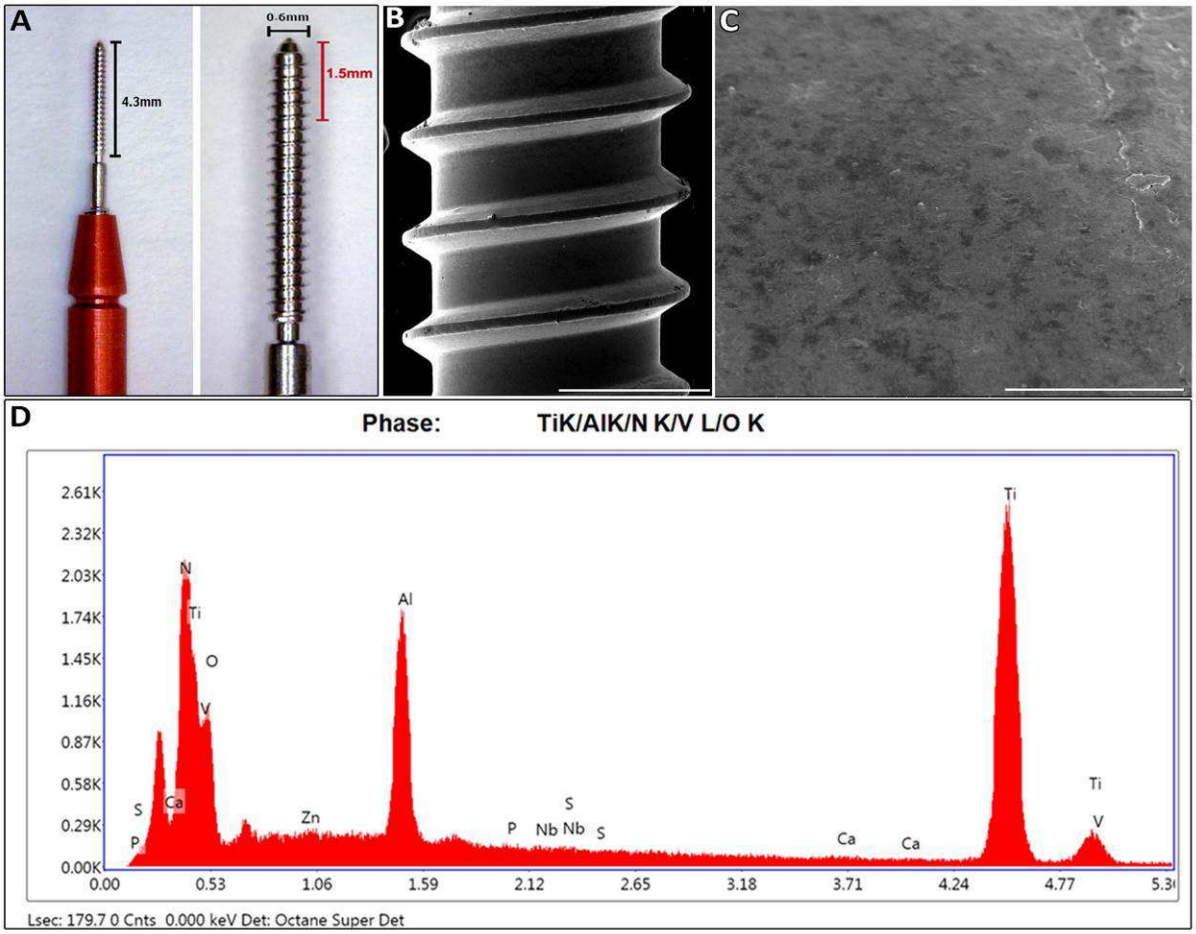

Figure 2- Ti screw used in oral osseintegration model in C57Bl/6 mice. A) Ti-screw (NTI-Kahla GmbH Rotary Dental Instruments, Kahla, Thüringen, Germany) of Ø0.6 mm was cut at length of 1.5 mm; B) Surface morphology of the body of titanium screw (385x magnification, scale bar 300 µm) and its (C) machined surface topography (5225x, scale bar 20 µm) from scanning electron microscopy (SEM) micrograph; D) Representative graph with surface composition from EDX analysis

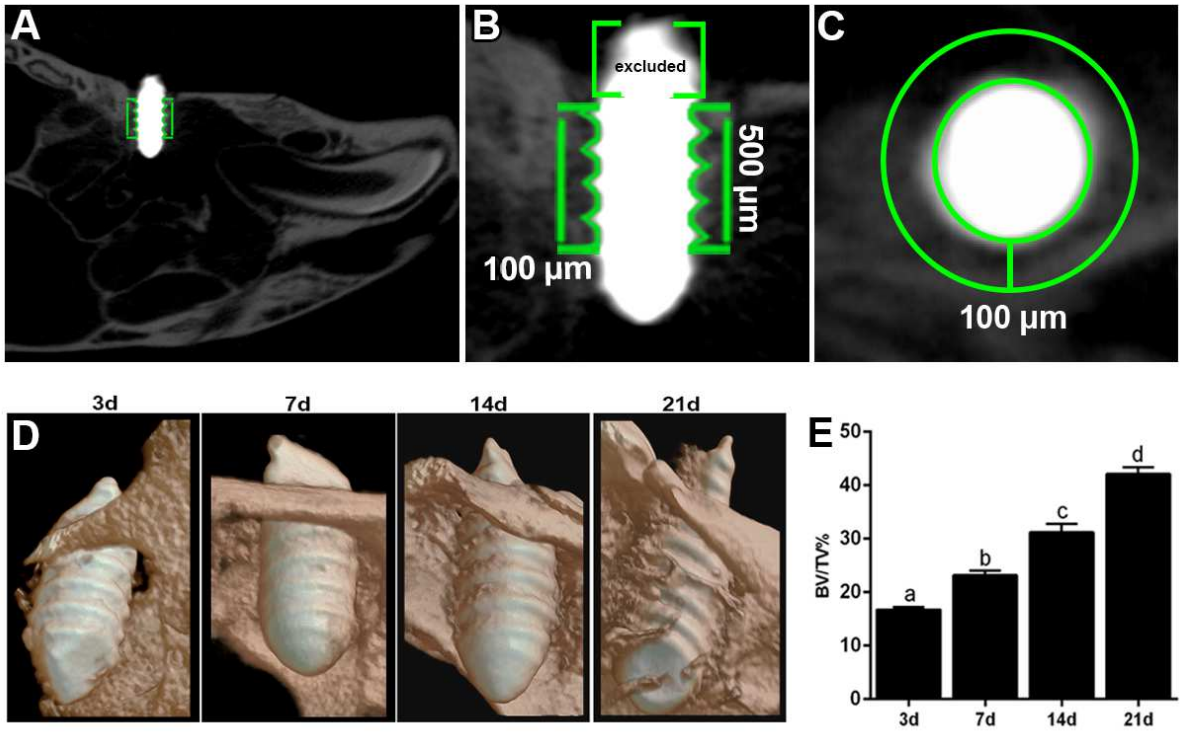

Figure 3- Micro-computed tomography (µCT) analysis of oral osseointegration model in C57Bl/6 mice. A) 2-D sagittal view of maxilla containing Ti screw for bone quantification; B) 2-D sagittal view with delimitation of a region of interest in the contact area of bone-to-implant, covering the region of contact bone threads throughout 500 µm of implant body and in the interface between the threads. The first 200 µm from the first third of Ti screw was excluded analysis in order to standardize the positioning for starting bone quantification in all specimens; (C) Axial view of Ti screw and bone inside the region of interest, considering 100 µm from the implant surface into the bone; D) Three-dimensional images were obtained with the CT-Vox software (Bruker Microct, Kontich, Belgium) along 3,7,14 and 21 days along osseointegration; E) Proportion of bone volume/tissue volume (BV/TV, %) in the interface bone-Ti were evaluated using CTAn software (Bruker Microct, Kontich, Belgium) to measure along days 3, 7, 14 and 21 post implantation. Different letters indicate significant statistical differences ($p<0.05$) among time periods

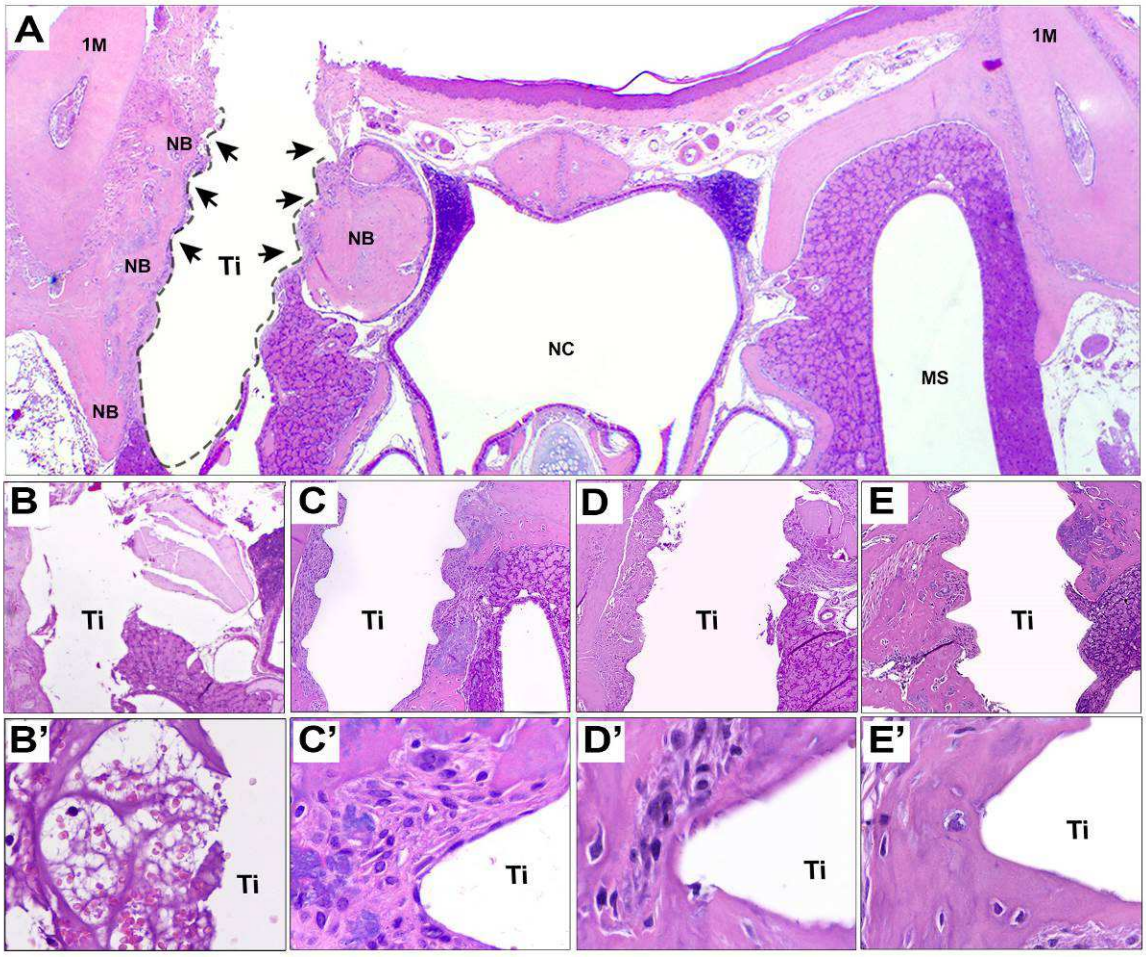

Figure 4- Hematoxylin & eosin (HE) staining of oral osseointegration model in C57Bl/6 mice and its histological aspects. A) Representative panoramic section of mouse maxilla and region of Ti implantation at day 14 post surgery. Arrows show threads space in direct contact with newly formed bone (NB); B-E') Chronology of oral osseointegration is observed throughout days 3 (B10x, B'40x), 7 (C10x, C'40x), 14 (D10x, D'40x) and 21 (E10x, E'40x). HE staining. NB= Newly formed bone. Ti= Ti screw space. 1M= first molar. NC= Nasal Cavity. MS= Maxillary sinus

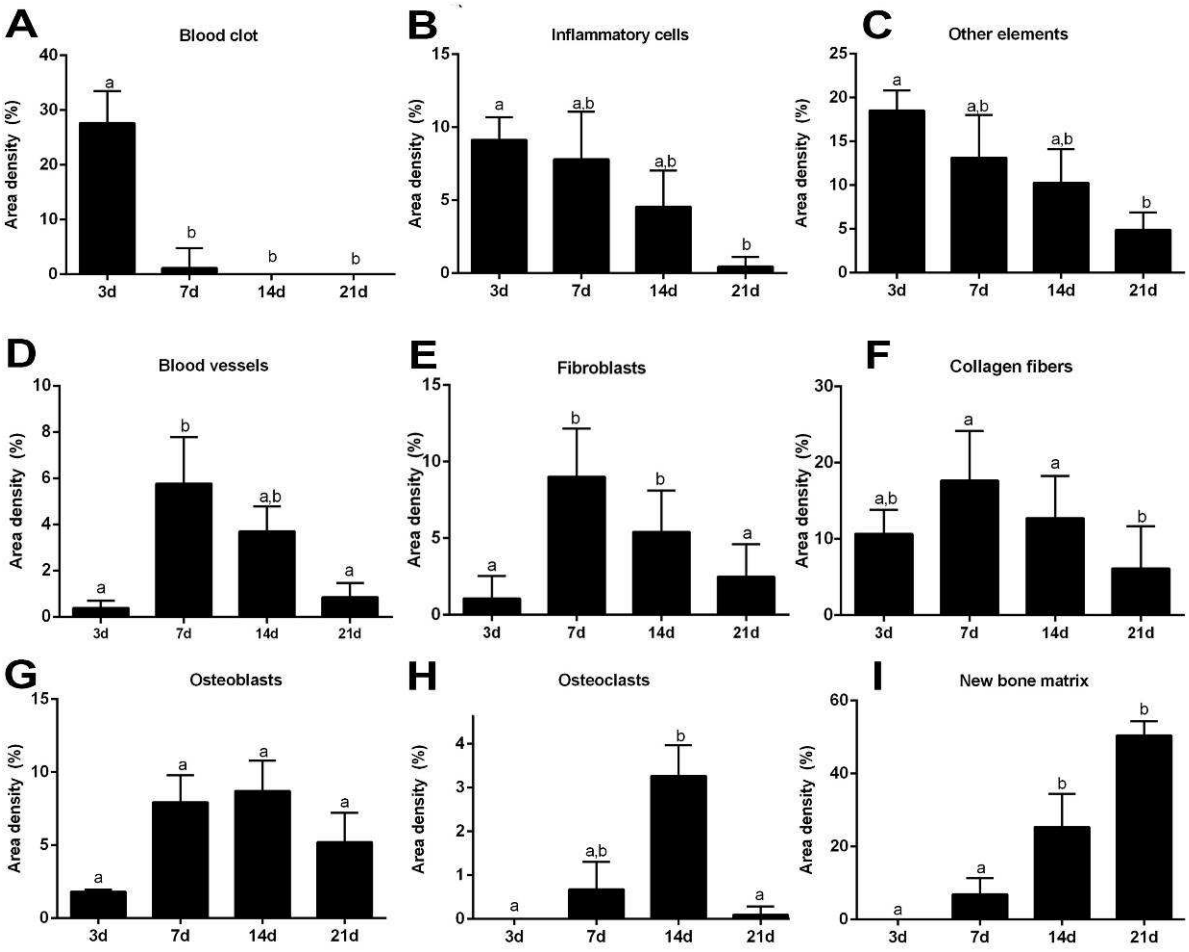

Figure 5- Histomorphometric analysis of healing components along oral osseintegration process in C57Bl/6-WT mice. Results are presented as the means (±SD) of area density for each component related to osseointegration process: (A) Blood clot; (B) Inflammatory cells; (C) Other elements; (D) Blood vessels; (E) Fibroblasts; (F) Collagen fibers; (G) osteoblasts; (H) Osteoclasts; (I) New bone matrix. Different letters indicate a statistically significant difference between the different time periods ($p<0.05$)

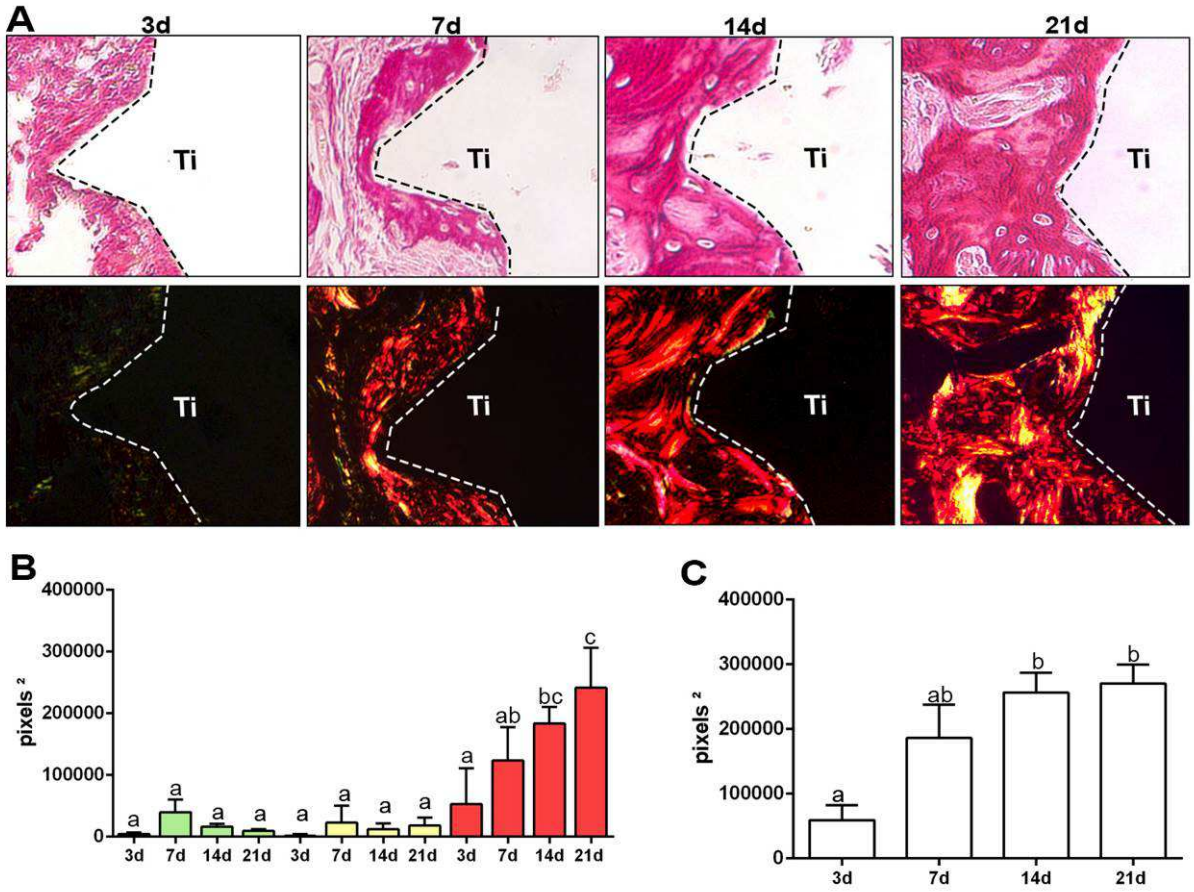

Figure 6- Birefringent fibers by picrosirius-polarization method in the oral osseointegration process. A) Representative sections from oral osseointegration process upon polarized and conventional light, to evaluate collagen fibers maturation along days 3, 7, 14 and 21 post-Ti-screw implantation. As visualized upon polarized light, green birefringence color indicates thin fibers; yellow and red colors at birefringence analysis indicate thick collagen fibers. Original magnification 40x; B-C) Intensity of birefringence measured from Image-analysis software (AxioVision, v. 4.8, Carl Zeiss Microscopy GmbH, Jena, Germany) to identify and quantify (B) area of collagen from each birefringence color (pixels 2) and total area of collagen fibers (pixel2) throughout experimental periods. Results are presented as the mean and SD of pixels2 for each color in the birefringence analysis. Different letters indicate a statistically significant difference (p 0.05) between the different time periods ($p<0.05$)

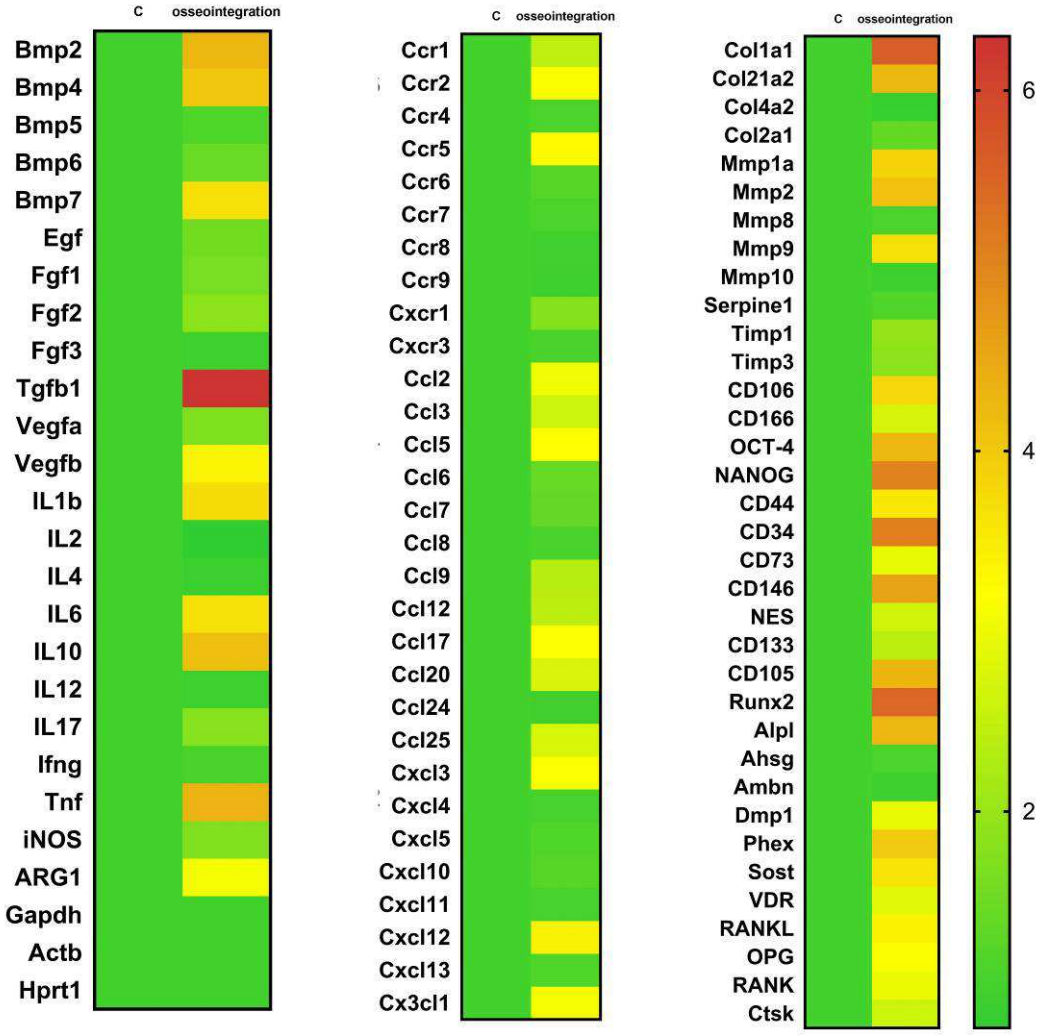

Figure 7- Gene expression patterns in the osseointegration process in C57Bl/6 mice. Molecular analysis of the gene expression patterns in the region of Ti screw implantation was comprised of an initial exploratory analysis by RealTimePCR array, considering a pool of samples from all the experimental time periods (3 d, 7 d, 14 d, 21 d). RealTimePCR array analysis was performed with the VIA7 system (Applied Biosystems Limited, Warrington,Cheshire, UK) using a customized qPCRarray comprised of the major targets from the Osteogenesis, Inflammatory Cytokines & Receptors and Wound Healing panels of the PCRarrayRT2 Profiler (SABiosciences/QIAGEN, Gaithersburg, MD, USA). Results are depicted as the fold increase change (and the standard deviation) in mRNA expression from triplicate measurements in relation to the control samples and normalized by internal housekeeping genes (GAPDH, HPRT, β-actin)

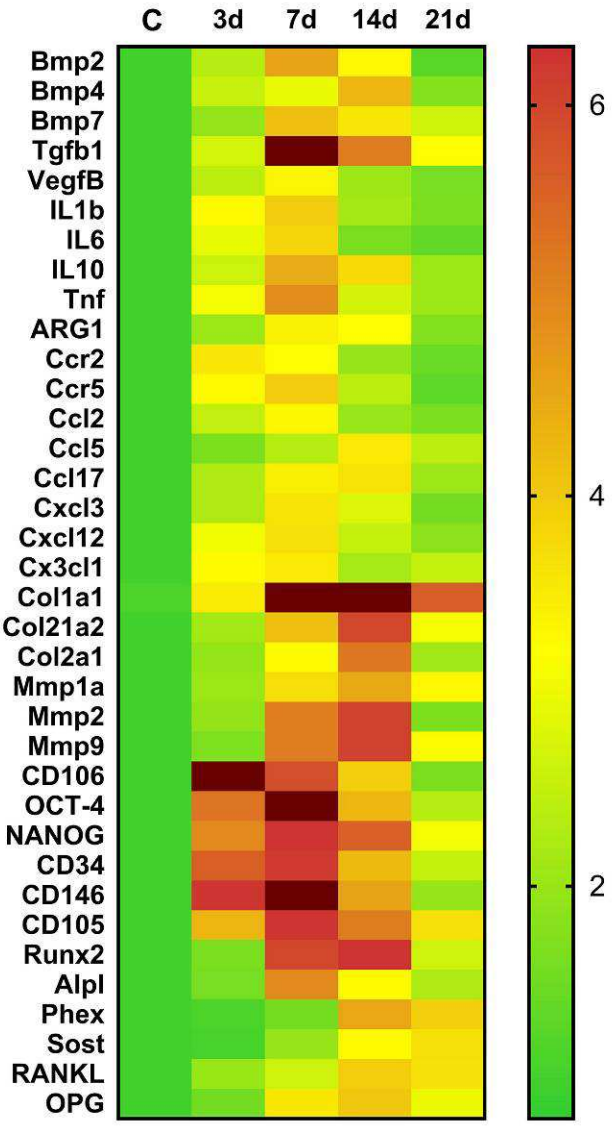

Figure 8- Kinetics of gene expression in the oral osseointegration process in C57Bl/6 mice. RealTimePCR array pooled from of all the experimental time periods was used to identify targets with a significant expression variation for their subsequent analyses in different time points along osseointegration process (0 h, 7 d, 14 d, 21 d). RealTimePCRarray analysis was performed with the VIA7 system (Applied Biosystems, Warrington, UK) using a customized qPCRarray comprised of the major targets from the Osteogenesis, Inflammatory Cytokines & Receptors and Wound Healing panels of the PCRarrayRT2 Profiler (SABiosciences/QIAGEN, Gaithersburg, MD, USA). Results are depicted as the fold increase change (and the standard deviation) in mRNA expression from triplicate measurements in relation to the control samples and normalized by internal housekeeping genes (GAPDH, HPRT, β-actin)

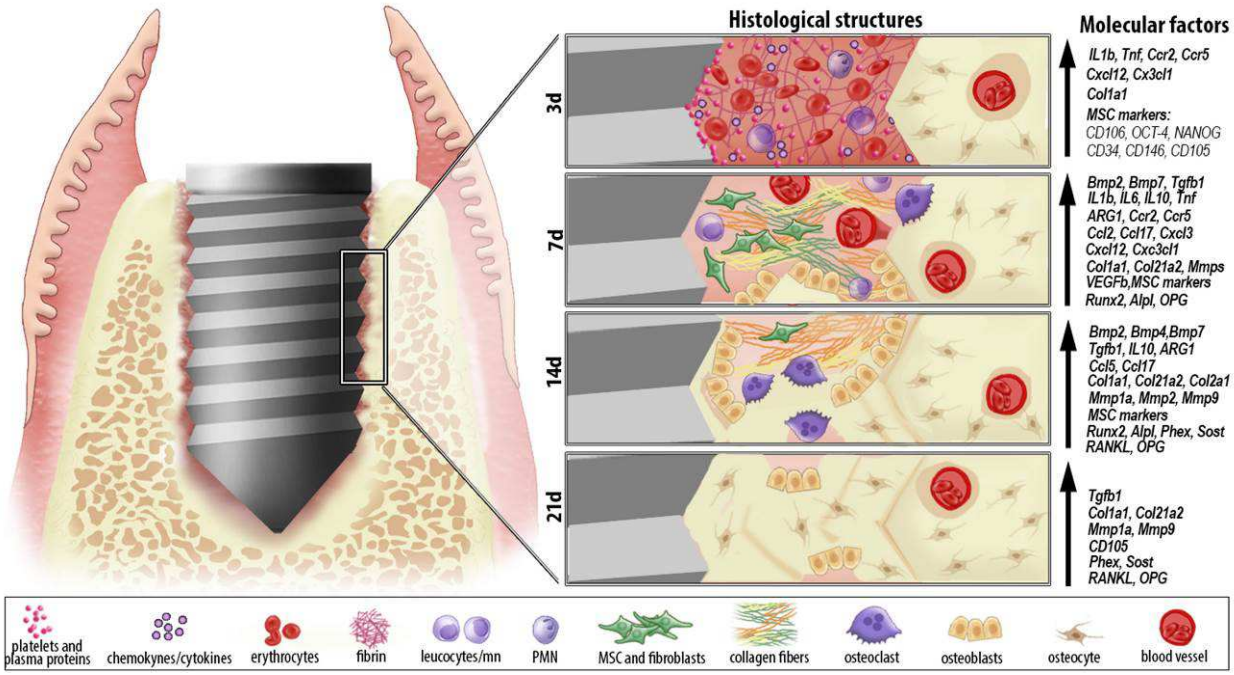

Figure 9- Graphic representation of microscopic and molecular events along oral osseointegration model in mice. Osseointegration process in oral cavity of C57Bl/6 exhibited overlapping phases along 3, 7, 14 and 21 days post Ti implantation. The healing process takes place with an organized blood clot an increased expression of growth factors (TGFb, VEGFb), immunological factors and MSC markers. Subsequently, a provisional granulation tissue is formed, with a high expression of growth factors and earlier osteogenic markers (BMPs, ALP and Runx2). Cytokines (TNF, IL6, IL1, IL10) chemokines (CXCL3, CCL2, CCL5, CC17, CXCL12 and CXC3CL1) and chemokine receptors (CCR2 and CCR5) regulate the infiltration of inflammatory cells and immune response. ARG1 (a M2 marker) is up regulated in implantation sites, indicating a predominance of a M2-type response for macrophages. At late time points (14 and 21 days), bone matrix is significantly increased, also followed by expression of Col1a1 and Col21a2. Remodeling/maturation process of bone is marked by a peak of MMPs, RANKL and OPG expression at 14 days, and an increased presence of osteoclasts. Finally, there is an intimate Ti/bone contact, with an expression of final osteoblast differentiation markers (PHEX, SOST)

2.2 ARTICLE 2 - Evidences of HGMB1 and RAGE contributions in the regenerative host response to Ti-based biomaterials. ACS Biomaterials Science & Engineering.

Abstract

DAMPs have been suggested to act as possible mediators of inflammation at biomaterial/host interface since theoretically they are released after the surgical trauma for biomaterial implantation. In this context, HMGB1 (the prototypic DAMP) and its cognate receptor RAGE, can comprise a potential regulatory axis for triggering inflammation and regulating healing outcomes. **Aim:** to investigate the impact of HMGB1 and RAGE on the constructive immune/inflammatory response and tissue repair around a classic biomaterial (Ti) implantation. **Material and Methods**: MC3T3-E1 and RAW 264.7 cells were treated with HMGB1 or HMGB1+ RAP (a RAGE inhibitor) for 48h, when the supernatants were collected for ELISA multiplex assays. C57Bl/6 mice received a subcutaneous implantation of Ti-disc (6AL-4V, Ø6mm, 2mm thick) and were euthanized at different time points, including early time points (0min, 5min, 4h, 24g, 48h, 72h, 7d) for DAMPs and acute inflammatory response analyses (microscopy, ELISA and PCR array) and healing time points (3d, 7d, 14d) for host response analysis (microscopy and PCR array). For host response analysis, mice were divided into 4 groups: Control; Vehicle (1.5% DMSO solution); GZA (Glycyrrhizic Acid) at a dosage of 200mg/Kg/day for HMGB1 inhibition; or RAP (RAGE Antagonistic Peptide) at a dosage of 4mg/Kg/day. **Results:** *In vivo* experiments showed different DAMPs (HMGB1, HSP60, HSP70, S100A9, Fibronectin and Biglycan) on Ti/host interface, mainly at early periods post Ti implantation. *In vitro* studies showed that antagonism of RAGE abolished the CCL5 production by MC3T3 cells and the HMGB1-induced VEGF production by RAW264-7 macrophages. Microscopic analysis *in vivo* evidenced a significant impairment of inflammatory response around Ti disc in GZA and RAP groups compared to the Control, with a drastic reduction of GR1+ cells and macrophages (F4/80+, CD80+, and CD206+ cells) in the implantation sites at 3 days. Molecular analysis demonstrated an up regulation of different immunological markers (e.g. TNFα, IL6, IL1b), including M2-type response markers (ARG1, IL10) in the control, while the same markers were significantly reduced in the GZA and RAP groups. At later time points, histological analysis evidenced a reduction of collagen deposition in GZA and RAP groups compared to the control. In parallel, the molecular analysis showed a drastic reduction of ECM formation and remodelling markers (e.g.Col1a2 and MMP9) in GZA and RAP groups compared to the control. **Conclusion:** Different DAMPs are released to the Ti/host interface. Particularly, the axis HMGB1/RAGE actively influences the inflammatory response post Ti implantation and the blockade of both molecules can negatively affect regenerative host response to Ti-based biomaterials.

Keywords: DAMP. HMGB1. RAGE. Macrophages. Regeneration. Titanium.

INTRODUCTION

Healing response associated with biomaterials grafting comprises an inflammatory immune reaction, which is theoretically triggered by host proteins adsorption at biomaterial surface [1]. Importantly, it has been suggested these initial events are directly connected to the positive outcome of classic permanent biomaterials used for osseointegration (such as Ti-based devices), supporting the recruitment of monocytes/macrophages and MSCs to the biomaterial surface [2-4]. In this context, the research on biomaterial science have focused on determinative interactions that take place in the biomaterial-cells/tissues interface, specially drawing the attention to the crosstalk between the first layer of protein deposited on biomaterial surface and macrophages, which is suggested to be critical for determining the biocompatibility and healing outcome [1, 5-7].

It is important to consider that host response to the biomaterial initiates immediately after the surgical procedure for a device implantation, which involves a tissue damage and consequently some damage degree of extracellular matrix (ECM), somatic cells and vasculature [8]. It has been postulated that mainly blood components, such as complement and clotting cascade proteins, adsorbs to the biomaterial surface and mediate the recognition of biomaterial by macrophages and MSCs [4, 9, 10]. In this context, the recent knowledge about ‘damage-associated molecular patterns’ (DAMPs) role on inflammatory immune response activation also brought to light the possible role of this molecules as host response triggers at the host/biomaterials interface [1, 11]. However, this putative interaction between DAMPs and biomaterials and its consequences for host response and healing outcomes remains unknown.

DAMPs are a family of endogenous molecules released upon cellular or tissue damage, which elicit the innate immune cells through binding to pattern recognition receptors (PRRs), such as Toll-like receptors (TLR2 and TLR4) and RAGE (receptor for advanced glycation endproducts); some of which are able to trigger inflammatory response by LPS (a pathogen associated molecular pattern – PAMP) binding [12-15]. DAMPs are contained in the nucleus (HMGB1), cytoplasm (e.g. S100A8 and S100A9, heat shock proteins in the exosomes [HSP60, HSP70])[15], and in the ECM (hialuronic acid, fibronectin and biglycan)[16]. Interestingly, the role of DAMPs have been investigated in a number destructive inflammatory conditions, such as tumour growth and local invasion, bone resorption during periodontitis, rheumatoid arthritis,

liver fibrosis and coagulopathies [11, 13, 14, 17-22]. However, recent studies have also suggested the potential contributions of DAMPs on tissue regeneration, especially HMBG1, the prototypical and most studied DAMP molecule [23].

HMBG1 has been associated with wound healing by stimulating the recruitment of inflammatory cells [24], MSCs migration, proliferation and differentiation [25], proliferation and collagen synthesis by osteoblasts [26, 27] and angiogenesis [24, 28]. Some studies demonstrate that HMGB1 can drastically change the pro-inflammatory cytokines production (e.g. TNFα, IL6) and expression of surface receptors (CD80/86) by macrophages, mainly via TLR receptors [29, 30]. Indeed, in pro-inflammatory conditions/environments, these interactions are suggested to facilitate M1-macrophage differentiation [31, 32], resembling the classic activation of macrophages by PAMPs (e.g. LPS) in infectious conditions. However, other studies suggest that immune system deals with DAMPs and PAMPs in a different way, discriminating molecules from damage and infection by means of additional receptors (such as CD24-Siglec G/10 receptor), which provide a fine-tunning to the signaling process resulting in different outcomes [33].

Importantly, among all receptors for HMGB1 binding, the most well established and studied is RAGE, which is not activated by PAMPs [34]. Interestingly, in the presence of complement protein C1q and RAGE, HMGB1 also can induce the differentiation of anti-inflammatory M2 phenotype [35]. Furthermore, the interaction of HMGB1 with already M2-polarized macrophages, has been associated with increased angiogenesis, in a manner RAGE dependent manner [36]. In this context, it is clear that the extracellular milieu and the predominance of specific receptors on cell surface, also influence the HMGB1 effects on cells.

At this point, understanding how HMGB1 and its receptors contribute to the biomaterial recognition and healing may provide important insight into the current knowledge of the role of host proteins in cell–biomaterial and tissue–biomaterial interactions. Thus, the aim of this study is to investigate the impact of HMGB1 or its cognate receptor RAGE on the constructive inflammatory response and tissue repair around a classic biomaterial (Ti) implantation.

MATERIALS AND METHODS

Material preparation. Machined 6AL-4V Titanium discs (Ti-discs) (Neodent®, Curitiba, PR, Brazil) of Ø6mm and 2mm thick from commercially pure grade 2 alloy were used for in vivo experiments. All Ti specimens were cleaned and autoclaved as previously describe [37].

Cell cultures. MC3T3-E1 subclone 4 (murine preosteoblasts) and RAW264-7 (murine macrophages) were purchased from American Type Culture Collection (ATCC®). MC3T3-E1 cells were cultured in Alpha Minimum Essential Media (αMEM) without ascorbic acid and supplemented with 10% Fetal Bovine Serum (FBS), while RAW264-7 cells were cultured in Dulbecco Minimal Essential Medium (DMEM) supplemented with 10% Fetal Bovine Serum (FBS). Both cell culture media were added with 1% penicillin-streptomycin (Gibco™) and 1% Fungiezone (Amphotericin B, HyClone™) antibiotics, 1% L-glutamine (Thermo Fisher®). During the culture period, cells were incubated at 37°C in a humidified atmosphere of 5% CO2, and the medium was replaced every 2 days. MC3T3-E1 confluent cells were sub-cultured through trypsinisation, with Gibco™ Trypsin-EDTA (0.5%). MC3T3-E1 osteoblasts and RAW264-7 macrophages were seeded in 96-well culture plates at a cell density of 1x104 cells per well for 24 hours. Then, both cell types were stimulated with HMGB1 (Recombinant Human HMGB1 Protein, R&D Systems, #1690-HMB-050) or LPS (Escherichia coli 0111:B4) as positive control. Additionally, one triplicate of each cell type was treated with a RAGE antagonist (RAP, Calbiochem, #553031) 10 minutes after HMGB1 addition. For MC3T3-E1 treatments were used 4µg/mL of LPS, 2 µg/mL of HMGB1 or 2 µg/mL of HMGB1+10 µM of RAP. For RAW264-7 treatments were used 8µg/mL of LPS, 1 µg/mL of HMGB1 or 1 µg/mL of HMGB1+40 µM of RAP. After 48h of treatment, the supernatants of MC3T3-E1 and RAW 264.7 cells were collected and then treated with protease inhibitor cocktail (cOmplete™, Sigma-Aldrich, #04693159001). The samples were subsequently analyzed by ELISA multiplex assays.

Cell secretion assays. The supernatants of MC3T3-E1 and RAW 264.7 cells were collected after all mentioned treatments and then treated with protease inhibitor cocktail (cOmplete™, Sigma-Aldrich, #04693159001). Subsequently, the supernatants were concentrated 5x using AMICON centrifugal filters units (3K) (Merck Millipore, MerckMillipore, Billerica, MA, USA). The average of protein

concentration was 1µg/µL. The cell response was evaluated by assaying the secreted concentration for a mouse inflammatory custom plate (MCYTOMAG 70K, MerckMillipore, Billerica, MA, USA) containing: IL6, TNFalpha, MCP1 (CCL2), RANTES (CCL5), VEGFa and LIX (IL8). The ELISA Multiplex assays were performed according to the manufacturer´s recommendations (MerckMillipore, Billerica, MA, USA).

Animals. Seventy five male wild-type mice (C57Bl/6) (10 weeks old, 25g of weight in average) were used in this study. The animals were bred in the animal facilities of University of Sao Paulo, School of Dentistry of Bauru (FOB/USP) and cared according the recommendations in the Guide for the Care and Use of Laboratory Animals of the National Institutes of Health[38]. Fifteen animals were used for very early experimental periods for kinetics of inflammatory cell migration on Ti-discs surface, considering 3 animals for each early time point post Ti-disc implantation (0 and 5min, 4, 24 and 48 hours), with no additional treatment. Sixty animals were used for analysis of host response to Ti-disc implantation at 3, 7 and 14 days and were distributed into 4 groups, containing 5 animals for each experimental period and group. Groups were divided according to each treatment: Control [with no treatment]; Vehicle [IP injection of 1.5% DMSO solution]; IP injection of Glycyrrhizic Acid (GZA, Sigma Aldrich) at a dosage of 200mg/Kg/day for HMGB1 inhibition [39]; or IP injection of RAGE antagonistic peptide (RAP, Merck Millipore, USA) at dosage of 4mg/Kg/day [17]. Vehicle or drugs were administered one day before the surgical procedure and were given until the end of experimental periods. The experimental protocol was approved by the local Institutional Committee for Animal Care and Use (#012/2014).

Animal experimentation protocol. For Ti implantation on subcutaneous tissue, mice were given intramuscular administration of 80 mg/kg of ketamine chloride (Dopalen®, Agribrands Brasil LTDA, Paulínia, SP, Brazil) and 160 mg/kg of xylazine chloride (Anasedan®, Agribrands Brasil LTDA, Paulínia, SP, Brazil) in the proportion 1:1, in order to provide anesthesia. Then, a longitudinal dermal incision was performed in the back of the animals, and a Ti-disc was implanted in each side. Immediately bellow Ti implantation, pockets were left empty for a sham sample, while the control region remained intact. Ti discs containing the surrounding tissues, as well sham and control samples were collected from the left side for microscopy (imunohistochemistry, H&E staining and collagen birefringence) and from the right

side for molecular analysis (ELISA assays and RealTimePCRarray analysis). Samples collected for microscopic analysis were fixed in PBS-buffered formalin (10%) solution (pH 7.2) for 24h at RT, then washed over-night in running water and processed for routine histology. Samples collected for molecular analysis were first rubbed on protein saver cards (Whatman®, Millipore Sigma, Darmstadt, Germany) for following ELISA assays of proteins adsorbed on Ti surface and the tissue surrounding the Ti was stored in RNAlater (Ambion, Austin, TX, USA) solutions for RealTimePCRarray [40].

In vivo DAMP adsorption assays. Ti-discs retrieved with surrounding tissues and the protein layer, as well the provisional matrix formed on Ti-disc surfaces, were absorbed onto five circles on Protein Saver cards (Whatman 903 Filter Protein Saver Cards, GE Healthcare Bio-Science Corp.; Whatman Biohazard). It was used one protein card, containing five circles/spots for sample collection, for each sample. The spots on the Protein Saver cards were dried overnight and storage at room temperature in foil barrier ziploc bags, following manufacture recommendations. Subsequently, the five spots from the cards impregnated with proteins were added to 24 wells plate containing 100-300 µl PBS-Tween and enzyme inhibitor (cOmplete™, Sigma-Aldrich, #04693159001). The plate was incubated at room temperature for 24hours on a rotary shaker to elute 100uL of samples from the spots. ELISA for DAMPs detection was performed according to the protocol recommended by the manufacturer, using a pool of five spots from each mice and the following kits (HMGB1 - LSBio, LifeSpan #LS-F4040; HSP60 - LSBio, LifeSpan #LS-F11128, HSP70 - R&DSystems #DYC1663E, Fibronectin - LSBio, LifeSpan, #LS-F3999,Biglycan - LSBio, LifeSpan #LS-F15938, S100A9 – LSBio, LifeSpan BioSciences #LS-F6833). The results were expressed as mean values ± standard deviation nanogram (ng) of protein per milligram of tissue, and represent values of duplicates of each sample obtained in two independent experiments.

Immunohistochemistry of subcutaneous tissue. After specimen's fixation with 4% paraformaldehyde, the Ti-discs from early time point (0 and 5min, 4, 24 and 48 hours) were removed from original implantation sites and the tissues were embedded in paraffin for sectioning at 4µm of thickness. Additionally, specimens from intact subcutaneous tissue were sectioned for a control. Three semi-serial sections (technical replicate) of each biological replicate were used for individual immunodetection of Ly6g-GR1 (sc-168490), F4/80 (a pan marker for murine

macrophages, sc-26642), CD80 (M1 macrophage, sc-376012) and CD206 (M2 macrophage, sc-34577), all primary antibodies purchased from Santa Cruz Biotechnology (Santa Cruz Biotechnology, Santa Cruz, CA, USA). Immunohistochemistry protocol was performed as previously described [40]. Briefly, histological sections were rehydrated and retrieved the antigens by boiling the histological slides in 10mM sodium citrate buffer pH6 for 30 minutes at 300°C. Subsequently, the sections were pre-incubated with 3% Hydrogen Peroxidase Block (Spring Bioscience Corporation, CA, USA) and subsequently incubated with 7% NFDM to block serum proteins. All primary antibodies were diluted at 1:100 in diluent solution for 1 hour at room temperature. Universal immuno-enzyme polymer method was used and sections were incubated in immunohistochemical staining reagent for 30 min at room temperature. The identification of antigen–antibody reaction was performed using 3-3'-diaminobenzidine (DAB) and counterstaining with Mayer's hematoxylin. Positive controls were performed by using mouse spleen for F4/80, CD80 and CD206 macrophages while Ly6g-Gr1+ were directly visualized in the inflamed tissues post surgical trauma.

Quantification of immunolabeled inflammatory cells. The analysis of immunolabeled cells (Gr1, F4/80, CD80, CD206) was performed by a single calibrated investigator using a 100x magnification, considering eight histological fields per section, comprising subcutaneous tissue surrounding the Ti-disc. Briefly, at least three samples (biological replicate) for each experimental period and strains were used for quantitative analysis and a total of 3 sections of each biological replicate were quantified. A grid image was superimposed on the histological photomicrographs, with 10 parallel lines and 100 points in a quadrangular area, by using Image J software (Version 1.51, National Institutes of Health, Bethesda, MD, USA). Only the points coincident with the immunolabeled cells were considered in cell counting and the mean for each section was obtained for statistical analysis.

Histological processing and staining. After 3, 7 and 14 days post Ti-disc implantation in control and all experimental groups (Vehicle, GZA and RAP), specimens were collected and fixed with 4% paraformaldehyde. After fixation, Ti-discs were removed from original implantation sites and the tissues were embedded in paraffin for sectioning at 4μm of thickness, following standardized procedures. Seven semi-serial sections (technical replicate) of each implanted area were stained

with hematoxylin-eosin (H&E) and four semi-serial (technical replicate) sections were stained with picrosirius red for subsequent birefringence analysis.

Histomorphometry. Eight histological fields per H&E stained section, comprising the region adjacent to the Ti-disc space were observed using a 100× immersion objective. Images from each histological field were captured with a Leica Imaging Software (LAX, Leica Microsystems Wetzlar GmbH, Wetzlar, Germany). A grid image was superimposed on the histological photomicrography, with 10 parallel lines and 100 points in a quadrangular area, by using Image J software (Version 1.51, National Institutes of Health, Bethesda, MD, USA) and the structures involving inflammatory and healing process surrounding the Ti-disc space (presence of blood clot, inflammatory cells, fibers, fibroblasts and blood vessels) were quantified. Only the points coincident with each structure were considered in the histomorphometry and the mean for each section was obtained for statistical analysis.

Birefringence analysis. Four histological fields picrosirius red sections were analyzed at 40x magnification through polarizing lens coupled to a binocular inverted microscope (Leica DM IRB/E, Leica Microsystems Wetzlar GmbH, Wetzlar, Germany) and images were captured with a Leica Imaging Software (LAX, Leica Microsystems Wetzlar GmbH, Wetzlar, Germany), as previously described [40]. Images from each field were captured and the measurements of each color spectrum (for green, yellow and red) for birefringent fibers were obtained using the software AxioVision 4.8 (Carl Zeiss Microscopy GmbH, Jena, Germany). Amount of each color pixels2 equivalent to the total area of each histological field was calculated and used in statistical analysis

Gene expression patterns of host response to Ti-disc implantation. Subcutaneous samples tissue of C57Bl/6 mice was retrieved after 3, 7 and 14 days post Ti-disc implantation of different experimental groups, weighed and homogenized. The extraction of total RNA from Ti-discs implantation sites into subcutaneous was performed with RNeasyFFPE kit (Qiagen Inc, Valencia, CA, USA) according to manufacturers' instructions. The integrity of RNA samples was checked by analyzing 1 mg of total RNA on 2100Bioanalyzer (Agilent Technologies, Santa Clara, CA, USA) according to manufacturers' instructions. Then, the complementary DNA was synthesized with 3 µg of RNA through a reverse transcription reaction (Superscript III, Invitrogen Corporation, Carlsbad, CA, USA). Viia7 instrument (LifeTechnologies, Carlsbad, CA, USA) was used for running the Real-time PCR

array plates, by using customized panels for "wound healing" (PAMM-121) and "inflammatory cytokines and receptors" (PAMM-011) for gene expression profiling. Subsequently, data were analyzed by RT2 Profiler PCR Array Data Analysis online software (SABiosciences, Frederick, MD, USA) for normalizing the initial geometric mean of three constitutive genes (GAPDH, ACTB, Hprt1), following normalizing the control group. Data were expressed as heat map fold change relative to the control group.

Statistical analysis. The statistical analysis was performed considering One-Way Analysis of variance (ANOVA) followed by Bonferroni's multiple comparison post-hoc test or student's t-test where applicable. For data which have not been in the distribution of normality Kruskal-Wallis test (followed by Dunn's test) and Mann-Whitney test were used The statistical significance of the experiment involving PCR Array was evaluated by the Mann-Whitney test, and the values tested for correction of Benjamini and Hochberg[41]. Values of $p<0.05$ were considered statistically significant. All statistical tests were performed with GraphPad Prism 5.0 software (GraphPad Software Inc., San Diego, CA, USA).

RESULTS AND DISCUSSION

Presence of DAMPs on Ti/host interface post subcutaneous Ti implantation

Our analysis confirmed that DAMPs characteristically released by cells (HMGB1, HSP60, HSP70, S100A9) and derived from ECM (Fibronectin and Biglycan) are found on Ti/host interface, mainly at very early periods post Ti implantation or post surgical trauma (Sham) (Figure 1). Importantly, HMGB1, S100A9, Biglycan and Fibronectin were similarly detected in both, Ti and Sham, demonstrating that the presence of Ti as a biomaterial in the surgical site does not cause the DAMPs release by itself. Indeed, such DAMPs are described to be released by different cell types after damage/stress [15] and from EMC [16].

Also, this result demonstrates that DAMPs are supposed to be adsorbed on Ti surface, constituting the protein layer with other molecules already described, such as blood proteins [42, 43].

DAMPs significantly decrease at day 7, as also demonstrated in the sham group. Thus, in regenerative conditions, DAMPs are present mainly in the initial inflammatory stages. As suggested by previous studies, this early host response to the biomaterial is activated by the contact of inflammatory cells and blood

components (coagulation proteins system and complement fragments) with exposed extracellular matrix proteins, as well the biomaterial surface by itself [1].

Role of HMGB1 and RAGE on MC3T3-E1 osteoblasts and RAW 264-7 macrophage cytokines and growth factors production.

When DAMPs are released in the tissue, these molecules bind in specific receptors on cells, such as TLR4 or RAGE, triggering the cellular/tissue/host response, which include the upregulation of pro-inflammatory cytokines, such as IL-6 and TNFα [12, 44]. Since macrophages and osteoblasts are the key players on Ti-mediated osseointegration, we evaluated the in vitro response of MC3T3-E1 osteoblasts and RAW-264.7 macrophages treated with HMGB1 (Figure 2). Importantly, these two cell lineages have been used for in vitro studies on osseointegration [45]. Additionally, an experimental group for both cell cultures was treated with RAP, an antagonist for RAGE, and after 10 minutes of RAP treatment, cells were treated with HMGB1. RAGE constitutes the prototypical receptor for HMGB1 and other DAMPs, such as S100A9, but not for PAMPs [15]. LPS was used as a positive control, since is a PAMP and can trigger a strong inflammatory response by binding in TLR4 [15].

The response of both cell types, MC3T3-E1 osteoblasts and RAW-264.7 macrophages was observed by the production of pro-inflammatory mediators (IL-6, CCL5, TNF-α), as well the growth factor VEGFa (Figure 2AB). CCL5 is a chemokine involved with macrophage recruitment to the chronic inflammation and has been positively correlated with high levels of M1-inflammatory macrophages markers (IL-6 and TNF-α) and macrophage survival in chronic inflammation [46]. Considering VEGF, besides its role as an angiogenic growth factor, it has also been supposed that it enhances osteoblasts differentiation and bone formation [47], as well as it induces M1 macrophages to shift to an M2 reparative phenotype [48].

In the present article, LPS induced high levels of IL6 and CCL5 by osteoblasts (Figure 2A), as expected by the activation of NFkB via TLR-MyD88-dependent mechanism [49]. Interestingly, HMBG1 it is also supposed to trigger an inflammatory response by treated cells, but in our results the stimulation of osteoblasts by HMGB1 did not induce increased levels of IL6 or CCL5. As previously observed, HMGB1 can cross-link TLR with another intracellular complex (CD24-Siglec G/10), which consequently brings SHP-1 to the signaling complex and inhibits NFkB activation;

thus, the immune system can be differently activated by PAMPs and DAMPs, even using the same PRRs [33]. Additionally, HMGB1 can activates other receptors which are not common for PAMPs, such as RAGE and CXCR4 [11]. In our results, the inhibition of RAGE completely abolished the CCL5 production by osteoblasts, evidencing the role of RAGE as a critical receptor for HMBG1 osteoblasts mediated responses [50] .

Considering the response of RAW264-7 macrophages, their activation with LPS increased the levels of IL6 and TNF-α compared to the control (Figure 2B). On the other hand, the stimulation with HMGB1 significantly increased the secretion of VEGFa. Additionally, RAGE antagonism significantly abolished the HMGB1-induced VEGF production by RAW264-7 macrophages. Since RAW264-7 is a cell line and not a primary culture, it is not possible to determine a state of M1/M2 polarization. However, the higher levels of HMGB1-induced VEGF, probably mediated by HMGB1/RAGE axis, indicate a potential contribution of this HMGB1 in the early stages of granulation tissue formation along tissue repair. Accordingly, it has been demonstrated that HMGB1 can significantly increase the VEGF production by M2-polarized macrophages via RAGE [36], also evidencing the importance of RAGE in macrophage responses and sterile inflammation.

Involvement of DAMPs on host response after subcutaneous Ti implantation

The inflammatory cell recruitment into the Ti disc could be triggered by the presence of DAMPs, also present in the Ti/host interface, such as HMGB1, S100A9, Fibronectin and Biglycan.

Considering the inflammatory cells recruited to the Ti-implantation sites, we evaluated the kinetics of GR1+, F4/80+, CD206+ and CD80+ cells migration along 0min, 5min, 4h, 24h, 48h, 72h and 7 days post implantation (the same stages involving protein layer formation and maturation) (Figure 3AB). Our study demonstrated migration of GR1+ cells with a peak at 48hours post Ti implantation and was drastically reduced by 3 to 7 days. In this context, GR1+ cells are mainly constituted by neutrophils, which are the first inflammatory cells recruited from adjacent blood vessels to the implantation site [1], followed by a sequence of events involving macrophages and other inflammatory cells. Accordingly, the cell number of F4/80+ macrophages peaked at 72hours post Ti-disc implantation, gradually decreasing at 7 days.

Macrophages are the major cells for determining biomaterial healing outcomes [51, 52], because of the range of biologically active mediators they are able to produce [30] and also because they determine the fate of functional or non-functional biomaterial incorporation [53, 54]. Indeed, macrophages are extremely plastic cells [30]; depending on the nature and balance of signalling molecules present in the microenvironment, they can reprogram their phenotypes toward a proinflammatory M1 profile or M2 profile. As mentioned, M1 pro-inflammatory macrophages is characterized by increased production of pro-inflammatory markers (TNF-α, IL-1, IL-6, IL-12, IL-23, IL17, INFγ), the expression of inducible NO synthase (iNOS), as well as surface markers, such as CD80/86. On the other hand, the cytokine profile for M2 anti-inflammatory macrophages includes increased production of IL-4, IL-10, TGFβ, VEGFa production, as well as expression of CD206, CD163, Arginase 1 (ARG1) [55]. These differential profiles are currently used as a tool to identify the distinctive macrophage population in tissue specimens [51, 56]. Importantly, the balance of macrophages quantities and states of polarization around implanted biomaterials is essential for determining a 'constructive' inflammatory and remodeling response or a persistent/foreign body response [51, 57].

In our results, while the CD80+ cells (suggested M1-phenotype) gradually decrease at 7 days, the CD206+ cells (suggested M2-phenotype) show a tendency of increasing along 3 and 7 days (Figure 3B) Interestingly, the mRNA levels of ARG1 (a M2 marker), as well IL10 and TGFβ, were significantly higher around Ti samples at 7 and 21days, compared to Sham group. These upregulation confirm the hypothesis of Ti as an immunomodulatory biomaterial, inducing a predominant M2-Type response along the resolution of inflammation [58, 59] (Figure 4).

Several growth factors (EGF, FGF1, FGF2, FGF3, FGF7, VGFa, TFGβ) and immunological markers (IL6, IL10, TNF, iNOS, ARG1, CXCL10, CXCL11, CXCL12) were positively regulated in the subcutaneous tissue repair in Ti and Sham samples compared to the control samples, evidencing their role along tissue healing. The molecules TGFβ, FGF1, FGF2 and VEGFa in Ti compared to the Sham samples. Indeed, TGFβ and FGFs are mainly related to regulation of cell proliferation and wound healing, while VEGFa contributes to the blood vessel development [45], reinforcing the beneficial role of Ti in mediating host response compared to sham group (Figure 4).

Host response kinetics to Ti-disc implantation disc under inhibition of HMGB1 (GZA 200mg/Kg/day) or RAGE (RAP 4mg/Kg/day).

After confirming the presence of DAMPs on Ti/host interface and their possible role on the modulation of M1/M2 macrophages, we next evaluated the host response post Ti-disc implantation under inhibition of HMGB1 or under the antagonism of RAGE. The subcutaneous tissue repair was evaluated at 3, 7 and 14 days post Ti-disc implantation by means of H&E description and histomorphometry (Figure 5), and birefringence (Figure 6). Molecular assays revealed target genes upregulated from pooled samples (Figure 7) and immunohistochemistry was performed to observe the impact of HMGB1 or RAGE inhibition on inflammatory cells. Besides the control group (animals with no treatment), mice were distributed into 3 experimental groups: Vehicle [IP injection of 1.5% DMSO solution]; IP injection of Glycyrrhizic Acid (GZA, Sigma Aldrich) at a dosage of 200mg/Kg/day for HMGB1 inhibition [39]; or IP injection of RAGE antagonistic peptide (RAP, Merck Millipore, USA) at dosage of 4mg/Kg/day [17]. All treatments were performed one day before the surgical Ti-disc implantation and were given until the end of experimental periods.

Control and vehicle treated mice showed a suitable blood clot formation and a slight inflammatory infiltrate at 3 days, followed by a dense connective tissue formation, containing fibroblasts and negligible quantities of inflammatory cells surrounding region of Ti-disc implantation at 14 days (Figure 5). Also, birefringence analysis revealed a yellow/red spectrum of collagen fibers surrounding the Ti at 14 days, consistent with an upregulation of Col1a2 and Col2a1 in Ti Control samples.

In parallel and in agreement with these microscopic results on Ti control, growth factors involved in cell proliferation (FGF1, FGF2, FGF3, TGFb1, EGF) and angiogenesis (VEGFa,b) [60-62] were significantly up-regulated in the Ti Control group compared to the endogenous control (Figure 7). Consistently, connective tissue growth factor (CTGF), integrins (ITGA-2,4,5) and vitronectin (VTN) are involved with cell adhesion and migration [60, 63]. Additionally, SERPINE 1, a molecule positively associated with cell adhesion and migration [60], was also up-regulated in the Ti control samples.

It is known that all these markers are positively related with tissue repair, and are in balance with ECM remodeling markers expression [40, 60, 62, 64] and cytokines [62]. Indeed, tissue healing and maturation of the ECM was also evidenced in Ti control by a high upregulation of ECM remodeling markers, such as

the matrix metalloproteinases (MMP1a, MMP2, MMP9) and their tissue inhibitors TIMPs (TIMP1, TIMP3), as well the protease cathepsin G (CTSG). Among the upregulated cytokines in Ti control samples, IL1β, IL6, TNF are up regulated in the inflammatory phase of healing [62], while IL10 contributes to the resolution of inflammation [65]. Also, CXCL10 and CXCL11 contribute to leucocytes recruitment, while CXCL12 is also related to angiogenesis, reepithelialization and MSC proliferation [62].

Importantly, the inhibition of HMGB1 by GZA treatment caused a disruption of blood clot formation at 3 days (arrow, Figure 5) and a persistence of blood clot and a decreased area density of blood vessels around Ti disc implantation at 7 days (Figure 5). Indeed, the HMGB1 is important to promote coagulation in vivo [20].

Similarly, both treatments, the inhibition of HMGB1 and the antagonism of RAGE, impaired the host response to the Ti disc by a decreased collagen fiber formation compared to the control and vehicle, but with no negative effects in the amount of fibroblasts (Figure 5,6).These results were compatible with decreased molecular analysis (Figure 7). Growth factors involved in cell proliferation, mainly for FGF family, were up regulated in GZA and RAP, such as in the Control group, while several ECM formation (Col1a2, Col2a1) and remodeling markers (MMP1a, MMP2, MMP9, , TIMP1, TIMP3, CTSG) were down regulated GZA and RAP compared to the control. Importantly, GZA and RAP group presented a downregulation of molecules involved in cell adhesion and migration (CTGF, VTN, ITGA2, ITGA4, ITGA5). All together, these results indicate a role of HMGB1 and RAGE on fibroblasts migration, differentiation and matrix deposition along tissue repair surrounding a classic biomaterial. Indeed, other studies have confirmed that HMGB1 is involved in MSCs migration, proliferation and differentiation [25], as well proliferation and collagen synthesis by osteoblasts [26, 27, 66], and some of these effects on MSCs have been related to the RAGE activation [66]. Also, the administration of RAP at the same dosage in this present study (4mg/Kg/day), significantly inhibit the cell migration in a subcutaneous model of tumor growth in mice and blocked NFκB activity induced by DAMPs, such as S100 and HMGB1 [17]. Despite of the differences and purposes between the cited study and the present study, it is clear that RAGE has an important role in triggering cell response mediated by DAMPs.

Despite of supposed effects of HMGB1 and RAGE on somatic cells (fibroblasts and MSCs), it is important to consider that HMGB1, such as other

DAMPs (S100A and fibronectin), were mainly detected at early phase post Ti disc implantation (1 day and 3 days) in this study, and can be responsible for triggering the inflammation (Figure 2).

Thus, the reduced tissue repair in GZA and RAP could be mainly associated with an ineffective inflammatory response caused by the inhibition of inflammatory signals induced by HMGB1 and RAGE. Definitely, the molecular analysis demonstrated a downregulation of chemokines (CXCL10, CXCL11) and pro-inflammatory cytokines (TNFα, IL6, IL1β). These results suggest that, HMGB1 and RAGE can play a role in triggering inflammation and leucocytes recruitment. In accordance with these results, the immuhistochemistry of GZA and RAP group also confirmed a drastic reduction of GR1+ cells and macrophages (F4/80+ cells, CD80+ cells, CD206+ cells) migration towards the implantation sites at 3 days post Ti implantation.

Finally, ARG1 (a marker for M2 macrophages) was upregulated in Ti control samples and downregulated in GZA and RAP. Considering the concept of constructive inflammatory environment, HMGB1 and RAGE seem to be involved with macrophage recruitment and their polarization states during the healing surrounding the biomaterial. In fact, the early stage of the host response around highly biocompatible biomaterials is mainly coordinate by immune/inflammatory cells and their mediators, when most of those cells are M1-macrophages, which efficiently switch from M1 to M2 phenotype along initial periods of inflammatory response, resulting in a suitable tissue repair [67].

Conclusion

In conclusion, this study demonstrated that different DAMPs from cellular (HMGB1, HSP60, HSP70, S100A9) and ECM (Fibronectin and Biglycan) origin are released at Ti implantation sites, and adhere to Ti surface. Importantly, HMGB1 and RAGE influence the host inflammatory immune response post biomaterial implantation in mice, and the blockade of both molecules negatively affect the subcutaneous tissue repair surrounding Ti discs.

Acknowledgments

The authors would like to thank Daniele Ceolin, Patricia Germino and Tania Cestari for their excellent technical assistance. This study was supported by grants (#2015/24637-3) and scholarships (#2014/09590-8, #2015/18162-2) from FAPESP.

References

1. Lin TH, Tamaki Y, Pajarinen J, Waters HA, Woo DK, Yao Z, et al. Chronic inflammation in biomaterial-induced periprosthetic osteolysis: NF-kappaB as a therapeutic target. Acta biomaterialia. 2014 Jan;10(1):1-10. PubMed PMID: 24090989. Pubmed Central PMCID: 3849197.

2. Davies JE. Understanding peri-implant endosseous healing. Journal of dental education. 2003 Aug;67(8):932-49. PubMed PMID: 12959168.

3. Trindade R, Albrektsson T, Wennerberg A. Current concepts for the biological basis of dental implants: foreign body equilibrium and osseointegration dynamics. Oral and maxillofacial surgery clinics of North America. 2015 May;27(2):175-83. PubMed PMID: 25753575.

4. Biguetti CC, Cavalla F, Silveira EM, Fonseca AC, Vieira AE, Tabanez AP, et al. Oral implant osseointegration model in C57Bl/6 mice: microtomographic, histological, histomorphometric and molecular characterization. Journal of Applied Oral Science. 2018 January 2018:1-24 (*in press*)

5. Corradetti B, Taraballi F, Corbo C, Cabrera F, Pandolfi L, Minardi S, et al. Immune tuning scaffold for the local induction of a pro-regenerative environment. Scientific reports. 2017 Dec 5;7(1):17030. PubMed PMID: 29208986. Pubmed Central PMCID: 5717048.

6.Anderson JM, Rodriguez A, Chang DT. Foreign body reaction to biomaterials. Seminars in immunology. 2008 Apr;20(2):86-100. PubMed PMID: 18162407. Pubmed Central PMCID: 2327202.

7.Brodbeck WG, Colton E, Anderson JM. Effects of adsorbed heat labile serum proteins and fibrinogen on adhesion and apoptosis of monocytes/macrophages on biomaterials. Journal of materials science Materials in medicine. 2003 Aug;14(8):671-5. PubMed PMID: 15348406.

8.Gorbet MB, Sefton MV. Biomaterial-associated thrombosis: roles of coagulation factors, complement, platelets and leukocytes. Biomaterials. 2004 Nov;25(26):5681-703. PubMed PMID: 15147815.

9.Ekdahl KN, Lambris JD, Elwing H, Ricklin D, Nilsson PH, Teramura Y, et al. Innate immunity activation on biomaterial surfaces: a mechanistic model and coping strategies. Advanced drug delivery reviews. 2011 Sep 16;63(12):1042-50. PubMed PMID: 21771620. Pubmed Central PMCID: 3166435.

10.Andersson J, Ekdahl KN, Lambris JD, Nilsson B. Binding of C3 fragments on top f adsorbed plasma proteins during complement activation on a model biomaterial surface. Biomaterials. 2005 May;26(13):1477-85. PubMed PMID: 15522749.

11.Kang R, Chen R, Zhang Q, Hou W, Wu S, Cao L, et al. HMGB1 in health and disease. Molecular aspects of medicine. 2014 Dec;40:1-116. PubMed PMID: 25010388. Pubmed Central PMCID: 4254084.

12.Fukata M, Vamadevan AS, Abreu MT. Toll-like receptors (TLRs) and Nod-like receptors (NLRs) in inflammatory disorders. Seminars in immunology. 2009 Aug;21(4):242-53. PubMed PMID: 19748439.

13.Land WG. The Role of Damage-Associated Molecular Patterns (DAMPs) in Human Diseases: Part II: DAMPs as diagnostics, prognostics and therapeutics in clinical medicine. Sultan Qaboos University medical journal. 2015 May;15(2):e157-70. PubMed PMID: 26052447. Pubmed Central PMCID: 4450777.

14.Sims GP, Rowe DC, Rietdijk ST, Herbst R, Coyle AJ. HMGB1 and RAGE in inflammation and cancer. Annual review of immunology. 2010;28:367-88. PubMed PMID: 20192808.

15.Tang D, Kang R, Coyne CB, Zeh HJ, Lotze MT. PAMPs and DAMPs: signal 0s that spur autophagy and immunity. Immunological reviews. 2012 Sep;249(1):158-75. PubMed PMID: 22889221. Pubmed Central PMCID: 3662247.

16.Anders HJ, Schaefer L. Beyond tissue injury-damage-associated molecular patterns, toll-like receptors, and inflammasomes also drive regeneration and fibrosis. Journal of the American Society of Nephrology : JASN. 2014 Jul;25(7):1387-400. PubMed PMID: 24762401. Pubmed Central PMCID: 4073442.

17.Arumugam T, Ramachandran V, Gomez SB, Schmidt AM, Logsdon CD. S100P-derived RAGE antagonistic peptide reduces tumor growth and metastasis. Clinical cancer research : an official journal of the American Association for Cancer Research. 2012 Aug 15;18(16):4356-64. PubMed PMID: 22718861. Pubmed Central PMCID: 3845828.

18. Charoonpatrapong K, Shah R, Robling AG, Alvarez M, Clapp DW, Chen S, et al. HMGB1 expression and release by bone cells. Journal of cellular physiology. 2006 May;207(2):480-90. PubMed PMID: 16419037.

19. Feng L, Xue D, Chen E, Zhang W, Gao X, Yu J, et al. HMGB1 promotes the secretion of multiple cytokines and potentiates the osteogenic differentiation of mesenchymal stem cells through the Ras/MAPK signaling pathway. Experimental and therapeutic medicine. 2016 Dec;12(6):3941-7. PubMed PMID: 28105126. Pubmed Central PMCID: 5228376.

20. Ito T, Kawahara K, Nakamura T, Yamada S, Nakamura T, Abeyama K, et al. High-mobility group box 1 protein promotes development of microvascular thrombosis in rats. Journal of thrombosis and haemostasis : JTH. 2007 Jan;5(1):109-16. PubMed PMID: 17239166.

21.Liu L, Deng J, Ji Q, Peng B. High-mobility Group Box 1 Is Associated with the Inflammatory Infiltration and Alveolar Bone Destruction in Rats Experimental Periapical Lesions. Journal of endodontics. 2017 Jun;43(6):964-9. PubMed PMID: 28389071.

22.Park SY, Lee SW, Kim HY, Lee WS, Hong KW, Kim CD. HMGB1 induces angiogenesis in rheumatoid arthritis via HIF-1alpha activation. European journal of immunology. 2015 Apr;45(4):1216-27. PubMed PMID: 25545169.

23.Yang H, Wang H, Chavan SS, Andersson U. High Mobility Group Box Protein 1 (HMGB1): The Prototypical Endogenous Danger Molecule. Molecular medicine. 2015 Oct 27;21 Suppl 1:S6-S12. PubMed PMID: 26605648. Pubmed Central PMCID: 4661054.

24.Schiraldi M, Raucci A, Munoz LM, Livoti E, Celona B, Venereau E, et al. HMGB1 promotes recruitment of inflammatory cells to damaged tissues by forming a complex with CXCL12 and signaling via CXCR4. The Journal of experimental medicine. 2012 Mar 12;209(3):551-63. PubMed PMID: 22370717. Pubmed Central PMCID: 3302219.

25.Degryse B, Bonaldi T, Scaffidi P, Muller S, Resnati M, Sanvito F, et al. The high mobility group (HMG) boxes of the nuclear protein HMG1 induce chemotaxis and cytoskeleton reorganization in rat smooth muscle cells. The Journal of cell biology. 2001 Mar 19;152(6):1197-206. PubMed PMID: 11257120. Pubmed Central PMCID: 2199202.

26.Li MJ, Li F, Xu J, Liu YD, Hu T, Chen JT. rhHMGB1 drives osteoblast migration in a TLR2/TLR4- and NF-kappaB-dependent manner. Bioscience reports. 2016 Jan 7;36(1):e00300. PubMed PMID: 26744383. Pubmed Central PMCID: 4759610.

27.Li Q, Yu B, Yang P. Hypoxia-induced HMGB1 in would tissues promotes the osteoblast cell proliferation via activating ERK/JNK signaling. International journal of clinical and experimental medicine. 2015;8(9):15087-97. PubMed PMID: 26628992. Pubmed Central PMCID: 4658881.

28.Schlueter C, Weber H, Meyer B, Rogalla P, Roser K, Hauke S, et al. Angiogenetic signaling through hypoxia: HMGB1: an angiogenetic switch molecule. The American journal of pathology. 2005 Apr;166(4):1259-63. PubMed PMID: 15793304. Pubmed Central PMCID: 1602384.

29.Martinez FO, Sica A, Mantovani A, Locati M. Macrophage activation and polarization. Frontiers in bioscience : a journal and virtual library. 2008 Jan 1;13:453-61. PubMed PMID: 17981560.

30.Mosser DM, Edwards JP. Exploring the full spectrum of macrophage activation. Nature reviews Immunology. 2008 Dec;8(12):958-69. PubMed PMID: 19029990. Pubmed Central PMCID: 2724991.

31.Su Z, Zhang P, Yu Y, Lu H, Liu Y, Ni P, et al. HMGB1 Facilitated Macrophage Reprogramming towards a Proinflammatory M1-like Phenotype in Experimental Autoimmune Myocarditis Development. Scientific reports. 2016 Feb 22;6:21884. PubMed PMID: 26899795. Pubmed Central PMCID: 4761996.

32.Schaper F, de Leeuw K, Horst G, Bootsma H, Limburg PC, Heeringa P, et al. High mobility group box 1 skews macrophage polarization and negatively influences phagocytosis of apoptotic cells. Rheumatology. 2016 Dec;55(12):2260-70. PubMed PMID: 27632996.

33.Liu Y, Chen GY, Zheng P. CD24-Siglec G/10 discriminates danger- from pathogen-associated molecular patterns. Trends in immunology. 2009 Dec;30(12):557-61. PubMed PMID: WOS:000272643500001. English.

34.Rauvala H, Rouhiainen A. RAGE as a receptor of HMGB1 (Amphoterin): roles in health and disease. Current molecular medicine. 2007 Dec;7(8):725-34. PubMed PMID: 18331230.

35.Son M, Porat A, He M, Suurmond J, Santiago-Schwarz F, Andersson U, et al. C1q and HMGB1 reciprocally regulate human macrophage polarization. Blood. 2016 Nov 3;128(18):2218-28. PubMed PMID: 27683415. Pubmed Central PMCID: 5095756.

36.Rojas A, Delgado-Lopez F, Perez-Castro R, Gonzalez I, Romero J, Rojas I, et al. HMGB1 enhances the protumoral activities of M2 macrophages by a RAGE-dependent mechanism. Tumor Biol. 2016 Mar;37(3):3321-9. PubMed PMID: WOS:000374903500056. English.

37.Abuna RP, Stringhetta-Garcia CT, Fiori LP, Dornelles RC, Rosa AL, Beloti MM. Aging impairs osteoblast differentiation of mesenchymal stem cells grown on titanium by favoring adipogenesis. Journal of applied oral science : revista FOB. 2016 Jul-Aug;24(4):376-82. PubMed PMID: 27556209. Pubmed Central PMCID: 4990367.

38.Institute of Laboratory Animal Resources (U.S.). Committee on Care and Use of Laboratory Animals. Guide for the care and use of laboratory animals. NIH publication. Bethesda, Md.: U.S. Dept. of Health and Human Services, Public Health Service. p. v.

39.Lau A, Wang S, Liu W, Haig A, Zhang ZX, Jevnikar AM. Glycyrrhizic acid ameliorates HMGB1-mediated cell death and inflammation after renal ischemia reperfusion injury. American journal of nephrology. 2014;40(1):84-95. PubMed PMID: 25059568.

40.Vieira AE, Repeke CE, Ferreira Junior Sde B, Colavite PM, Biguetti CC, Oliveira RC, et al. Intramembranous bone healing process subsequent to tooth extraction in mice: micro-computed tomography, histomorphometric and molecular characterization. PloS one. 2015;10(5):e0128021. PubMed PMID: 26023920. Pubmed Central PMCID: 4449187.

41.Benjamini YH, Y. Controlling the False Discovery Rate: A Practical and Powerful Approach to Multiple Testing. Journal of the Royal Statistical Society Series B (Methodological). 1995;1(57):11.

42.Vishwakarma A, Bhise NS, Evangelista MB, Rouwkema J, Dokmeci MR, Ghaemmaghami AM, et al. Engineering Immunomodulatory Biomaterials To Tune the Inflammatory Response. Trends in biotechnology. 2016 Jun;34(6):470-82. PubMed PMID: 27138899.

43.Othman Z, Cillero Pastor B, van Rijt S, Habibovic P. Understanding interactions between biomaterials and biological systems using proteomics. Biomaterials. 2018 Mar 12;167:191-204. PubMed PMID: 29571054.

44.Kokkola R, Andersson A, Mullins G, Ostberg T, Treutiger CJ, Arnold B, et al. RAGE is the major receptor for the proinflammatory activity of HMGB1 in rodent macrophages. Scandinavian journal of immunology. 2005 Jan;61(1):1-9. PubMed PMID: 15644117.

45.Thalji G, Cooper LF. Molecular assessment of osseointegration in vitro: a review of current literature. The International journal of oral & maxillofacial implants. 2014 Mar-Apr;29(2):e171-99. PubMed PMID: 24683582.

46.Keophiphath M, Rouault C, Divoux A, Clement K, Lacasa D. CCL5 promotes macrophage recruitment and survival in human adipose tissue. Arteriosclerosis, thrombosis, and vascular biology. 2010 Jan;30(1):39-45. PubMed PMID: 19893003.

47.Hu K, Olsen BR. Osteoblast-derived VEGF regulates osteoblast differentiation and bone formation during bone repair. The Journal of clinical investigation. 2016 Feb;126(2):509-26. PubMed PMID: 26731472. Pubmed Central PMCID: 4731163.

48.Wheeler KC, Jena MK, Pradhan BS, Nayak N, Das S, Hsu CD, et al. VEGF may contribute to macrophage recruitment and M2 polarization in the decidua. PloS one. 2018;13(1):e0191040. PubMed PMID: 29324807. Pubmed Central PMCID: 5764356.

49.Souza JA, Rossa C, Jr., Garlet GP, Nogueira AV, Cirelli JA. Modulation of host cell signaling pathways as a therapeutic approach in periodontal disease. Journal of applied oral science : revista FOB. 2012 Mar-Apr;20(2):128-38. PubMed PMID: 22666826. Pubmed Central PMCID: 3894752.

50. Zhou Z, Xiong WC. RAGE and its ligands in bone metabolism. Frontiers in bioscience. 2011 Jan 1;3:768-76. PubMed PMID: 21196410. Pubmed Central PMCID: 3815642.

51.Ogle ME, Segar CE, Sridhar S, Botchwey EA. Monocytes and macrophages in tissue repair: Implications for immunoregenerative biomaterial design. Experimental biology and medicine. 2016 May;241(10):1084-97. PubMed PMID: 27229903. Pubmed Central PMCID: 4898192.

52.Spiller KL, Anfang RR, Spiller KJ, Ng J, Nakazawa KR, Daulton JW, et al. The role of macrophage phenotype in vascularization of tissue engineering scaffolds. Biomaterials. 2014 May;35(15):4477-88. PubMed PMID: 24589361. Pubmed Central PMCID: 4000280.

53.Taraballi F, Corradetti B, Minardi S, Powel S, Cabrera F, Van Eps JL, et al. Biomimetic collagenous scaffold to tune inflammation by targeting macrophages. Journal of tissue engineering. 2016 Jan-Dec;7:2041731415624667. PubMed PMID: 26977285. Pubmed Central PMCID: 4765811.

54.Ma QL, Zhao LZ, Liu RR, Jin BQ, Song W, Wang Y, et al. Improved implant osseointegration of a nanostructured titanium surface via mediation of macrophage polarization. Biomaterials. 2014 Dec;35(37):9853-67. PubMed PMID: 25201737.

55.Antonios JK, Yao Z, Li C, Rao AJ, Goodman SB. Macrophage polarization in response to wear particles in vitro. Cellular & molecular immunology. 2013 Nov;10(6):471-82. PubMed PMID: 24013843. Pubmed Central PMCID: 3818297.

56.Das A, Sinha M, Datta S, Abas M, Chaffee S, Sen CK, et al. Monocyte and macrophage plasticity in tissue repair and regeneration. The American journal of pathology. 2015 Oct;185(10):2596-606. PubMed PMID: 26118749. Pubmed Central PMCID: 4607753.

57.Anderson DE, Bean JF, Holt NE, Keel JC, Bouxsein ML. Computed tomography-based muscle attenuation and electrical impedance myography as indicators of trunk muscle strength independent of muscle size in older adults. American journal of physical medicine & rehabilitation. 2014 Jul;93(7):553-61. PubMed PMID: 24508931. Pubmed Central PMCID: 4105177.

58.Thalji GN, Nares S, Cooper LF. Early molecular assessment of osseointegration in humans. Clinical oral implants research. 2014 Nov;25(11):1273-85. PubMed PMID: 24118318.

59.Albrektsson T, Dahlin C, Jemt T, Sennerby L, Turri A, Wennerberg A. Is marginal bone loss around oral implants the result of a provoked foreign body reaction? Clinical implant dentistry and related research. 2014 Apr;16(2):155-65. PubMed PMID: 24004092.

60.Garlet GP, Horwat R, Ray HL, Jr., Garlet TP, Silveira EM, Campanelli AP, et al. Expression analysis of wound healing genes in human periapical granulomas of progressive and stable nature. Journal of endodontics. 2012 Feb;38(2):185-90. PubMed PMID: 22244633.

61. Bodnar RJ. Epidermal Growth Factor and Epidermal Growth Factor Receptor: The Yin and Yang in the Treatment of Cutaneous Wounds and Cancer. Advances in wound care. 2013 Feb;2(1):24-9. PubMed PMID: 24527320. Pubmed Central PMCID: 3840479.

62. Barrientos S, Stojadinovic O, Golinko MS, Brem H, Tomic-Canic M. Growth factors and cytokines in wound healing. Wound repair and regeneration : official publication of the Wound Healing Society [and] the European Tissue Repair Society. 2008 Sep-Oct;16(5):585-601. PubMed PMID: 19128254.

63. Song Y, Kim JS, Choi EK, Kim J, Kim KM, Seo HR. TGF-beta-independent CTGF induction regulates cell adhesion mediated drug resistance by increasing collagen I in HCC. Oncotarget. 2017 Mar 28;8(13):21650-62. PubMed PMID: 28423507. Pubmed Central PMCID: 5400613.

64. Barrientos S, Brem H, Stojadinovic O, Tomic-Canic M. Clinical application of growth factors and cytokines in wound healing. Wound repair and regeneration : official publication of the Wound Healing Society [and] the European Tissue Repair Society. 2014 Sep-Oct;22(5):569-78. PubMed PMID: 24942811. Pubmed Central PMCID: 4812574.

65. Claudino M, Trombone AP, Cardoso CR, Ferreira SB, Jr., Martins W, Jr., Assis GF, et al. The broad effects of the functional IL-10 promoter-592 polymorphism: modulation of IL-10, TIMP-3, and OPG expression and their association with periodontal disease outcome. Journal of leukocyte biology. 2008 Dec;84(6):1565-73. PubMed PMID: 18725394.

66. Lin F, Zhang W, Xue D, Zhu T, Li J, Chen E, et al. Signaling pathways involved in the effects of HMGB1 on mesenchymal stem cell migration and osteoblastic differentiation. International journal of molecular medicine. 2016 Mar;37(3):789-97. PubMed PMID: 26846297.

67. Sridharan R, Cameron AR, Kelly DJ, Kearney CJ, O'Brien FJ. Biomaterial based modulation of macrophage polarization: a review and suggested design principles. Mater Today. 2015 Jul-Aug;18(6):313-25. PubMed PMID: WOS:000356184700013. English.

FIGURES AND LEGENDS

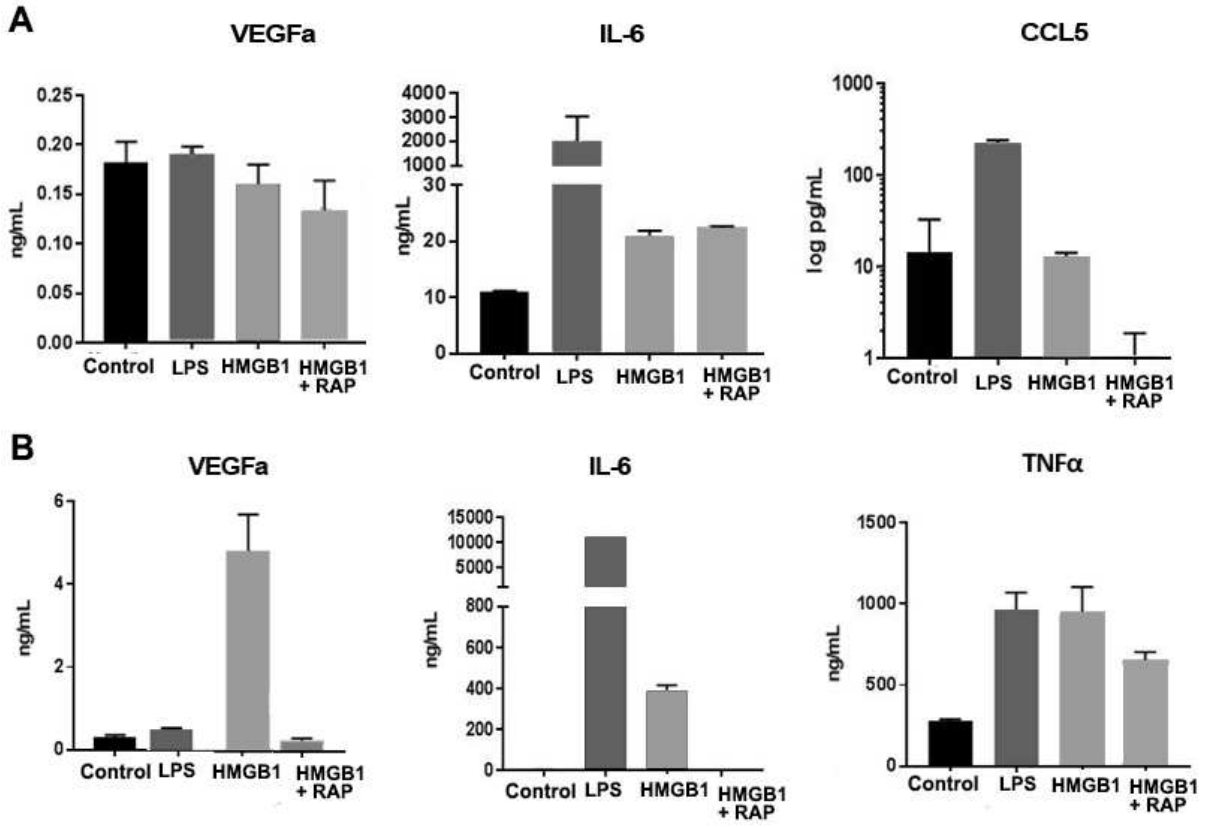

Figure 1. Protein concentrations from MC3T3-E1 and RAW 264-7 cells treated with HMGB1 in presence or absence of RAGE antagonist. A) VEGFa, IL-6 and CCL5 protein concentrations were analyzed from supernatant of MC3T3 cells using ELISA multiplex assay. B) VEGFa, IL-6 and TNFα protein concentrations were analyzed from supernatant of RAW264.7 cells using ELISA multiplex assay. Briefly, MC3T3-E1 or RAW 264.7 cells were seeded *in* 96-well culture plates at a cell density of $1x10^4$ cells/well for 24 hour until treatment with LPS (positive control), HMGB1 or HMGB1+RAP. The supernatant were collected after 48h of treatment. Columns = triplicates from 3 independent experiments; bars, ±SD. *$p < 0.05$ vs Control.

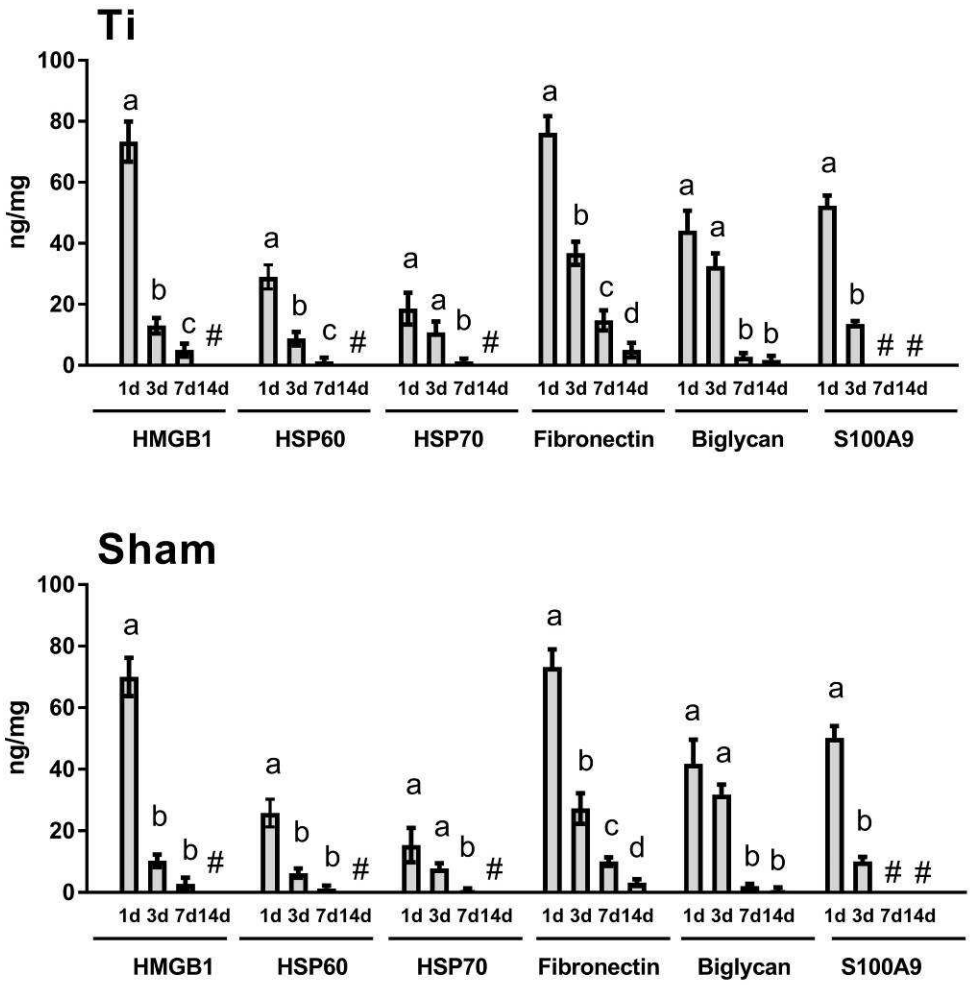

Figure 2. DAMPs adsorption on Ti/host interface and in the inflammatory exudates post subcutaneous Ti implantation. Ti-discs were retrieved from subcutaneous tissue of C57Bl/6 mice after 1d, 3d, 7d and 14d post implantation. Surrounding tissues and the protein layer Ti-disc samples were absorbed onto five circles on Protein Saver cards (Whatman 903 Filter Protein Saver Cards, GE Healthcare Bio-Science Corp.; Whatman Biohazard). Sham samples were submitted to the same treatment and were used for comparison. After elution and treatment of proteins, ELISA for DAMPs detection was performed according to the manufacturer, using a pool of five spots from each mice and the following kits (HMGB1 - LSBio, LifeSpan #LS-F4040; HSP60 - LSBio, LifeSpan #LS-F11128, HSP70 - R&DSystems #DYC1663E, Fibronectin - LSBio, LifeSpan, #LS-F3999,Biglycan - LSBio, LifeSpan #LS-F15938, S100A9 – LSBio, LifeSpan BioSciences #LS-F6833). The results were expressed as mean values ± standard deviation nanogram (ng) of protein per milligram of tissue, and represent values of duplicates of each sample obtained in two independent experiments. Different letters indicate significant differences in each time point ($p<0.05$)

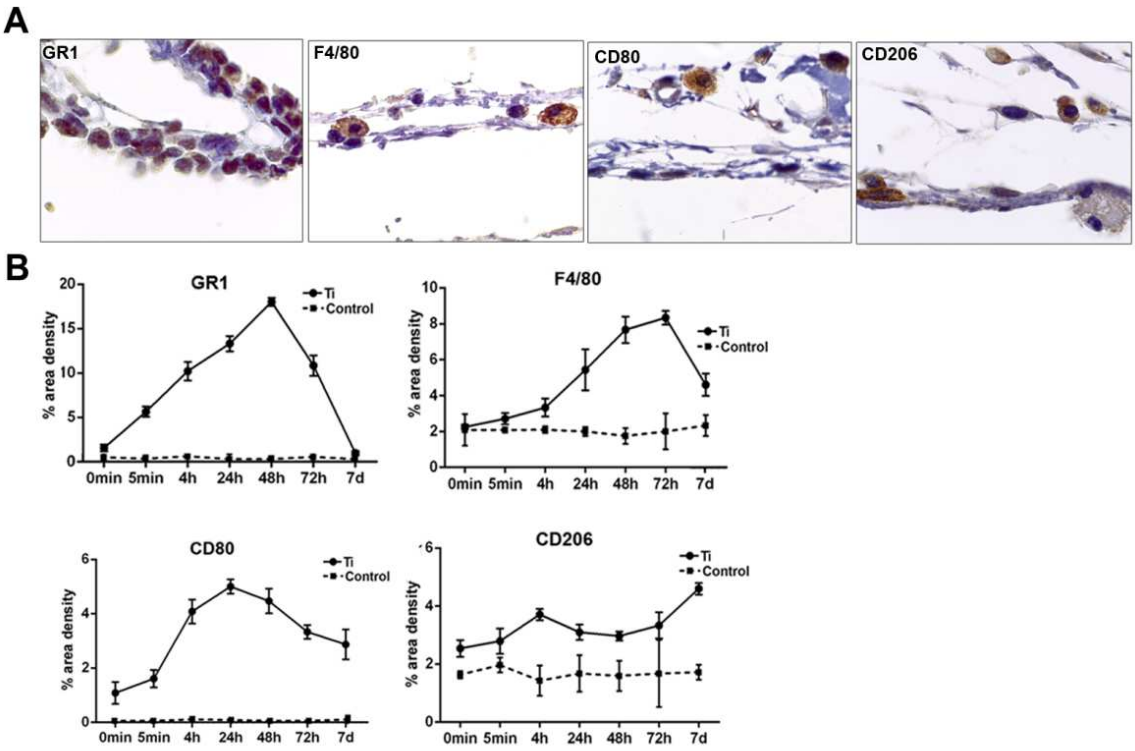

Figure 3. Inflammatory cells recruited to the Ti disc implantation sites in early periods post Ti implantation in subcutaneous tissue of C57Bl/6 mice. Mice received Ti-disc implantation in the subcutaneous tissue and were divided into 7 early experimental periods: 0min, 5min, 4h, 24h, 48h, 72h and 7 days. (A) Representative sections from subcutaneous tissue surrounding the Ti disc at 72 hours post Ti disc implantation with immunolabeling for GR1+, F4/80+, CD80+ and CD206+ cells (40x magnification). (B) Quantitative analysis of GR1+, F4/80+, CD80+ and CD206+ cells post Ti disc implantation. Results are presented as mean and SD.

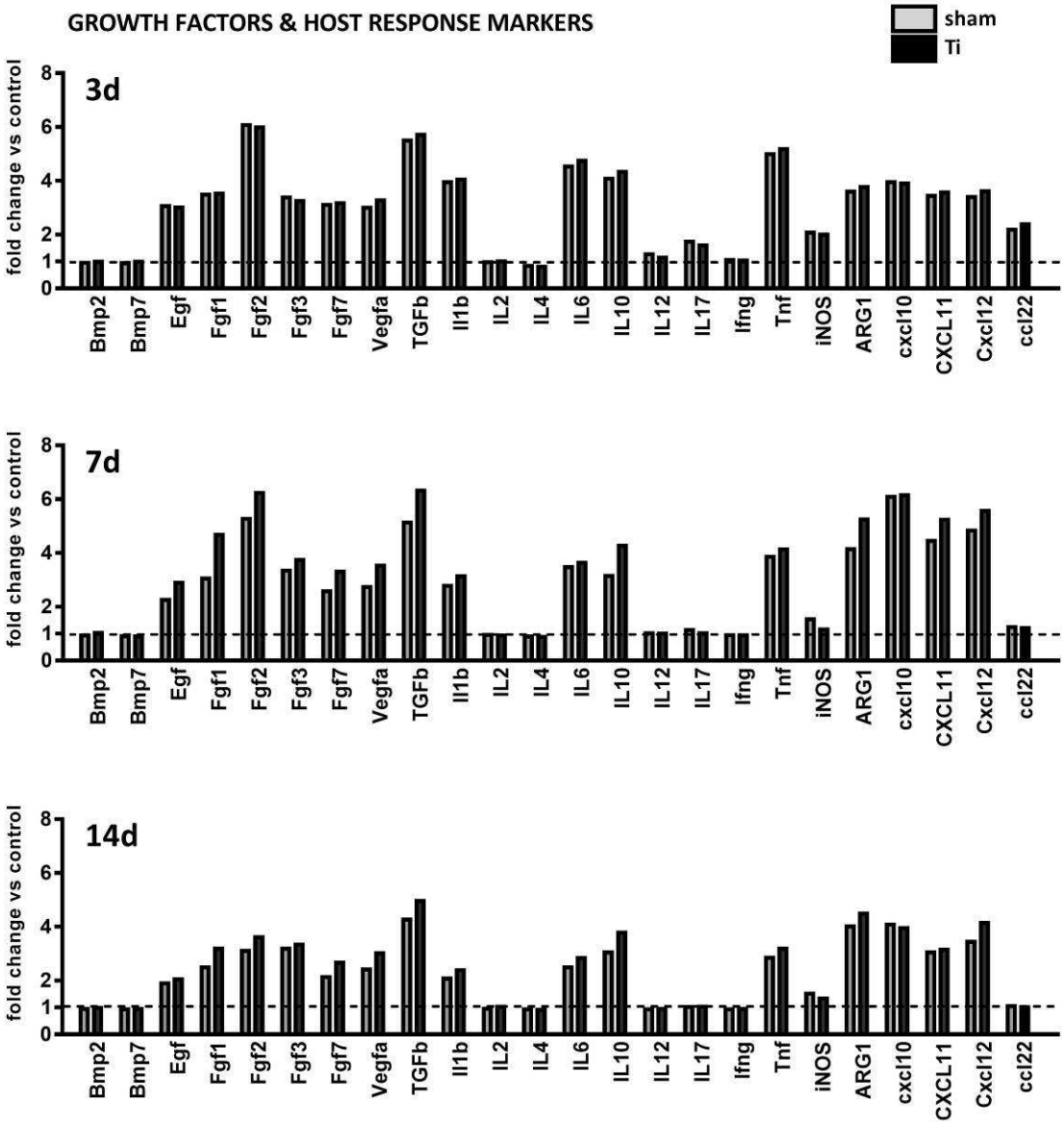

Figure 4. Kinetics of gene expression patterns post subcutaneous Ti disc implantation in C57Bl/6 mice. Mice received Ti-disc implantation in the subcutaneous tissue and were divided into 3 experimental periods: 3d, 7d and 14d. Immediately down from Ti implantation, pockets were left empty for a sham sample, while the control region remained intact. Ti discs containing the surrounding tissues, as well sham and control samples were collected in RNAlater solution (Ambion, Austin, TX, USA) and then homogenized for extraction of total RNA according to manufacturers' instructions (RNeasyFFPE kit, Qiagen Inc, Valencia, CA, USA). Gene expression was performed by using exploratory analysis by RealTimePCR array, with the VIA7 system (Applied Biosystems, Warrington, UK) and a customized qPCRarray comprised of the major targets (Inflammatory Cytokines & Receptors and Wound Healing panels) of the PCRarrayRT2 Profiler (SABiosciences/QIAGEN).

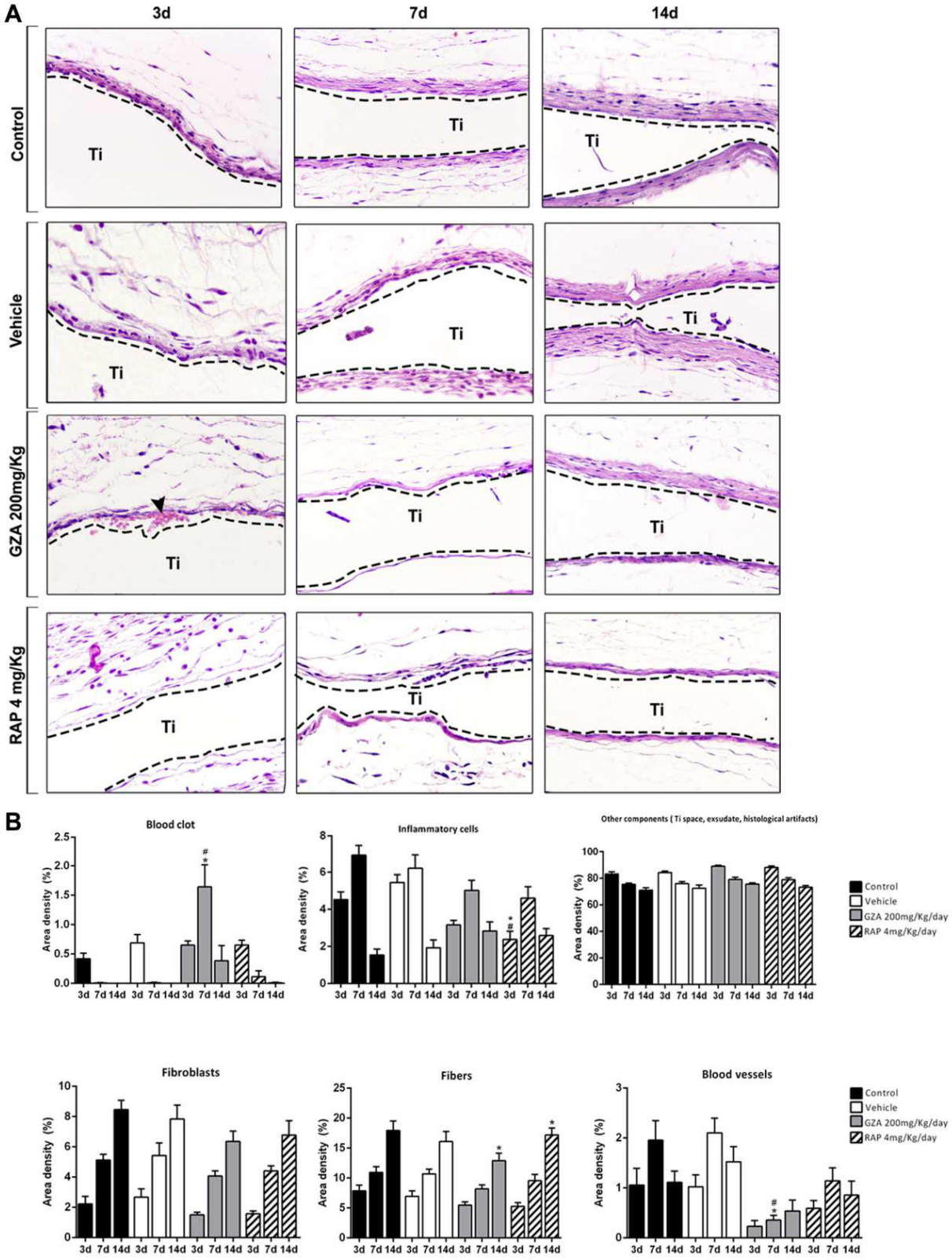
A
3d
7d
14d
Control
Vehicle
GZA 200mg/Kg
RAP 4 mg/Kg
Ti
B
Blood clot
Inflammatory cells
Other components (Ti space, exsudate, histological artifacts)
Fibroblasts
Fibers
Blood vessels
Area density (%)
3d 7d 14d
Control
Vehicle
GZA 200mg/Kg/day
RAP 4mg/Kg/day

Figure 5. Histophatological and histomorphometric analysis of subcutaneous tissue post implantation of Ti-disc in C57Bl/6 mice treated with HMGB1 inhibitor or RAGE antagonist. Mice received Ti-disc implantation in the subcutaneous tissue and were divided in according to each treatment: Control (C group, with no treatment); Vehicle (1.5% DMSO solution); Glycyrrhizic Acid at a dosage of 200mg/Kg/day (GZA group); or RAGE antagonistic peptide at dosage of 4mg/Kg/day (RAP group). Vehicle or drugs were administered one day before the surgical procedure and were given until the end of experimental periods (3d, 7d and 14d). (A) Comparative morphology of the healing phases post Ti disc implantation for each group, stained with H&E (40 x magnification). (B) Results from histomorphometry of healing parameters (blood clot, inflammatory cells, fibroblasts, fibers and blood vessels) are presented as the mean of area density for each structure measured in each examined group. Symbols indicates a statistically significant difference ($p<0.05$) between experimental groups (GZA and RAP) vs Control* and experimental groups vs Vehicle$^{\#}$ at the same time point.

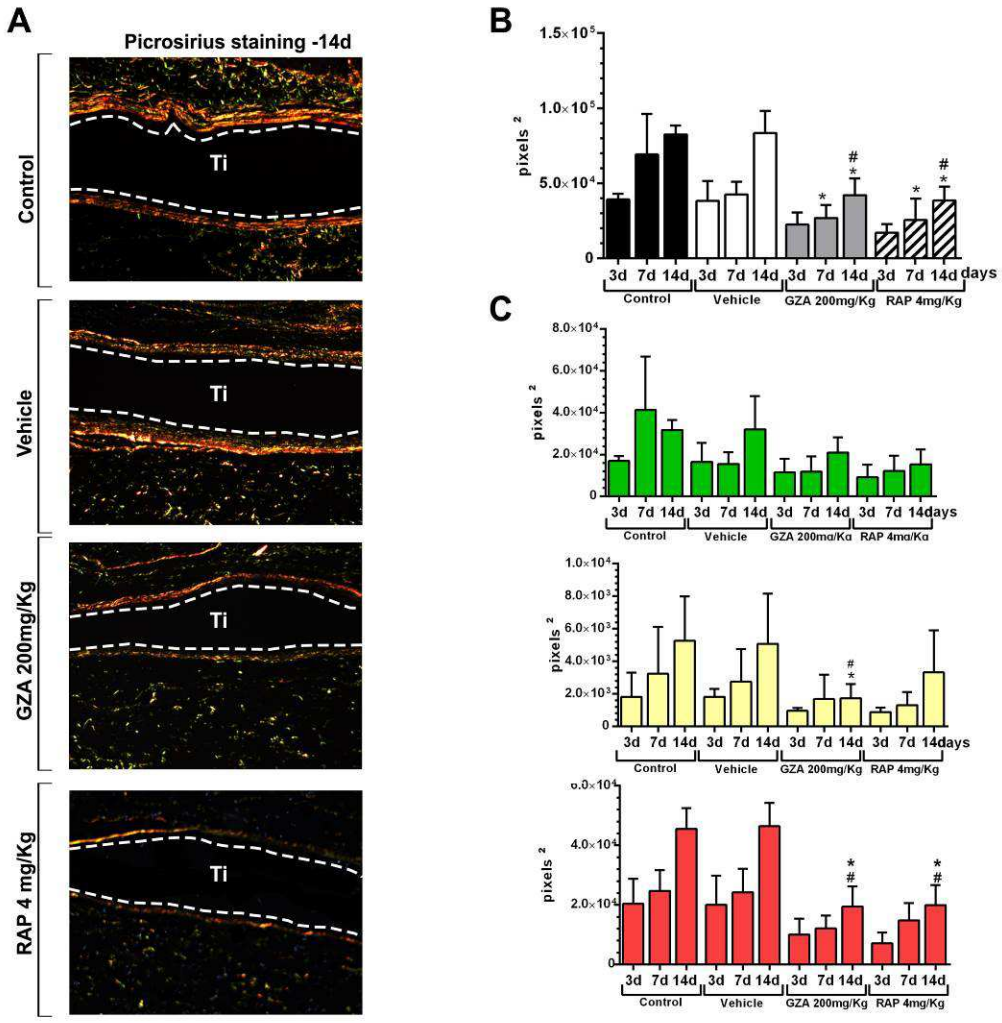

Figure 6. Birefringence analysis of collagen fibers post Ti-disc implantation in C57Bl/6 mice treated with HMGB1 inhibitor or RAGE antagonist. Mice received Ti-disc implantation in the subcutaneous tissue and were divided in according to each treatment: Control (C group, with no treatment); Vehicle (1.5% DMSO solution); Glycyrrhizic Acid at a dosage of 200mg/Kg/day (GZA group); or RAGE antagonistic peptide at dosage of 4mg/Kg/day (RAP group). Vehicle or drugs were administered one day before the surgical procedure and were given until the end of experimental periods (3d, 7d and 14d). (A) Representative sections from subcutaneous tissue surrounding Ti implantation space at 14 days post Ti implantation. Staining: Picrosirius red upon polarized (20x magnification). Green birefringence color indicates thin fibers, while yellow and red colors indicate thick collagen fibers. (B) Intensity of birefringence performed using image-analysis software (AxioVision, v. 4.8, CarlZeiss) for total area of collagen fibers (pixels 2) and (C) from each color spectrum. Results are presented as mean and SD of pixels2. Symbols indicates a statistically significant difference ($p<0.05$) between experimental groups (GZA and RAP) vs Control* and experimental groups vs Vehicle# at the same time point.

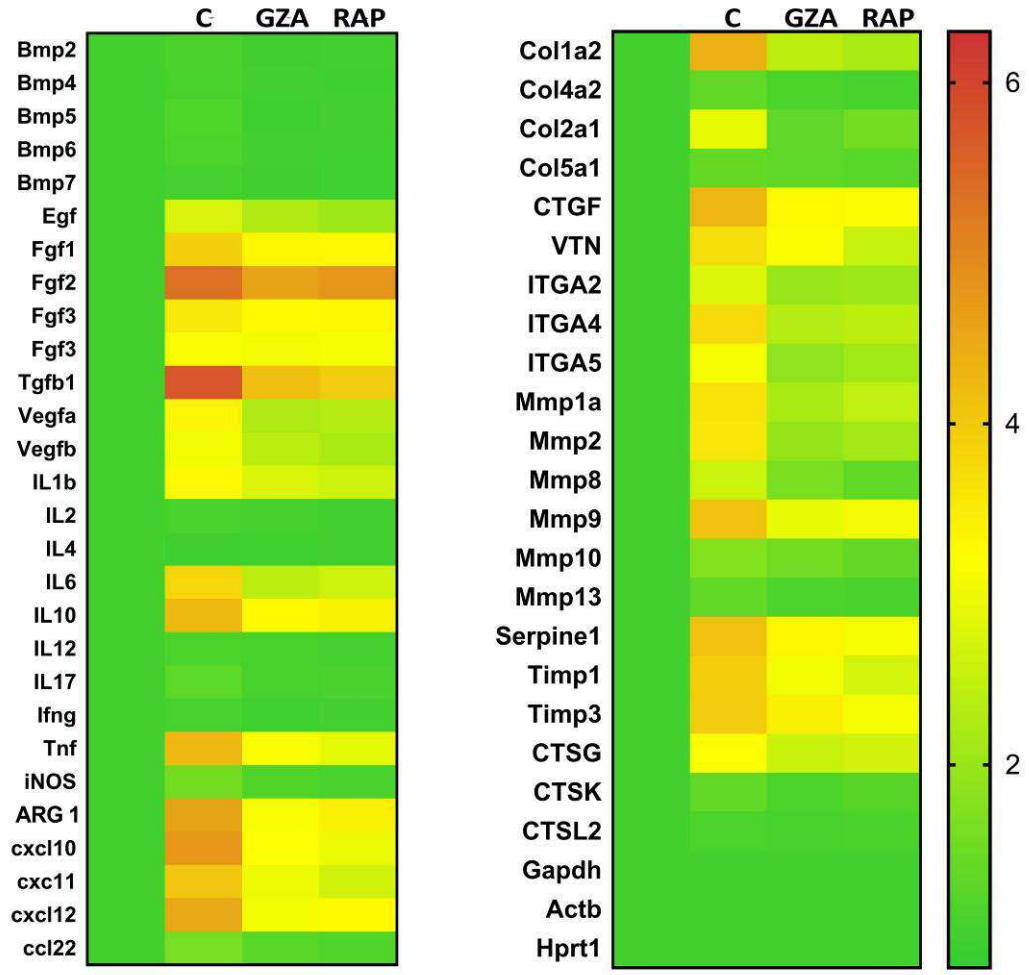

Figure 7. Gene expression patterns post subcutaneous Ti disc implantation in C57Bl/6 mice treated with HMGB1 inhibitor or RAGE antagonist. Mice received Ti-disc implantation in the subcutaneous tissue and were divided in according to each treatment: Control (C group, with no treatment); Glycyrrhizic Acid at a dosage of 200mg/Kg/day (GZA group); or RAGE antagonistic peptide at dosage of 4mg/Kg/day (RAP group). Subcutaneous tissue samples were removed at 3, 7 and 14 days post Ti implantation and a pool of samples from all the experimental time periods in each experimental group was used for a gene expression pattern analysis. Samples of subcutaneous tissue without surgery were used as control. Gene expression was performed by using exploratory analysis by RealTimePCR array, with the VIA7 system (Applied Biosystems, Warrington, UK) and a customized qPCRarray comprised of the major targets (Inflammatory Cytokines & Receptors and Wound Healing panels) of the PCRarrayRT2 Profiler (SABiosciences/QIAGEN). Results are depicted as the fold increase change (and the standard deviation) in mRNA expression from triplicate measurements in relation to the control samples and normalized by internal housekeeping genes (GAPDH, HPRT, β-actin).

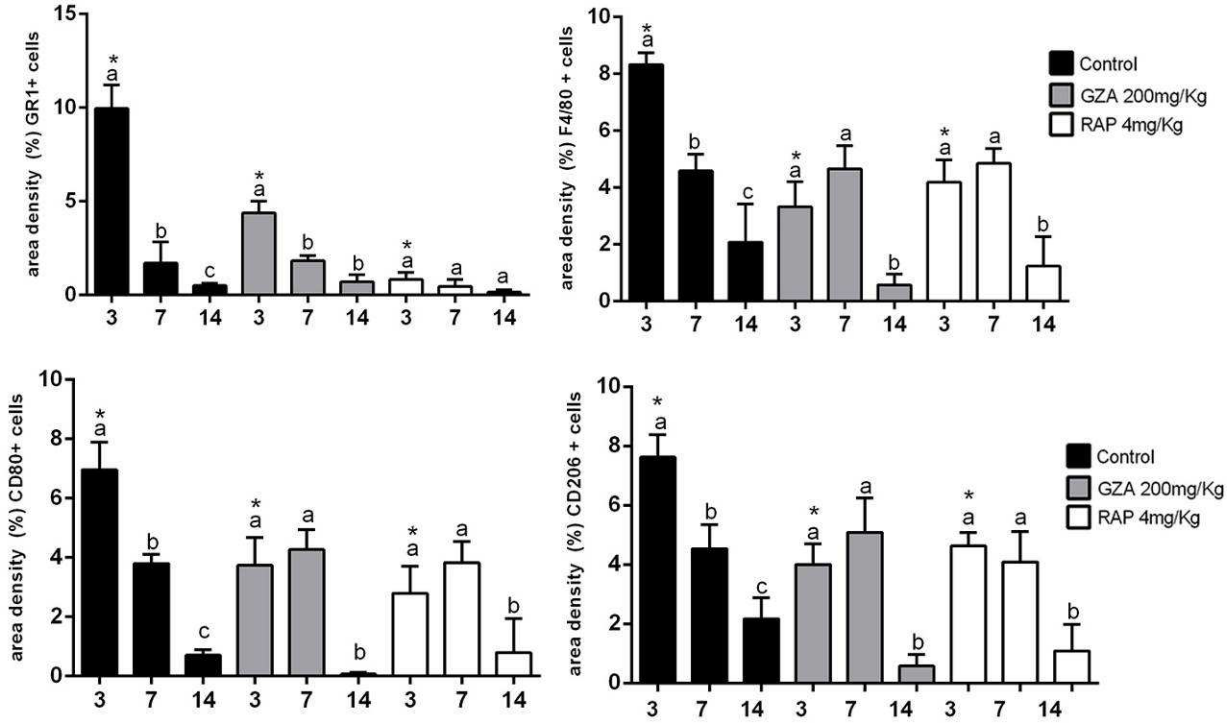

Figure 8. Inflammatory cells recruited to the Ti disc implantation sites in C57Bl/6 mice treated with HMGB1 inhibitor or RAGE antagonist. Mice received Ti-disc implantation in the subcutaneous tissue and were divided in according to each treatment: Control (C group, with no treatment); Vehicle (1.5% DMSO solution); Glycyrrhizic Acid at a dosage of 200mg/Kg/day (GZA group); or RAGE antagonistic peptide at dosage of 4mg/Kg/day (RAP group). Vehicle or drugs were administered one day before the surgical procedure and were given until the end of experimental periods (3d, 7d and 14d). Quantitative analysis of GR1+, F4/80+, CD80+cells, CD206+ cells was performed for each group at days 3, 7 and 14 days post Ti implantation. Different letters indicate significant differences in each time point ($p<0.05$); symbol * indicate significant differences between experimental groups (GZA and RAP) vs control at the same time point. Results are presented as mean and SD.

2.3 ARTICLE 3 – HGMB1 and RAGE mediates Ti oral osseointegration in C57Bl/6 mice. Acta biomaterialia.

Abstract.

The releasing of HMGB1 into extracellular environment and its binding with RAGE has been implicated with several cellular effects which are important for triggering inflammation and regulating healing outcomes. While several studies have identified HMBG1/RAGE signaling effects in different tissues and by distinct approaches, mainly considering inflammatory diseases, their role on osseointegration remains unexplored. **Aim:** In this study, we investigated the effects of HMGB1 or RAGE inhibition in the Ti-mediated osseointegration in C57Bl/6 mice. **Material and Methods**: C57Bl/6 mice received a Ti implant placement in the edentulous alveolar crest and peri-implant sites were evaluated by means microscopic and molecular analysis in different time points (3, 7, 14 and 21 days). According to each treatment, mice were divided into 4 groups: Control (with no treatment); Vehicle (IP% DMSO solution); GZA (IP injection of Glycyrrhizic Acid for HMGB1 inhibition); RAP (IP injection of RAGE antagonistic peptide). **Results:** Effectively, the inhibition of both HMGB1 and RAGE caused the impairment of Ti-mediated osseointegration in mice C57Bl/6 mice, affecting the dynamics of mineralized bone and organic matrix deposition. The administration of GZA significantly disrupted the blood clot formation, affecting fibrin network formation. Stages of osseointegration were marked by a slight inflammatory response at early time points, followed by a gradual bone apposition and matrix maturation in the C and Vehicle group. On the other, GZA and RAP treated mice presented a foreign body reaction (FBR) around Ti threads, with persistence of macrophages along experimental groups, as well FBGC and necrotic bone. C group presented a balance between M1 and M2-type response, with a higher expression of ARG1, IL10, TGFb, VEGFb, CXCL12 and several MSC markers. Conversely, the GZA and RAP group present a higher expression pro-inflammatory cytokines (IL1b, IL6, TNFα), chemokines (CCL5 and CXCL3), chemokine receptors (CCR2, CCR5) and MMPs (MMP1a, MMP2, and MMP9). Finally, Col1a and a number of bone differentiation/remodelling markers were significantly up-regulated in C group compared to the RAP and GZA treated mice. **Conclusions:** This study demonstrated that HMGB1 and RAGE have a role in the osseointegration process, influencing the genesis and regulation of inflammatory immune response, which include the modulation of macrophages polarization state, MSC migration and differentiation in bone cells and consequent bone deposition.

Keywords: DAMP. HMBG1. RAGE. Macrophages. Osseointegration. Titanium.

1. INTRODUCTION

Ti-based devices are classically used in dentistry, due to its osseointegration capacity which is translated in a remarkable clinical success [1-3]. However, the understanding of molecular interactions at Ti/host interface which provides a beneficial equilibrium between immune/inflammatory response and subsequent bone apposition towards Ti surface remains unclear and constitute a delicate task in biomaterial science [3], mainly because of the limited tools available in this field.

In this context, in a recent study of molecular and histological characterization of Ti mediated osseointegration in C57Bl/6 mice [4] a highly orchestrated and transient inflammation coordinating the early stages of osseointegration was demonstrated. Indeed, in the beginning of the osseointegration several bone healing [VEGFb, BMPs, ALP and Runx2] and inflammation-related molecules [TNF, IL6, IL1, CXCL3, CCL2, CCL5 and CXC3CL1]) are up-regulated, with a predominance of macrophage M2-type response. The balance of M1 (pro-inflammatory) and/or M2 (regenerative) macrophage polarization is suggested as a crucial step for determining the success or failure of biomaterial osseointegration [5-7]. Indeed, macrophages play regulatory functions by secreting a range of different mediators (chemokines, cytokines, enzymes and growth factors) in the inflammatory microenvironment, which consequently drives the intensity and duration of immune response, affecting the healing outcomes [7, 8].

Macrophage polarization around biomaterial begins immediately after the biomaterial implantation, with biomaterial surface recognition and a transient polarization state, which are influenced by varying microenvironmental cues, some of which biomaterial-based [7]. In this way, it has been supposed that the type and the quantity of proteins adsorbed on biomaterial and influenced by its surface critically affects its recognition by macrophages and consequently influence the ratio of M1:M2 polarized macrophages [7, 9].

Considering the candidate proteins for adsorbing on Ti surface, it is known that the surgical trauma caused by the biomaterial placement results in a number of released proteins, which are from blood extravasations, but also proteins from necrotic cells and disrupted extracellular matrix, constituting a group of ‘danger signals’ called danger-associated molecular patterns (DAMPs) [10]. While blood exudates consist of platelets forming a fibrin-rich clot and serves as a depot for

cytokines and growth factors at host/biomaterial interface [10, 11], the role o DAMPs is still not described on osseointegration sites.

DAMPs or ‘danger signals’ are a group of endogenous intracellular or extracellular molecules, which are released from their original sites into the microenvironment upon a breakage of tissue components caused by trauma or stress [12]. After their release from damage, DAMPs are recognized by a number of pattern recognition receptors (PRRs) primarily expressed on macrophages [8, 13, 14]. Among several DAMPs already described in the literature, the High Mobility Group Box 1 (HMGB1) is the prototypical and most well-studied HMG family protein and has been highly associated with the activation of inflammatory responses, but also with wound healing [15].

HMGB1 is a 30-kDa abundant non-histone nuclear protein and can also be secreted by activated macrophages or injured cells [15]. Either alone or associated with other molecules, HMGB1 can play pleiotropic functions by activating multiple receptors (TLR4 and TLR2, RAGE, CD24, Integrin/Mac1, TIM3, CXCR4) and consequently can generate different effects (cytokine and growth factors release, cell migration, angiogenesis and/or anti-inflammatory effects), depending on the context and intensity of immune/inflammatory response [15-17]. Among all receptors for HMGB1 binding, the most well established and studied is RAGE [18, 19] and constitute the major receptor for studying HMGB1 activities in rodent macrophages [20]. Importantly, the axis HMGB1/RAGE is related with several cellular effects which are important to inflammatory and healing outcomes, such as: neurovascular remodeling and recovery [21], induction of inflammatory response in endothelial cells [22], inhibition and protection of apoptosis in somatic cells [23], stimuli of muscle satellite cell for muscle regeneration [24], RANKL-induced osteoclastogenesis [25] and angiogenesis by M2 macrophages [19] and endothelial cells [26]. Importantly, these previous studies have identified HMBG1/RAGE functions in different tissues and for distinct approaches, while their possible role on macrophages on biomaterial recognition and also in bone regenerative therapies remains non-explored.

In this present study, we investigate the role of HMGB1 along Ti-mediated oral osseointegration in C57Bl/6 mice and its impact on macrophage responses, by means a cause-effect study of pharmacological inhibition of the HMGB1 or its cognate receptor RAGE.

2. MATERIALS AND METHODS

2.1 Material preparation

Titanium implant screws (titanium-6 aluminum-4 vanadium alloy, NTI-Kahla GmbH Rotary Dental Instruments, Kahla, Thüringen, Germany) of Ø 0.6 mm were cut at length of 1.5 mm and sterilized by autoclaving before surgical procedures, as previously described in oral osseointegration model in C57Bl/6 mice.

2.2 Animals

A total of hundred sixty male wild-type mice (C57Bl/6) (10 weeks old, 25g of weight in average) were used in this study. The animals were bred in the animal facilities of University of Sao Paulo, School of Dentistry of Bauru (FOB/USP) and cared for according to the recommendations in the Guide for the Care and Use of Laboratory Animals of the National Institutes of Health [27]. Animals were distributed according to experimental periods (3, 7, 14 and 21 days) into 4 experimental groups, containing 10 animals for each experimental period and group. Of 10 animals for each group and time point, 6 animals were used for microscopic analysis (microCT, histological, and birefringence analysis) and 4 animals were used for molecular assays. Experimental groups were divided according each treatment: Control [with no treatment]; Vehicle [IP injection of 1.5% DMSO solution]; IP injection of Glycyrrhizic Acid (GZA, Sigma Aldrich) at a dosage of 200mg/Kg/day for HMGB1 inhibition[28]; or IP injection of RAGE antagonistic peptide (RAP, Merck Millipore, USA) at dosage of 4mg/Kg/day[29]. Mice were given IP injections of drugs or vehicle one day before the surgical procedure, continuing by the end of experimental periods. Mice were provided sterile water ad libitum and were fed with sterile standard solid mice chow (Nuvital, Curitiba, PR, Brazil) along all experimental periods of this study, except throughout the first 72 hours post-Ti implantation, in which diet was crumbled. No antibiotics and anti-inflammatory drugs were administered to the animals after implantation surgery, in order to avoid interferences on investigated immunological pathways [30]. The experimental protocol was performed according to ARRIVE guidelines [31] and approved by the local Institutional Committee for Animal Care and Use (#012/2014).

2.3 Experimental protocol

The Ti-implant placement in edentulous alveolar crest of the oral cavity of C57Bl/6 mice was performed as previously described (Biguetti et al, 2018). Briefly, mice were anesthetized previous to the surgery by intramuscular administration of 80 mg/kg of ketamine chloride (Dopalen®, Agribrands Brasil LTDA, Paulínia, SP, Brazil) and 160 mg/kg of xylazine chloride (Anasedan®, Agribrands Brasil LTDA, Paulínia, SP, Brazil) in the proportion 1:1, which was determined according to animal weight. Then, the mouse was placed in dorsal decubitus position and the 4 limbs were affixed to a surgical table, under a stereomicroscope (DF Vasconcellos S.A., Sao Paulo, SP, Brazil), and oral mucosa was cleaned using topical chlorhexidine solution for 1 min. An incision of 2 mm width parallel to the palatal crease and 1 mm in front of the left first maxillary molar was made and the subjacent bone was drilled using a pilot drill of Ø 0.50 mm (NTI-Kahla GmbH Rotary Dental Instruments, Kahla, Thüringen, Germany) adapted to a surgical motor (NSK-Nakanishi International, Kanuma,Tochigi, Japan), with a speed of 600 rpm. The Ti-implant was screwed down in the implant bed using a Castro Viejo Micro Needle Holder (Fine Science Tools®, British Columbia, CA, USA). The right edentulous alveolar crest was used as control side, without implant placement. At the end of experimental periods, mice were killed by anesthetic overdose and maxillae were removed for microscopic (microtomographic, histological, histomorphometric) or molecular analysis. Samples selected for microscopic analysis were fixed in PBS-buffered formalin (10%) solution (pH 7.2) for 48h at room temperature, washed overnight in running water and maintained in alcohol fixative (70% hydrous ethanol) until the conclusion of the µCT scanning. Then, the specimens were decalcified in 4.13% EDTA (pH 7,2) for following histological processing protocols. Samples for molecular analysis were stored in RNAlater (Ambion, Austin, TX, USA) solutions [32].

2.4 Micro-computed tomography (µCT) assessment

Mice maxillae containing the Ti-implants were scanned by Skyscan 1176 System (Bruker Microct, Kontich, Belgium) at 80 kV, 300 µA, 180 degrees of rotation and exposure range of 1 degree. After scanning and previous reconstructions (NRecon software, Bruker Microct, Kontich, Belgium), representative three-dimensional images were obtained by CT-Vox 2.3 software, while quantitative

evaluation of bone to implant interface was assessed using CTAn 1.1.4.1 software (Bruker Microct, Kontich, Belgium) in accordance with recommended guidelines [33] and previous standardization for this model [4]. Briefly, for quantification of bone volume proportion (BV/TV, %) at the implant-bone interface area, a cylindrical region of interest (ROI) with axis length of 500 µm and diameter of 700 µm and the bone quantification. After binarization and separation between titanium body and bone by the difference of hyperdensities, the BV/TV was acquired.

2.5 Histomorphometry

The mice maxillae used for microCT scanning were processed for histological analysis following standardized procedures (Biguetti et al, 2018). Semi-serial sections were cut with 4 µm thickness, and nine serial sections from the central region of implantation sites were taken for hematoxylin and eosin [H&E] staining. The histomorphometry was performed by a single calibrated investigator with a binocular microscope (Olympus Optical Co., Tokyo, Honshu, Japan) using a 100x immersion objective. Briefly, six histological fields per HE section, comprising the region adjacent to thread spaces, were observed under a 100 points grid in a quadrangular area, by using Image J software (Version 1.51, National Institutes of Health, Bethesda, MD, USA). Points were quantified coinciding with the following structures found in the osseointegration sites or in implant failure sites: blood clot, inflammatory cells, blood vessels, fibroblasts and fibers, osteoblasts, osteoclasts, bone matrix, necrotic bone and foreign body giant cells (FBGC) and other elements (empty spaces left by implant space). Results were presented as the mean area density for each structure considered in each examined group.

2.6 Birefringence analysis

A total of 4 sections with 4 µm thickness from the central region of bone to implant contact were used for picrosirius red staining and birefringence analysis. As previously described [4, 32], green birefringence color indicates thin fibers; yellow and red colors at birefringence analysis indicate thick collagen fibers. Three fields from each section were analyzed through polarizing lens coupled to a binocular inverted microscope (Leica DM IRB/E, Leica Microsystems Wetzlar GmbH, Wetzlar,

Germany), by using 40x magnification immersion objective. Images were captured with a Leica Imaging Software (LAX, Leica Microsystems Wetzlar GmbH, Wetzlar, Germany) and the quantification of birefringence brightness was performed using the software AxioVision 4.8 (Carl Zeiss Microscopy GmbH, Jena, Germany) considering green, yellow and red spectra pixels2 . Mean values of 4 sections from each animal were calculated and submitted to statistical analysis.

2.7 RealTimePCR array reactions

To comprehensively compare the osseointegration and impact of DAMPs or its receptors inhibition on investigated mediators along this process, a robust molecular method by RealTimePCR array was applied. Maxillae from all experimental groups and time points were dissected and samples containing only the region of the implant bed were storage in RNA Stabilization Solution (RNAlater®, Thermofisher, Waltham, MA, USA) until RealTime PCR array reactions, while samples from the right side (without implant placement) were used and a control. RealTimePCR array reactions were performed as previously described [32], using first a pool of all experimental time-points (3 d, 7 d, 14 d and 21d) for each group, in order to select targets in which expression variation presented a significant variation compared to the control side. Upregulated targets were analyzed regarding their kinetics of expression for specific time points of 3, 7, 14 and 21-days during osseointegration process or osseointegration failures. Briefly, the extraction of total RNA from implantation sites or controls was performed with RNeasyFFPE kit (Qiagen Inc, Valencia, CA, USA) according to manufacturers' instructions. The integrity of RNA samples was checked by analyzing 1 mg of total RNA on 2100Bioanalyzer (Agilent Technologies, Santa Clara, CA, USA) according to manufacturers' instructions, and the complementary DNA was synthesized using 3 µg of RNA through a reverse transcription reaction (Superscript III, Invitrogen Corporation, Carlsbad, CA, USA). As previously standardized bone repair models in mice [4], the Real-time PCR array was performed in a Viia7 instrument (LifeTechnologies, Carlsbad, CA, USA) using custom panels for "wound healing" (PAMM-121), "inflammatory cytokines and receptors" (PAMM-011) and "Osteogenesis" (PAMM-026) (SABiosciences, Frederick, MD, USA) for gene expression profiling. Data obtained post amplifications were analyzed by RT2 Profiler PCR Array Data Analysis online software (SABiosciences, Frederick, MD, USA) for

normalizing the initial geometric mean of three constitutive genes (GAPDH, ACTB, Hprt1), following normalizing the control group. Data are expressed as heat map fold change relative to the control group.

2.8 Statistical analysis

Statistical treatment of quantitative data was performed using GraphPad Prism 5.0 software (GraphPad Software Inc., San Diego, CA, USA).Normally distributed data were analyzed using One-Way Analysis of variance (ANOVA) followed by Bonferroni's multiple comparison post-hoc tests or student's t-test where applicable. For non-normal distributions, data were analyzed by means Kruskal-Wallis test (followed by Dunn's test) and Mann-Whitney test. The statistical significance of the experiment involving PCR Array was evaluated by the Mann-Whitney test, and the values tested for correction of Benjamini and Hochberg[34]. Values of $p<0.05$ were considered statistically significant.

3. Results

3.1 µCT assessment of bone apposition along osseointegration

Qualitative and quantitative analyses of mineralized bone matrix revealed a non-significant quantity of bone around Ti threads at 3 days among all groups, which just characterize the native bone supporting the Ti-implant (Figure 1AB). Detectable, but not statistically significant newly formed bone matrix was observed at 7 days (22.33±1.93) compared to 3 days (17.18±1.11) post Ti-implantation in the Control group, and the osseointegration was achieved throughout a gradual and proportion of bone apposition (BV/TV, %) around implant threads at 14 d (32.88±3.16%) and 21d (42.25±3.86%) (Figure1B). On the other hand, RAP and GZA treated animals showed a significantly reduced BV/TV around Ti threads at 14 and 21 days compared to the Control group (Figure1B), and vehicle treated group as well (data not shown). The mean of BV/TV around implant threads in RAP treated animals was 18.53±1.60% at 14 days and 23.69±1.40% at 21 days, while in the GZA treated animals was 14.76±4.06% at 14 days and 16.58±3.40% at 21 days. The vehicle treated group also achieved osseointegration with no statistical differences compared to the control (data not shown).

3.2 Birefringence of collagen fibers on granulation tissue and bone matrix

To comprehensively analyze the impact of HGMB1 inhibition or RAGE antagonism along the quality of organic bone matrix during the osseointegration process in mice, we quantified green, yellow and red spectrum fibers from the bone matrix and initial granulation tissue of Control and Experimental groups (Figure 2AB). All groups showed a negligible quantity of collagen fibers starting at 3 days around the Ti threads, emitting birefringence in the green spectrum (i.e. immature and thinner fibers). From 7 to 21 days, the control group showed a gradual and significant increase of yellow and red collagen fibers, resulting in evidenced matrix maturation along osseointegration. Conversely, RAP treated mice showed impaired formation and maturation of collagen fibers, with a significantly reduced amount of total fibers at 14 and 21 days compared to the control. In the same way, GZA treated mice had a drastic impairment of collagen fibers formation, with significantly reduced amount of all birefringent type of fibers from 7 to 21 days compared to the control. No significant differences were observed in the dynamic of collagen fibers formation and maturation along osseointegration between control vehicle treated group (data not shown).

3.3 Histopathological description and histomorphometry of healing components along osseointegration

Histopathological analysis revealed a suitable osseointegration process in the control group, with an intramembranous bone healing following overlapping phases from 3 days to 21 days post Ti-implant placement in mice (Figure 3). Similar histological dynamics of osseointegration were observed in the vehicle treated group (Supplementary Figure 1). On the other hand, both experimental groups treated with RAP or GZA, exhibited failure of osseointegration, with the typical presence of fibrous connective tissue and FBGC along 14 and 21 days post-Ti implantation (14 and 21 days).

At 3 days the bone-implant interface in the control group was filled predominantly by a blood clot (Figure 4A) providing support for cell infiltration (Figure 3). At 7 days increased quantities of granulation tissue components were observed (blood vessels, fibroblasts and fibers) (Figure 4CD), as well an initial differentiation of

osteoblasts and bone matrix from the Ti threads and bone edges (Figure 3, arrowheads). At 14 and 21 days, granulation tissue components significantly decreased around Ti threads spaces, followed by an increased quantity of osteoblasts and bone matrix in the same regions (Figure 3, Figure 4E and G) resulting in a direct contact between the implant and bone (Figure 3, arrowheads). Furthermore, control and vehicle group exhibited osteoclastic resorption lacunae and a few quantities of osteoclasts were found around bone debris and pre-existing bone along 3 and 7 days post Ti implantation, followed by osteoclastic remodeling of newly formed bone at 14 and 21 days.

Comparatively to the Control group, RAP treated mice also showed a suitable blood clot formation the bone-implant interface, but in a slighted reduced number, surrounded by an eosinophilic and slight matrix of fibrin network, with identifiable support for cell migration (Figure 3, arrows). On the other hand, GZA treated mice presented a disorganized blood clot, with agglomerated platelets and red blood cells separated from the malformed fibrin networks (MFN) (Figure 4, GZA group) and a drastically reduced area density of this component (Figure 4A). Both RAP and GZA treated mice showed necrotic/non-viable bone persisting at 7 days to 21 days post Ti-implantation, as well a foreign body reaction (FBR) with the presence of FBGC (Figure 3, Figure 4H-I). RAP group exhibited a negligible higher quantity of osteoblasts and bone formation in scattered areas surrounding Ti thread spaces compared to GZA group (Figure 3, Figure 4E). No statistical differences were observed in quantitative results for other elements (empty spaces, artifacts and Ti space) (data not shown).

Gene expression patterns in the osseointegration sites under HGMB1 inhibition or RAGE antagonism

A pool of samples from all periods post-Ti implantation were initially analyzed by means of an exploratory RealTimePCR array (Figure 5), considering molecules involved in inflammatory response and bone healing (growth factors; immunological/inflammatory markers; extracellular matrix, MSC and bone markers). Osseointegration experimental groups (C, GZA and RAP) were depicted as the fold increase change in relation to control samples (C*), which are from the right side of maxilla of C57Bl/6 untreated mice, without surgery.

Among growth factors, TGFβ1 and VEGFb were significantly upregulated in C group, such as several MSC putative markers (CD206, OCT-4, NANOG, CD44, CD34, CD73, CD146, CD105, CXCL12); while GZA and RAP presented an important reduction in the mRNA levels for all these targets. In the same way, several bone markers related to osteoblasts differentiation (BMP2, BMP4, BMP7, Runx2, ALPL, DMP1, Phex, Sost, VDR) and bone remodeling (RANKL, OPG, CTSK), were positively upregulated in C group during osseointegration, whereas their expression were drastically reduced in GZA and RAP group. On the other hand, especially RAP group present an upregulation for FGF1 and FGF2.

Considering immunological markers for M1/M2 macrophages, a higher expression of ARG1 and IL10 was particularly found on C group, but not observed in GZA and RAP groups. The majority of chemokines and their receptors involved in inflammatory cells migration (CCR1, CCR2, CCR5, CCL2, CCL3, CCL5, CCL9, CCL12, CCL17, CCL20, CCL25, CXCL3, CXC3CL1) were upregulated in all osseointegration groups. GZA and RAP presented a higher expression of CCR2, CCR5, CCL5 and CXCL3 compared to the control. Also, pro-inflammatory cytokines were differentially expressed in C group compared to the GZA and RAP. IL1b, IL6, TNF were upregulated in the three osseointegration groups (C, GZA and RAP), but with increased mRNA levels in GZA and RAP groups compared to the C.

Among the extracellular matrix markers, Col1a2, MMP1a, MMP2 and MMP9 were upregulated during osseointegration process in all groups. However, mRNA levels of Col1a2 were higher in the C group, while GZA and RAP group presented higher mRNA levels for MMPs.

Discussion

In this present article, it was hypothesized that HMGB1 (as a DAMP released from tissue damage during the aseptic surgical trauma) might interact with Ti/host interface and might influence inflammatory and healing responses upon the oral osseointegration. Consequently, to investigate the role of HMGB1 along osseointegration process, C57Bl/6 mice were subjected to Ti-implant surgical placement in the edentulous area and were treated with GZA (an HMGB1 inhibitor), at concentrations previously used in C57Bl/6 mice [28]. Additionally, considering that RAGE is cognate receptor for HMGB1 [18] and is the major receptor involving

HMGB1 pro-inflammatory signalling in rodents [20], an additional experimental group was treated with RAP, a RAGE antagonist, at a dosage previously described for using in C57Bl/6 [29].

Effectively, the inhibition of both, HMGB1 or RAGE, caused the failure of Ti-mediated osseointegration in mice C57Bl/6 mice, affecting the dynamics of mineralized (Figure 1) and organic (Figure 2) bone matrix formation. Despite the limited information about a connection between bone healing and HMGB1, the inhibition of HMGB1 in a model of tooth extraction in mice (by using an anti-HMGB1 antibody), significantly delayed the bone healing process, but without inhibiting it completely [17]. It is important to remind, in our present experimental model, the presence of a biomaterial is an important variable in the healing site, which requires a more delicate balance compared to the bone repair by itself.

Subsequently, the histological and molecular analysis were used in parallel for a detailed exploration of GZA and RAP effects on the unsuccessful osseointegration compared to the successful osseointegration along the events of acute inflammation, cell proliferation and differentiation, and finally bone apposition in the specific time points post Ti implant placement.

The process of osseointegration starts by preparing the bone defect for implant placement, when coagulation proteins from blood are released and then activated to provide the clot formation and consequently a provisional matrix for cell recruitment and migration [10]. A suitable blood clot was evidenced at the host/Ti interface around 3 days in the control, vehicle and RAP treated mice. However, the GZA treatment caused a disruption of fibrin network formation and impairment in the blood clot structure (Figure 3, 4). Indeed, it has been demonstrated that HMGB1 acts synergistically with thrombin to promote coagulation in vivo, evidencing its role as an organizer in post-injury wound healing [35]. Thus, the failure of osseointegration in GZA was initially caused by the disruption of the blood clot, the first provisional matrix around Ti threads.

Previous studies demonstrated that HMGB1 promotes the secretion of multiple cytokines in the injury sites, strongly activating and driving the acute inflammatory response [36]. In this context, the activation of inflammatory response at acute phase post biomaterial implantation is an essential step for triggering a suitable healing [7]. In our histological and histomorphometric analysis, while control and vehicle treated mice presented a peak of inflammatory cells at 3 days and significantly decreased at

7 and 14 days, RAP and GZA treated mice had a disruption in the inflammatory response, resulting in higher counts of inflammatory cells around Ti threads until the late periods post Ti implantation, mainly macrophages as suggested by the cellular morphology. Indeed, GZA and RAP presented a higher expression of CCR2, CCR5, CCL5 and CXCL3 compared to the C group. While CCR2, CCR5 and CCL5 are mainly involved in monocyte/macrophages migration [8], the CXCL3 plays a role in PMN recruitment [37]. Consistently, in the first phase of biomaterial recognition and the beginning of inflammatory cascade, the balance of quality and quantities of blood clot components (e.g. platelets), neutrophils (PMN) and macrophages is considered critical for healing outcomes [5]. For example, the persistence of macrophages along late periods post biomaterial implantation is implicated with biomaterial encapsulation [3].

In this present study, we observed a persistence of macrophages and fibroblasts around Ti threads in GZA and RAP groups. Accordingly, RAP presented an upregulation of mRNA for growth factors involved in fibroblasts proliferation (FGF1 and FGF2), compatible with a fibrous soft tissue demonstrated at birefringence. In this way, it has been suggested that a persistence of macrophages and fibroblasts along late periods post biomaterial implantation is implicated with a dysregulation of macrophage phenotype (M1: M2 ratios) [5]. Accordingly, the expression of ARG1 and IL10, related to a M2-type response, were particularly found on C group, but not in GZA and RAP. Furthermore, GZA and RAP group showed increased mRNA levels of IL1β, IL6, TNFα, suggesting a persistence of M1-type response.

Thus, it is evident that HMGB1 and RAGE contribute to the ratio of M1:M2 polarized macrophages in the healing sites post biomaterial implantation. As a consequence, both GZA and RAP treated mice had impairment in the area density of blood vessels at 7 days compared to the control, and also a decreased expression of growth factors involving angiogenesis (VEGFb) and MSCs recruitment and proliferation (TGFβ1, CXCL12) [32]. Indeed, mRNA levels of MSC putative markers (CD206, OCT-4, NANOG, CD44, CD34, CD73, CD146, CD105) were also significantly reduced in GZA and RAP groups compared to the control (CD206, OCT-4, NANOG, CD44, CD34, CD73, CD146, CD105). Accordingly, it has been demonstrated that HMGB1 can induce VEGFa expression by M2-type macrophages [19] and in sites of injury [26] in a manner dependent on RAGE, in both situations. Additionally, endothelial cells also express RAGE in their surface and are

demonstrated to respond to HMGB1 stimulation through multiple mechanisms, including endothelial cell proliferation, migration and sprouting, and upregulation of proangiogenic factors [38, 39].

The primary clinical failure of implants is characterized by an enveloping soft tissue layer around the Ti, also known as FBR [3]. Here we demonstrated a FBR with increasing quantities of necrotic remaining bone and FBGC in GZA and RAP treated mice. The reduced quantities of osteoclasts in GZA and RAP treated mice were in according to reduced expression of remodelling bone markers (RANKL, OPG, CTSK) in these both groups, compared to the C group. As a consequence, FBGC were observed around bone fragments, in a temptation to remove remaining necrotic bone, besides of the encapsulation of biomaterial in both, GZA and RAP group. Indeed, it has been suggested that apoptotic osteocytes can release HMGB1 as a danger signal to activate RANKL-induced bone resorption in non-viable bone [40], and this activation has been reported to occur in a manner dependent on RAGE [25, 41]. Thus, inhibition of HMGB1 and RAGE significantly impaired the removal of non-viable bone in the implantation sites after drilling.

Finally, after the deposition of higher amounts of ECM around biomaterial (predominantly collagens type I) during the proliferative phase, starts the remodeling phase [4]. The remodelling phase is important for bone maturation and begins with a higher balance of MMPs- and tissue inhibitor of metalloproteinase (TIMP), and also bone matrix enzymes (e.g. CTSK), mediating the degradation and remodelling of the newly deposited bone matrix and generally resulting in bone remodelling and maturation [32]. In accordance, these stages were observed along osseointegration in the C group, in parallel with an upregulation of osteoblast differentiation markers (BMP2, BMP4, BMP7, Runx2, ALPL, DMP1, Phex, Sost, VDR) and Col1a2. Conversely, the expression of bone markers were drastically reduced in GZA and RAP group. Also, in the birefringence analysis, the quality and quantities of collagen fibers were drastically impaired, mainly in GZA group, but also with the RAGE antagonism. At this moment, it was reported that HMGB1 could stimulate osteoblasts migration in a toll-like receptor (TLR) 2/TLR4- and NF-κB-dependent manner [42], osteogenic differentiation from adipocytes [43] and also can induce matrix mineralization by human dental pulp cells via RAGE expression [44]. However, considering the presence of HMGB1 mainly at acute inflammatory stage as a DAMP, the negative effects of GZA and RAP on bone healing could also be associated with

the imbalance of M1:M2 macrophages and the negative impact on macrophage activation. Indeed, the inhibition of HMGB1 and RAGE negatively affect the triggering of a constructive inflammatory response, culminating in a cascade of negative effects on osseointegration.

Finally, despite the inflammatory roles implicated to HMGB1 in destructive inflammatory environments, several studies have suggested that HMGB1 can also act as a regenerative mediator [15-18, 26, 36, 38], as also demonstrated by this cause-effect study. Furthermore, since the animals received the GZA and RAP along all experimental periods, future studies are required to investigate the inhibition HMGB1 and/or RAGE only in initial time points along Ti-mediated osseointegration, when these molecules are main required, in order to determine their role in each phase of osseointegration.

Conclusion

Taking together, our findings suggest that HMGB1 and RAGE actively influence the osseointegration process, by their influence in the balance of inflammatory markers, macrophages polarization state, MSC migration and differentiation in bone cells and consequent bone deposition.

Acknowledgments

The authors would like to thank Daniele Ceolin, Patricia Germino and Tania Cestari for their excellent technical assistance. This study was supported by grants (#2015/24637-3) and scholarships (#2014/09590-8, #2015/18162-2) from FAPESP.

REFERENCES

1. Adell R, Lekholm U, Rockler B, Branemark PI. A 15-year study of osseointegrated implants in the treatment of the edentulous jaw. International journal of oral surgery. 1981 Dec;10(6):387-416. PubMed PMID: 6809663.

2. Branemark PI, Hansson BO, Adell R, Breine U, Lindstrom J, Hallen O, et al. Osseointegrated implants in the treatment of the edentulous jaw. Experience from a 10-year period. Scandinavian journal of plastic and reconstructive surgery Supplementum. 1977;16:1-132. PubMed PMID: 356184.

3. Albrektsson T, Dahlin C, Jemt T, Sennerby L, Turri A, Wennerberg A. Is marginal bone loss around oral implants the result of a provoked foreign body reaction? Clinical implant dentistry and related research. 2014 Apr;16(2):155-65. PubMed PMID: 24004092.

4. Biguetti CC, Cavalla F, Silveira EM, Fonseca AC, Vieira AE, Tabanez AP, et al. Oral implant osseointegration model in C57Bl/6 mice: microtomographic, histological, histomorphometric and molecular characterization. Journal of Applied Oral Science. 2018 January 2018:1-24.

5. Brown BN, Ratner BD, Goodman SB, Amar S, Badylak SF. Macrophage polarization: an opportunity for improved outcomes in biomaterials and regenerative medicine. Biomaterials. 2012 May;33(15):3792-802. PubMed PMID: 22386919. Pubmed Central PMCID: 3727238.

6. Trindade R, Albrektsson T, Wennerberg A. Current concepts for the biological basis of dental implants: foreign body equilibrium and osseointegration dynamics. Oral and maxillofacial surgery clinics of North America. 2015 May;27(2):175-83. PubMed PMID: 25753575.

7. Sridharan R, Cameron AR, Kelly DJ, Kearney CJ, O'Brien FJ. Biomaterial based modulation of macrophage polarization: a review and suggested design principles. Mater Today. 2015 Jul-Aug;18(6):313-25. PubMed PMID: WOS:000356184700013. English.

8. Mosser DM, Edwards JP. Exploring the full spectrum of macrophage activation. Nature reviews Immunology. 2008 Dec;8(12):958-69. PubMed PMID: 19029990. Pubmed Central PMCID: 2724991.

9. Corradetti B, Taraballi F, Corbo C, Cabrera F, Pandolfi L, Minardi S, et al. Immune tuning scaffold for the local induction of a pro-regenerative environment. Scientific reports. 2017 Dec 5;7(1):17030. PubMed PMID: 29208986. Pubmed Central PMCID: 5717048.

10. Vishwakarma A, Bhise NS, Evangelista MB, Rouwkema J, Dokmeci MR, Ghaemmaghami AM, et al. Engineering Immunomodulatory Biomaterials To Tune the Inflammatory Response. Trends in biotechnology. 2016 Jun;34(6):470-82. PubMed PMID: 27138899.

11. Davies JE. Understanding peri-implant endosseous healing. Journal of dental education. 2003 Aug;67(8):932-49. PubMed PMID: 12959168.

12. Land WG. The Role of Damage-Associated Molecular Patterns (DAMPs) in Human Diseases: Part II: DAMPs as diagnostics, prognostics and therapeutics in clinical medicine. Sultan Qaboos University medical journal. 2015 May;15(2):e157-70. PubMed PMID: 26052447. Pubmed Central PMCID: 4450777.

13. Fukata M, Vamadevan AS, Abreu MT. Toll-like receptors (TLRs) and Nod-like receptors (NLRs) in inflammatory disorders. Seminars in immunology. 2009 Aug;21(4):242-53. PubMed PMID: 19748439.

14. Sims GP, Rowe DC, Rietdijk ST, Herbst R, Coyle AJ. HMGB1 and RAGE in inflammation and cancer. Annual review of immunology. 2010;28:367-88. PubMed PMID: 20192808.

15. Kang R, Chen R, Zhang Q, Hou W, Wu S, Cao L, et al. HMGB1 in health and disease. Molecular aspects of medicine. 2014 Dec;40:1-116. PubMed PMID: 25010388. Pubmed Central PMCID: 4254084.

16. Schiraldi M, Raucci A, Munoz LM, Livoti E, Celona B, Venereau E, et al. HMGB1 promotes recruitment of inflammatory cells to damaged tissues by forming a complex with CXCL12 and signaling via CXCR4. The Journal of experimental medicine. 2012 Mar 12;209(3):551-63. PubMed PMID: 22370717. Pubmed Central PMCID: 3302219.

17. Aoyagi H, Yamashiro K, Hirata-Yoshihara C, Ideguchi H, Yamasaki M, Kawamura M, et al. HMGB1-induced inflammatory response promotes bone healing in murine tooth extraction socket. Journal of cellular biochemistry. 2018 Jan 27. PubMed PMID: 29377249.

18. Rauvala H, Rouhiainen A. RAGE as a receptor of HMGB1 (Amphoterin): roles in health and disease. Current molecular medicine. 2007 Dec;7(8):725-34. PubMed PMID: 18331230.

19. Rojas A, Delgado-Lopez F, Perez-Castro R, Gonzalez I, Romero J, Rojas I, et al. HMGB1 enhances the protumoral activities of M2 macrophages by a RAGE-dependent mechanism. Tumor Biol. 2016 Mar;37(3):3321-9. PubMed PMID: WOS:000374903500056. English.

20. Kokkola R, Andersson A, Mullins G, Ostberg T, Treutiger CJ, Arnold B, et al. RAGE is the major receptor for the proinflammatory activity of HMGB1 in rodent macrophages. Scandinavian journal of immunology. 2005 Jan;61(1):1-9. PubMed PMID: 15644117.

21. Tian X, Sun L, Feng D, Sun Q, Dou Y, Liu C, et al. HMGB1 promotes neurovascular remodeling via Rage in the late phase of subarachnoid hemorrhage. Brain research. 2017 Sep 1;1670:135-45. PubMed PMID: 28606778.

22. Luo Y, Li SJ, Yang J, Qiu YZ, Chen FP. HMGB1 induces an inflammatory response in endothelial cells via the RAGE-dependent endoplasmic reticulum stress pathway. Biochemical and biophysical research communications. 2013 Sep 6;438(4):732-8. PubMed PMID: 23911608.

23. Su Z, Wang T, Zhu H, Zhang P, Han R, Liu Y, et al. HMGB1 modulates Lewis cell autophagy and promotes cell survival via RAGE-HMGB1-Erk1/2 positive feedback during nutrient depletion. Immunobiology. 2015 May;220(5):539-44. PubMed PMID: 25578401.

24. Riuzzi F, Sorci G, Sagheddu R, Donato R. HMGB1-RAGE regulates muscle satellite cell homeostasis through p38-MAPK- and myogenin-dependent repression of Pax7 transcription. Journal of cell science. 2012 Mar 15;125(Pt 6):1440-54. PubMed PMID: 22328527.

25. Zhou Z, Han JY, Xi CX, Xie JX, Feng X, Wang CY, et al. HMGB1 regulates RANKL-induced osteoclastogenesis in a manner dependent on RAGE. Journal of

bone and mineral research : the official journal of the American Society for Bone and Mineral Research. 2008 Jul;23(7):1084-96. PubMed PMID: 18302500. Pubmed Central PMCID: 2679382.

26. Lei C, Zhang S, Cao T, Tao W, Liu M, Wu B. HMGB1 may act via RAGE to promote angiogenesis in the later phase after intracerebral hemorrhage. Neuroscience. 2015 Jun 4;295:39-47. PubMed PMID: 25813710.

27. Institute of Laboratory Animal Resources (U.S.). Committee on Care and Use of Laboratory Animals. Guide for the care and use of laboratory animals. NIH publication. Bethesda, Md.: U.S. Dept. of Health and Human Services, Public Health Service. p. v.

28. Lau A, Wang S, Liu W, Haig A, Zhang ZX, Jevnikar AM. Glycyrrhizic acid ameliorates HMGB1-mediated cell death and inflammation after renal ischemia reperfusion injury. American journal of nephrology. 2014;40(1):84-95. PubMed PMID: 25059568.

29. Arumugam T, Ramachandran V, Gomez SB, Schmidt AM, Logsdon CD. S100P-derived RAGE antagonistic peptide reduces tumor growth and metastasis. Clinical cancer research : an official journal of the American Association for Cancer Research. 2012 Aug 15;18(16):4356-64. PubMed PMID: 22718861. Pubmed Central PMCID: 3845828.

30. Araujo-Pires AC, Biguetti CC, Repeke CE, Rodini Cde O, Campanelli AP, Trombone AP, et al. Mesenchymal stem cells as active prohealing and immunosuppressive agents in periapical environment: evidence from human and experimental periapical lesions. Journal of endodontics. 2014 Oct;40(10):1560-5. PubMed PMID: 25260726.

31. Kilkenny C, Browne WJ, Cuthi I, Emerson M, Altman DG. Improving bioscience research reporting: the ARRIVE guidelines for reporting animal research. Veterinary clinical pathology. 2012 Mar;41(1):27-31. PubMed PMID: 22390425.

32. Vieira AE, Repeke CE, Ferreira Junior Sde B, Colavite PM, Biguetti CC, Oliveira RC, et al. Intramembranous bone healing process subsequent to tooth extraction in mice: micro-computed tomography, histomorphometric and molecular characterization. PloS one. 2015;10(5):e0128021. PubMed PMID: 26023920. Pubmed Central PMCID: 4449187.

33. Bouxsein ML, Boyd SK, Christiansen BA, Guldberg RE, Jepsen KJ, Muller R. Guidelines for assessment of bone microstructure in rodents using micro-computed tomography. Journal of bone and mineral research : the official journal of the American Society for Bone and Mineral Research. 2010 Jul;25(7):1468-86. PubMed PMID: 20533309.

34. Benjamini YH, Y. Controlling the False Discovery Rate: A Practical and Powerful Approach to Multiple Testing. Journal of the Royal Statistical Society Series B (Methodological). 1995;1(57):11.

35. Ito T, Kawahara K, Nakamura T, Yamada S, Nakamura T, Abeyama K, et al. High-mobility group box 1 protein promotes development of microvascular thrombosis in rats. Journal of thrombosis and haemostasis : JTH. 2007 Jan;5(1):109-16. PubMed PMID: 17239166.

36. Feng L, Xue D, Chen E, Zhang W, Gao X, Yu J, et al. HMGB1 promotes the secretion of multiple cytokines and potentiates the osteogenic differentiation of mesenchymal stem cells through the Ras/MAPK signaling pathway. Experimental and therapeutic medicine. 2016 Dec;12(6):3941-7. PubMed PMID: 28105126. Pubmed Central PMCID: 5228376.

37. Reutershan J, Stockton R, Zarbock A, Sullivan GW, Chang D, Scott D, et al. Blocking p21-activated kinase reduces lipopolysaccharide-induced acute lung injury by preventing polymorphonuclear leukocyte infiltration. American journal of respiratory and critical care medicine. 2007 May 15;175(10):1027-35. PubMed PMID: 17322107. Pubmed Central PMCID: 1899271.

38. Biscetti F, Straface G, De Cristofaro R, Lancellotti S, Rizzo P, Arena V, et al. High-mobility group box-1 protein promotes angiogenesis after peripheral ischemia in diabetic mice through a VEGF-dependent mechanism. Diabetes. 2010 Jun;59(6):1496-505. PubMed PMID: 20200317. Pubmed Central PMCID: 2874711.

39. Schlueter C, Weber H, Meyer B, Rogalla P, Roser K, Hauke S, et al. Angiogenetic signaling through hypoxia: HMGB1: an angiogenetic switch molecule. The American journal of pathology. 2005 Apr;166(4):1259-63. PubMed PMID: 15793304. Pubmed Central PMCID: 1602384.

40. Plotkin LI. Apoptotic osteocytes and the control of targeted bone resorption. Current osteoporosis reports. 2014 Mar;12(1):121-6. PubMed PMID: 24470254. Pubmed Central PMCID: 3952244.

41. Charoonpatrapong K, Shah R, Robling AG, Alvarez M, Clapp DW, Chen S, et al. HMGB1 expression and release by bone cells. Journal of cellular physiology. 2006 May;207(2):480-90. PubMed PMID: 16419037.

42. Li MJ, Li F, Xu J, Liu YD, Hu T, Chen JT. rhHMGB1 drives osteoblast migration in a TLR2/TLR4- and NF-kappaB-dependent manner. Bioscience reports. 2016 Jan 7;36(1):e00300. PubMed PMID: 26744383. Pubmed Central PMCID: 4759610.

43. Hsu LW, Goto S, Nakano T, Chen KD, Wang CC, Lai CY, et al. The effect of exogenous histone H1 on rat adipose-derived stem cell proliferation, migration, and osteogenic differentiation in vitro. Journal of cellular physiology. 2012 Oct;227(10):3417-25. PubMed PMID: 22223405.

44. Qi SC, Cui C, Yan YH, Sun GH, Zhu SR. Effects of high-mobility group box 1 on the proliferation and odontoblastic differentiation of human dental pulp cells. International endodontic journal. 2013 Dec;46(12):1153-63. PubMed PMID: 23600680.

FIGURES AND LEGENDS

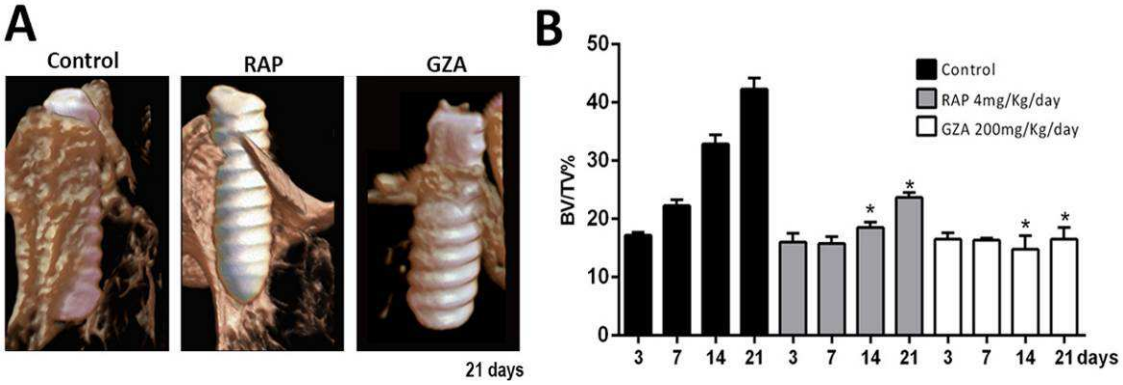

Figure 1. Micro-computed tomography (µCT) analysis of oral osseointegration model in C57Bl/6 mice under RAGE antagonism (RAP 4mg/Kg/day) or HMGB1 inhibition (GZA 200mg/Kg/day). Mice received Ti-screw implantation in the edentulous ridge of maxilla and were divided in according to each treatment: Control (C group, with no treatment); Glycyrrhizic Acid at a dosage of 200mg/Kg/day (GZA group); or RAGE antagonistic peptide at dosage of 4mg/Kg/day (RAP group). A) Three-dimensional representative images obtained with the CT-Vox software at 21 days post Ti implantation from Control, RAP and GZA groups. B) Quantitative analysis of bone volume/tissue volume (BV/TV, %) in the interface bone-Ti along days 3, 7, 14 and 21 post implantation for Control, RAP and GZA groups. Symbol * indicate significant statistical differences ($p<0.05$) in comparison with control.

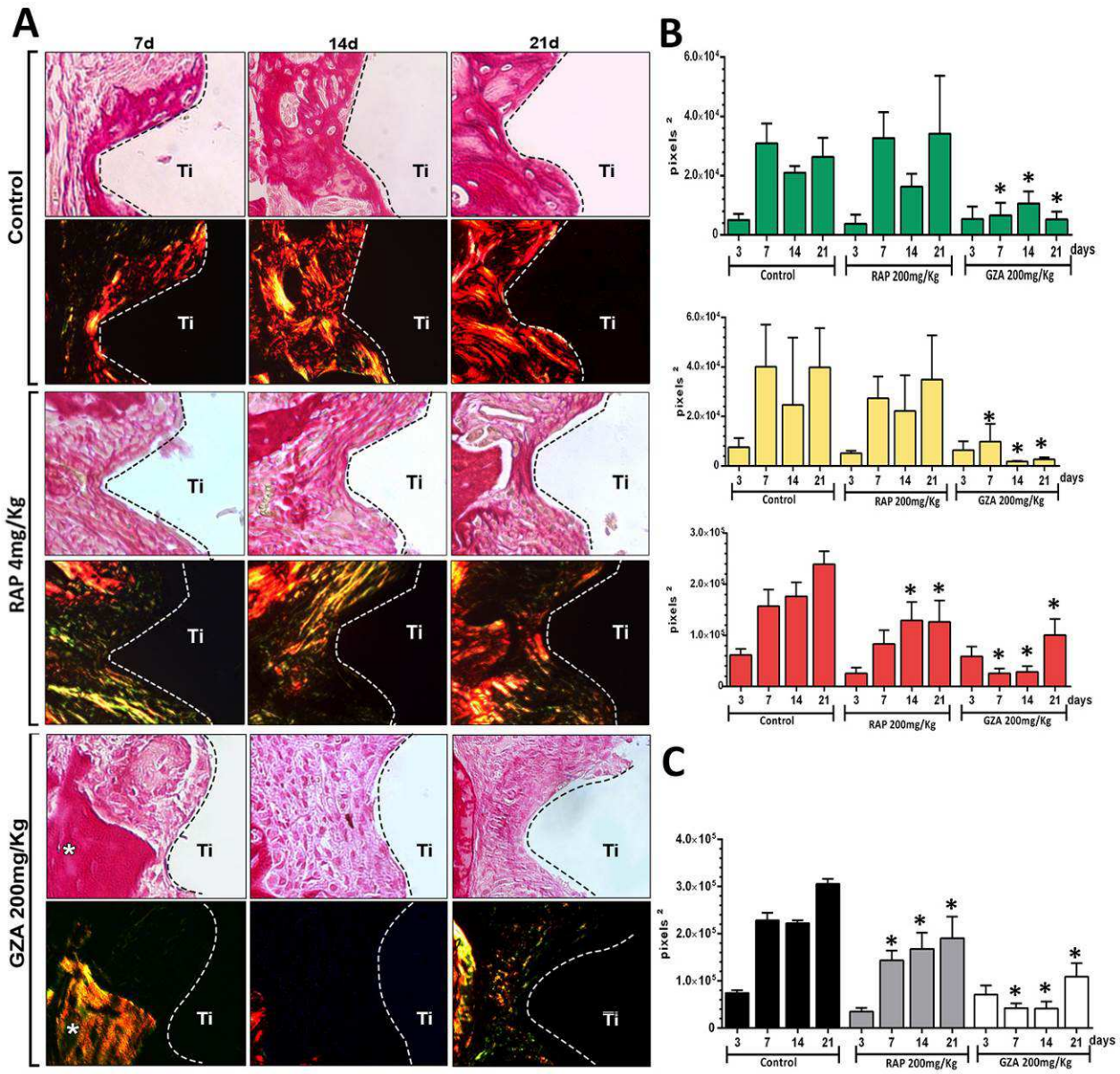

Figure 2 – Birefringence analysis of collagen fibers along osseointegration model in C57Bl/6 mice under RAGE antagonism (RAP 4mg/Kg/day) or HMGB1 inhibition (GZA 200mg/Kg/day). Mice received Ti-screw implantation in the edentulous ridge of maxilla and were divided in according to each treatment: Control (C group, with no treatment); Glycyrrhizic Acid at a dosage of 200mg/Kg/day (GZA group); or RAGE antagonistic peptide at dosage of 4mg/Kg/day (RAP group). A) Representative sections from oral osseointegration process upon polarized and conventional light, to evaluate collagen fibers maturation along days 3, 7, 14 and 21 post-Ti-screw implantation in the different experimental groups. As visualized upon polarized light, green birefringence color indicates thin fibers; yellow and red colors at birefringence analysis indicate thick collagen fibers. Original magnification 40x. B) Intensity of birefringence measured from Image-analysis software (AxioVision, v. 4.8, CarlZeiss) to identify and quantify area of collagen from each birefringence color (pixels 2) and C) total area of collagen fibers (pixel2) throughout experimental periods. Results are presented as the mean and SD of pixels2 for each color in the birefringence analysis. Symbol * indicate a statistically significant difference vs control ($p<0.05$).

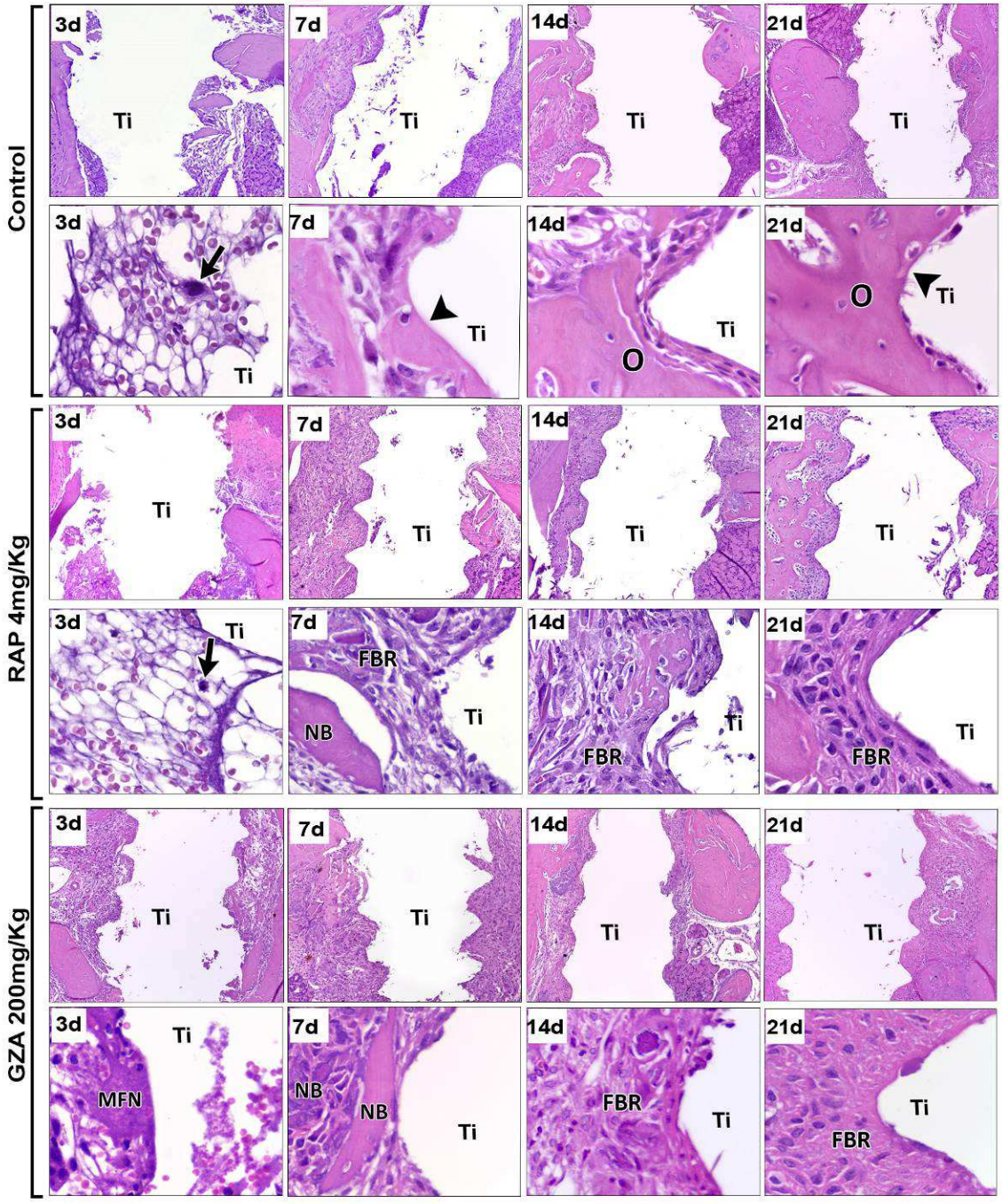

Figure 3. Histopathological analysis along oral osseointegration model in C57Bl/6 mice under RAGE antagonism (RAP 4mg/Kg/day) or HMGB1 inhibition (GZA 200mg/Kg/day). Mice received Ti-screw implantation in the edentulous ridge of maxilla and were divided in according to each treatment: Control (C group, with no treatment); Glycyrrhizic Acid at a dosage of 200mg/Kg/day (GZA group); or RAGE antagonistic peptide at dosage of 4mg/Kg/day (RAP group). Chronology of oral osseointegration is observed throughout days 3, 7, 14 and 21 days. Histological slides were stained with H&E and images were captured at 10 and 100x magnification. Ti = Ti screw space. BC = Blood clot. Arrows = fibrin supporting cell migration. Arrowheads = bone/Ti contact region. O = osseointegration. MFN = Malformed fibrin network. NB = Necrotic bone. FBR = Foreign bone reaction.

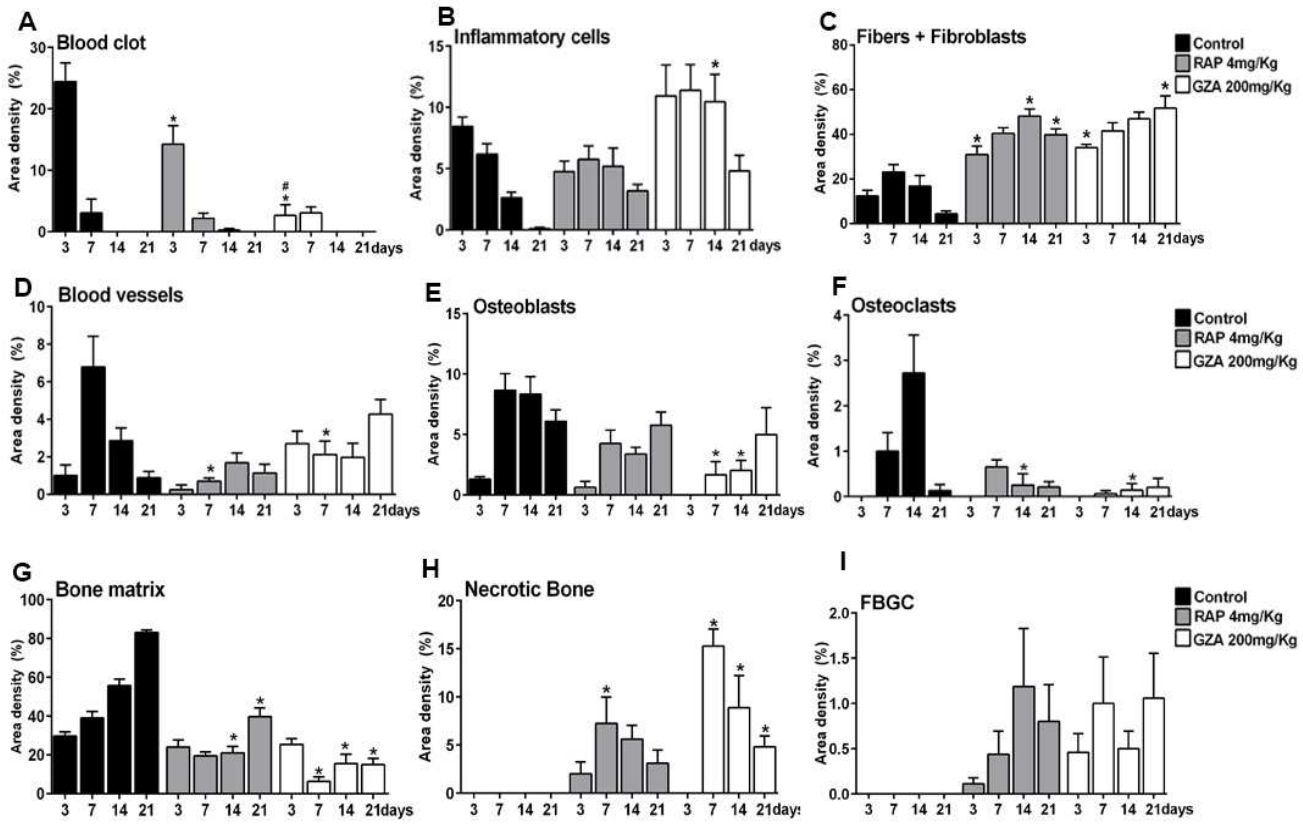

Figure 4. Histomorphometric analysis of healing components along oral osseointegration model in C57Bl/6 mice under RAGE antagonism (RAP 4mg/Kg/day) or HMGB1 inhibition (GZA 200mg/Kg/day). Mice received Ti-screw implantation in the edentulous ridge of maxilla and were divided in according to each treatment: Control (C group, with no treatment); Glycyrrhizic Acid at a dosage of 200mg/Kg/day (GZA group); or RAGE antagonistic peptide at dosage of 4mg/Kg/day (RAP group). Results are presented as the means (±SD) of area density for each component related to osseointegration process: (A) Blood Clot, (B) Inflammatory cells, (C) Fibers + Fibroblasts, (D) Blood vessels, (E) Osteoblasts, (F) Osteoclasts, (G) Bone matrix, (H) Necrotic Bone and (I) FBGC. Symbol *indicate a statistically significant difference vs control, # indicate differences between RAP and GZA groups ($p<0.05$).

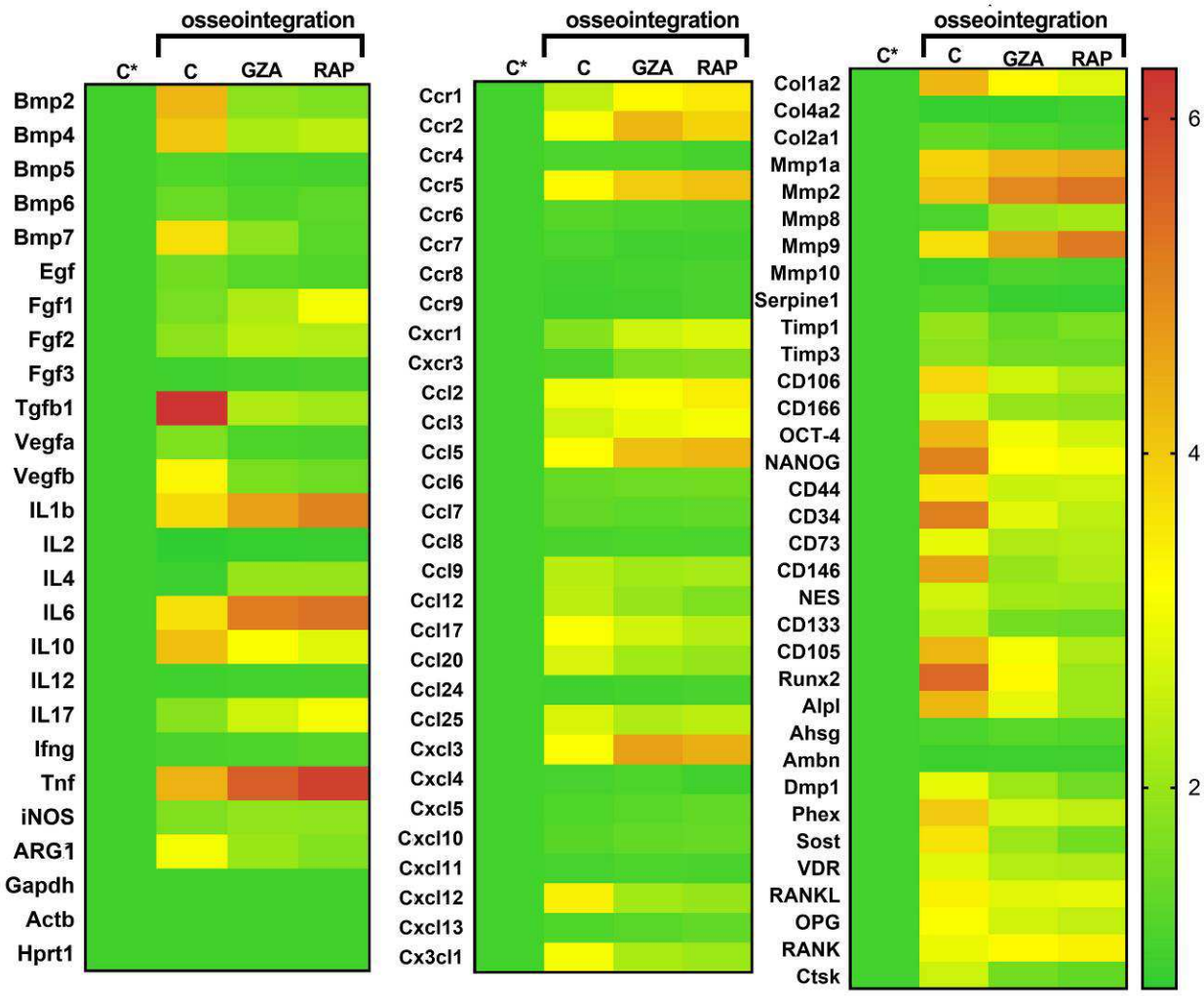

Figure 5. Gene expression patterns in the osseointegration sites under inhibition of HMGB1 (GZA 200mg/Kg/day) or RAGE antagonism (RAP 4mg/Kg/day). Mice received Ti-screw implantation in the edentulous ridge of maxilla and were divided in according to each treatment: Control (C group, with no treatment); Glycyrrhizic Acid at a dosage of 200mg/Kg/day (GZA group); or RAGE antagonistic peptide at dosage of 4mg/Kg/day (RAP group). Right side without Ti-screw implantation was used as tissue control and represented as **C***. Molecular analysis of the gene expression patterns in the region of Ti screw implantation was comprised of an initial exploratory analysis by RealTimePCR array for each experimental group (Control, GZA and RAP), considering a pool of samples from all the experimental periods (3 d, 7 d, 14 d, 21 d). RealTimePCR array analysis was performed with the VIA7 system (Applied Biosystems Limited, Warrington,Cheshire, UK) using a customized qPCRarray comprised of the major targets from the Osteogenesis, Inflammatory Cytokines & Receptors and Wound Healing panels of the PCRarrayRT2 Profiler (SABiosciences/QIAGEN, Gaithersburg, MD, USA). Results are depicted as the fold increase change (and the standard deviation) in mRNA expression from triplicate measurements in relation to the control samples and normalized by internal housekeeping genes (GAPDH, HPRT, β-actin)

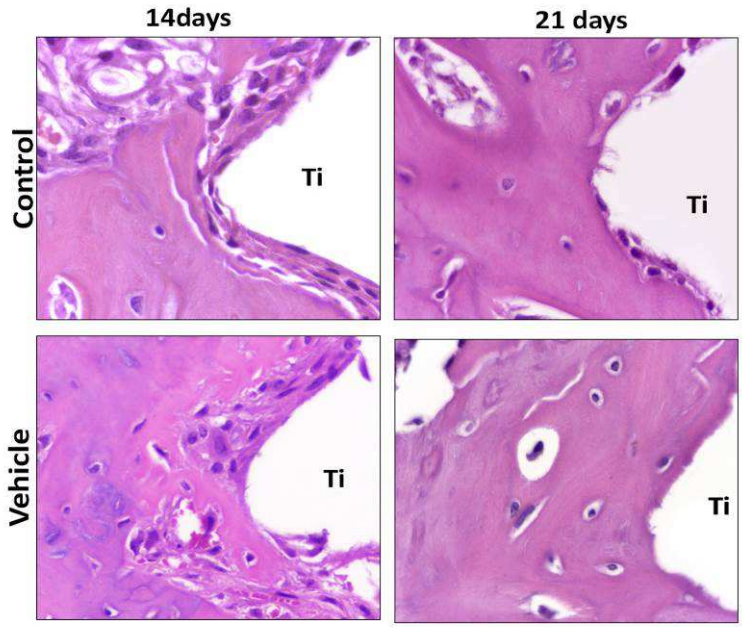

Supplementary figure 1. Oral osseointegration model in C57Bl/6 mice at 14 and 21 days post Ti implantation. H&E stained histological images captured at 100x magnification. Ti = Ti screw space.

3 DISCUSSION

3 DISCUSSION

In this present thesis, we focused on the role of DAMPs in the modulation of inflammatory response, especially considering macrophage response, upon a classic biomaterial (Ti) implantation and its impact in the subsequent repair (article 2) and osseointegration processes (article 1 and 3). Particularly, we used Ti as a model of a traditional biomaterial widely used in dentistry and orthopedics, because of its high biocompatibility and osseointegration capacity (DAVIES 2003; ALBREKTSSON et al, 2014). In fact, Ti has been suggested as an immunomodulatory biomaterial rather than an inert metal, partially because of TiO2 surface layer created immediately post Ti implantation, which is supposed to drive a favorable protein adsorption into the biomaterial and contribute to modulate the biological environment (OTHMAN et al., 2018).

At this moment, the initial biological reaction that leads to Ti-mediated osseointegration is still not fully understood, since a number of studies are at the stage identifying proteins adsorbed on the Ti surface, and describing the process of protein adsorption by artificial methods *in vitro* (OTHMAN et al., 2018). Additionally, immunological mechanisms upon protein adsorption stages that coordinate this 'constructive' host response at the Ti/host interface remain unclear, partly because of the limited methodological tools and animal models currently used for these purposes.

In order to solve this limitation, the article 1 provides a comprehensive description of an oral Ti implant osseointegration model in C57Bl/6 mice, with a microtomographic, histological, histomorphometric and molecular characterization (BIGUETTI et al., 2018). This oral osseointegration in C57Bl/6 mice resembles healing events described along osseointegration in other larger animal models and in humans. Importantly, in this article we demonstrated potential immunological targets responsible for orchestrating cell migration, proliferation, ECM deposition and maturation, angiogenesis, bone formation and remodeling at the bone-implant interface. Therefore, animal model and strain was used in the next studies as suitable tool for the assessment of biological events upon osseointegration and repair process.

Previous *in vitro* studies, using artificial Ti incubation with plasma serum (ROMERO-GAVILAN et al., 2017) or bone powder (SUGIMOTO et al., 2016) have shown that Ti surfaces are able to attract bone proteins, ECM proteins, growth factors, as well immunological mediators. Of note, this information is useful for the comprehension of the blood and bone proteins adsorption on the biomaterial and suggests some insights about Ti surface properties and regenerative capacity. However, it is important to remind that the *in vivo* host/biomaterial interface is substantially more complex than simulated conditions *in vitro and* controlled environments. In this context, we suggest that the protein layer might have DAMPs originated from the surgical for biomaterial implantation, as also considered in recent reviews in biomaterial science-(VISHWAKARMA et al., 2016)

In the article 2, Ti-discs were placed in the subcutaneous tissue of C57Bl/6 mice and collected at different time periods (1d,3d,7d,14d) for ELISA assays. Our analysis confirmed that DAMPs from cellular (HMGB1, HSP60, HSP70, S100A9) and ECM (Fibronectin and Biglycan) origin are found in Ti/host interface, mainly at 1day post-Ti implantation or post-surgical trauma (Sham), gradually decreasing at 3days, as also demonstrated in the sham group.

Subsequently or simultaneously to the protein adsorption step, macrophages recruited to the host/biomaterial interface will recognize and interact with all these molecules (SRIDHARAN et al., 2015). In the article 2, the kinetics of inflammatory cells demonstrated a peak of GR1+ cells (neutrophils) at 48hours post Ti implantation, which are the first leucocytes recruited from adjacent blood vessels to the implantation site(LIN et al. 2014), followed by a sequence of events involving macrophages (F4/80+, CD80+ and CD206+). Interestingly, the mRNA levels of ARG1, IL10, TGFβ (M2-markers), were significantly upregulated in Ti implantation sites, at 7 and 21days, confirming that Ti can favor an M2-Type along tissue repair (ALBREKTSSON et al., 2014; THALJI et al., 2014).

Considering that protein layer on Ti surface establishes the biomaterial-cells interface (ALBREKTSSON et al., 2014; OTHMAN et al., 2018), the presence of DAMPs mediating Ti/host interactions could be a critical step for triggering the host response, which in turn will direct cell migration and differentiation into a suitable healing. In this context, the role of HMGB1 and its cognate receptor RAGE was investigated upon Ti implantation. In this context, the pharmacological inhibition/antagonism of these molecules was the rational approach in providing

strategies for studying a cause-effect relation between the HMGB1 and RAGE on the host response post-Ti implantation in subcutaneous tissue (article 2) and bone (article 3).

Of note, the inhibition of HMGB1 (GZA 200mg/Kg/day) and the antagonism of RAGE (RAP 4mg/Kg/day) negatively impacted the host response to the Ti disc implantation in subcutaneous tissue, evidenced by a decreased collagen fiber formation, reduced mRNA levels for ECM markers (Col1a2, Col2a1, MMP1a, MMP2, MMP9, TIMP1, TIMP3, CTSG) and molecules involved in cell adhesion and migration (CTGF, VTN, ITGA2,ITGA4, ITGA5). Furthermore, an ineffective inflammatory response was demonstrated in the mice treated with GZA (HMGB1 inhibitor) and RAP (RAGE antagonist), with a reduced expression of chemokines (CXCL10, CXCL11) and pro-inflammatory cytokines (TNFα, IL6, IL1b) in pooled samples, followed by a reduction of GR1+ cells and macrophages (F4/80+ cells, CD80+ cells, CD206+ cells) at 3 days post Ti implantation. Finally, the mRNA levels of ARG2 (a marker for M2 macrophages) was increased in the Control and reduced in GZA and RAP treated mice.

Considering the concept of constructive inflammatory environment, our results in the article 2 indicated that HMGB1 and RAGE influence different steps of Ti-mediated tissue repair, including: blood clot formation (only observed in GZA group), inflammatory cell recruitment, macrophages polarization into a M2 phenotype, angiogenesis, cell proliferation and migration, collagen deposition and matrix remodeling.

In the article 3, the emphasis was placed on the role HMGB1 and RAGE on the Ti-mediated osseointegration. As expected based on the results of subcutaneous tissue, the blockade of HMGB1 or RAGE caused the failure of Ti-mediated osseointegration in mice C57Bl/6 mice, affecting the dynamics of bone cells differentiation, bone deposition and decreased mRNA levels of bone markers. As also observed on subcutaneous Ti-implantation model (article 2), the GZA group caused a disruption of blood clot formation in the oral osseointegration model in mice (article 3). In fact, HMGB1 is supposed to act synergistically with thrombin to promote blood coagulation in vivo (ITO et al., 2007). Thus, the failure of osseointegration in GZA was initially caused by the disruption of the blood clot, which is the first provisional matrix for MSCs and inflammatory cells recruitment around Ti threads.

The failure of osseointegration in GZA and RAP group was marked with a persistent FBR. Importantly, FBR around Ti implants is demonstrated as a persistence of macrophages and fibroblasts along late periods post biomaterial implantation, and is correlated with a dysregulation of macrophage phenotype (M1: M2 ratios) (BROWN et al., 2012). In this way, is desirable to have a predominance of M1-type response along acute inflammatory response and a predominance of M2-type response along the resolution of inflammation and regenerative phase (Brown et al., 2012). Importantly, the expression of ARG1 and IL10, related to M2-type response, were particularly found on C group along with a suitable osseointegration, but not in GZA and RAP treated mice. On the other hand, GZA and RAP group showed increased mRNA levels of IL1b, IL6, TNFα, suggesting a persistence of M1-type response. In face of these findings, it reasonable to hypothesize that HMGB1 and RAGE contribute to the ratio of M1:M2 polarized macrophages along osseointegration process.

Finally, it is important to consider that mRNA expression quantitative analyses were performed from pooled samples in the article 2 and article 3 and not for experimental periods separately. Thus, in future studies we will perform the kinetics of mRNA expression for up-regulated targets in the pooled samples from Control and GZA and RAP groups. The final purpose of our investigations is to provide some contributions to the present knowledge about osseointegration phenomena from an immunological point of view. We believe that immunological studies in biomaterial science can contribute to the development of new immunomodulatory strategies, with the ultimate goal of improving clinical predictability.

4 CONCLUSIONS

4 CONCLUSIONS

In conclusion, this study originally demonstrated

- C57Bl/6 mice oral osseointegration model comprise a suitable tool for the assessment of biological events upon osseointegration process, evidencing potential elements responsible for orchestrating cell migration, proliferation, ECM deposition and maturation, angiogenesis, bone formation and remodeling at the bone-implant interface in parallel with a novel microscopic analysis (article 1).
- Different DAMPs from cellular (HMGB1, HSP60, HSP70, S100A9) and ECM (Fibronectin and Biglycan) origin are released at Ti implantation sites, and adhere to Ti surface (article 2)
- HMGB1 and RAGE influence the host inflammatory immune response post biomaterial implantation in mice, and the blockade of both molecules negativelly affect the subcutaneous tissue repair surrounding Ti discs (article 2)
- The inhibition HMGB1 or RAGE impaired the Ti-mediated osseointegration in mice C57Bl/6 mice, affecting the balance of inflammatory markers, macrophages polarization state, MSC migration and differentiation in bone cells and consequent bone deposition (article 3)

REFERENCES

REFERENCES

Abid S, Houssaini A, Mouraret N, Marcos E, Amsellem V, Wan F, et al. P21-dependent protective effects of a carbon monoxide-releasing molecule-3 in pulmonary hypertension. Arteriosclerosis, thrombosis, and vascular biology. 2014;34(2):304-12.

Ai-Aql ZS, Alagl AS, Graves DT, Gerstenfeld LC, Einhorn TA. Molecular mechanisms controlling bone formation during fracture healing and distraction osteogenesis. Journal of dental research. 2008;87(2):107-18..

Albrektsson T, Dahlin C, Jemt T, Sennerby L, Turri A, Wennerberg A. Is marginal bone loss around oral implants the result of a provoked foreign body reaction? Clinical implant dentistry and related research. 2014;16(2):155-65.

Alvarez MM, Liu JC, Trujillo-de Santiago G, Cha BH, Vishwakarma A, Ghaemmaghami AM, et al. Delivery strategies to control inflammatory response: Modulating M1-M2 polarization in tissue engineering applications. Journal of controlled release : official journal of the Controlled Release Society. 2016 28;240:349-63.

Anderson JM, Rodriguez A, Chang DT. Foreign body reaction to biomaterials. Seminars in immunology. 2008;20(2):86-100.

Aoyagi H, Yamashiro K, Hirata-Yoshihara C, Ideguchi H, Yamasaki M, Kawamura M, et al. HMGB1-induced inflammatory response promotes bone healing in murine tooth extraction socket. 2018, Journal of cellular biochemistry.

Araujo-Pires AC, Francisconi CF, Biguetti CC, Cavalla F, Aranha AM, Letra A, et al. Simultaneous analysis of T helper subsets (Th1, Th2, Th9, Th17, Th22, Tfh, Tr1 and Tregs) markers expression in periapical lesions reveals multiple cytokine clusters accountable for lesions activity and inactivity status. Journal of applied oral science : revista FOB. 2014;22(4):336-46.

Araujo-Pires AC, Biguetti CC, Repeke CE, Rodini Cde O, Campanelli AP, Trombone AP, et al. Mesenchymal stem cells as active prohealing and immunosuppressive agents in periapical environment: evidence from human and experimental periapical lesions. Journal of endodontics. 2014 ;40(10):1560-5..

Becher OJ, Holland EC. Genetically engineered models have advantages over xenografts for preclinical studies. Cancer research. 2006 01;66(7):3355-8, discussion 8-9.

Biguetti CC, Cavalla F, Silveira EM, Fonseca AC, Vieira AE, Tabanez AP, et al. Oral implant osseointegration model in C57Bl/6 mice: microtomographic, histological, histomorphometric and molecular characterization. 2018; Journal of Applied Oral Science. (*in press*)

Biscetti F, Straface G, De Cristofaro R, Lancellotti S, Rizzo P, Arena V, et al. High-mobility group box-1 protein promotes angiogenesis after peripheral ischemia in diabetic mice through a VEGF-dependent mechanism. Diabetes. 2010;59(6):1496-505..

Brancato SK, Albina JE. Wound macrophages as key regulators of repair: origin, phenotype, and function. The American journal of pathology. 2011;178(1):19-25.

Brown BN, Ratner BD, Goodman SB, Amar S, Badylak SF. Macrophage polarization: an opportunity for improved outcomes in biomaterials and regenerative medicine. Biomaterials. 2012;33(15):3792-802.

Chen Z, Yuen J, Crawford R, Chang J, Wu C, Xiao Y. The effect of osteoimmunomodulation on the osteogenic effects of cobalt incorporated beta-tricalcium phosphate. Biomaterials. 2015;61:126-38.

Colnot C, Romero DM, Huang S, Rahman J, Currey JA, Nanci A, et al. Molecular analysis of healing at a bone-implant interface. Journal of dental research. 2007 ;86(9):862-7.

Cooper LF, Masuda T, Yliheikkila PK, Felton DA. Generalizations regarding the process and phenomenon of osseointegration. Part II. In vitro studies. The International journal of oral & maxillofacial implants. 1998;13(2):163-74.

Davies JE. Understanding peri-implant endosseous healing. Journal of dental education. 2003;67(8):932-49.

Degryse B, Bonaldi T, Scaffidi P, Muller S, Resnati M, Sanvito F, et al. The high mobility group (HMG) boxes of the nuclear protein HMG1 induce chemotaxis and cytoskeleton reorganization in rat smooth muscle cells. The Journal of cell biology. 2001 19;152(6):1197-206.

Fabbro MD, Taschieri S, Canciani E, Addis A, Musto F, Weinstein R, et al. Osseointegration of Titanium Implants With Different Rough Surfaces: A Histologic and Histomorphometric Study in an Adult Minipig Model. Implant dentistry. 2017;26(3):357-66.

Ferraz EP, Sverzut AT, Freitas GP, Sa JC, Alves C, Jr., Beloti MM, et al. Bone tissue response to plasma-nitrided titanium implant surfaces. Journal of applied oral science : revista FOB. 2015;23(1):9-13.

Fukata M, Vamadevan AS, Abreu MT. Toll-like receptors (TLRs) and Nod-like receptors (NLRs) in inflammatory disorders. Seminars in immunology. 2009;21(4):242-53.

Garlet GP, Cardoso CR, Silva TA, Ferreira BR, Avila-Campos MJ, Cunha FQ, et al. Cytokine pattern determines the progression of experimental periodontal disease induced by Actinobacillus actinomycetemcomitans through the modulation of MMPs, RANKL, and their physiological inhibitors. Oral microbiology and immunology. 2006 ;21(1):12-20.

Gittens RA, Scheideler L, Rupp F, Hyzy SL, Geis-Gerstorfer J, Schwartz Z, et al. A review on the wettability of dental implant surfaces II: Biological and clinical aspects. Acta biomaterialia. 2014 ;10(7):2907-18.

Graves DT, Oates T, Garlet GP. Review of osteoimmunology and the host response in endodontic and periodontal lesions. Journal of oral microbiology. 2011;3.

Ito T, Kawahara K, Nakamura T, Yamada S, Nakamura T, Abeyama K, et al. High-mobility group box 1 protein promotes development of microvascular thrombosis in rats. Journal of thrombosis and haemostasis : JTH. 2007;5(1):109-16.

Jaguin M, Houlbert N, Fardel O, Lecureur V. Polarization profiles of human M-CSF-generated macrophages and comparison of M1-markers in classically activated macrophages from GM-CSF and M-CSF origin. Cellular immunology. 2013;281(1):51-61.

Kang R, Chen R, Zhang Q, Hou W, Wu S, Cao L, et al. HMGB1 in health and disease. Molecular aspects of medicine. 2014;40:1-116.

Kokkola R, Andersson A, Mullins G, Ostberg T, Treutiger CJ, Arnold B, et al. RAGE is the major receptor for the proinflammatory activity of HMGB1 in rodent macrophages. Scandinavian journal of immunology. 2005;61(1):1-9.

Land WG. The Role of Damage-Associated Molecular Patterns (DAMPs) in Human Diseases: Part II: DAMPs as diagnostics, prognostics and therapeutics in clinical medicine. Sultan Qaboos University medical journal. 2015;15(2):e157-70.

Lin TH, Tamaki Y, Pajarinen J, Waters HA, Woo DK, Yao Z, et al. Chronic inflammation in biomaterial-induced periprosthetic osteolysis: NF-kappaB as a therapeutic target. Acta biomaterialia. 2014;10(1):1-10.

Lin Z, Rios HF, Volk SL, Sugai JV, Jin Q, Giannobile WV. Gene expression dynamics during bone healing and osseointegration. Journal of periodontology. 2011;82(7):1007-17.

Liu Y, Chen GY, Zheng P. CD24-Siglec G/10 discriminates danger- from pathogen-associated molecular patterns. Trends in immunology. 2009;30(12):557-61.

Mantovani A, Sica A, Sozzani S, Allavena P, Vecchi A, Locati M. The chemokine system in diverse forms of macrophage activation and polarization. Trends in immunology. 2004;25(12):677-86.

Martinez FO, Sica A, Mantovani A, Locati M. Macrophage activation and polarization. Frontiers in bioscience : a journal and virtual library. 2008;13:453-61.

Martinez-Ibanez M, Murthy NS, Mao Y, Suay J, Gurruchaga M, Goni I, et al. Enhancement of plasma protein adsorption and osteogenesis of hMSCs by functionalized siloxane coatings for titanium implants. Journal of biomedical materials research Part B, Applied biomaterials. 2017

Mosser DM, Edwards JP. Exploring the full spectrum of macrophage activation. Nature reviews Immunology. 2008;8(12):958-69.

Mountziaris PM, Mikos AG. Modulation of the inflammatory response for enhanced bone tissue regeneration. Tissue engineering Part B, Reviews. 2008;14(2):179-86.

Mouraret S, Hunter DJ, Bardet C, Brunski JB, Bouchard P, Helms JA. A pre-clinical murine model of oral implant osseointegration. Bone. 2014;58:177-84.

Murray PJ, Allen JE, Biswas SK, Fisher EA, Gilroy DW, Goerdt S, et al. Macrophage activation and polarization: nomenclature and experimental guidelines. Immunity. 2014 17;41(1):14-20.

Othman Z, Cillero Pastor B, van Rijt S, Habibovic P. Understanding interactions between biomaterials and biological systems using proteomics. Biomaterials. 2018 12;167:191-204.

Ogle OE. Implant surface material, design, and osseointegration. Dental clinics of North America. 2015;59(2):505-20.

Park JE, Barbul A. Understanding the role of immune regulation in wound healing. American journal of surgery. 2004;187(5A):11S-6S.

Rojas A, Delgado-Lopez F, Perez-Castro R, Gonzalez I, Romero J, Rojas I, et al. HMGB1 enhances the protumoral activities of M2 macrophages by a RAGE-dependent mechanism. Tumor Biol. 2016;37(3):3321-9.

Romero-Gavilan F, Gomes NC, Rodenas J, Sanchez A, Azkargorta M, Iloro I, et al. Proteome analysis of human serum proteins adsorbed onto different titanium surfaces used in dental implants. Biofouling. 2017;33(1):98-111.

Sang LC, Vinu A, Coppens MO. General description of the adsorption of proteins at their iso-electric point in nanoporous materials. Langmuir : the ACS journal of surfaces and colloids. 2011 15;27(22):13828-37.

Schiraldi M, Raucci A, Munoz LM, Livoti E, Celona B, Venereau E, et al. HMGB1 promotes recruitment of inflammatory cells to damaged tissues by forming a complex with CXCL12 and signaling via CXCR4. The Journal of experimental medicine. 2012 12;209(3):551-63.

Sridharan R, Cameron AR, Kelly DJ, Kearney CJ, O'Brien FJ. Biomaterial based modulation of macrophage polarization: a review and suggested design principles. Mater Today. 2015;18(6):313-25.

Sugimoto K, Tsuchiya S, Omori M, Matsuda R, Fujio M, Kuroda K, et al. Proteomic analysis of bone proteins adsorbed onto the surface of titanium dioxide. Biochemistry and biophysics reports. 2016;7:316-22.

Tang D, Kang R, Coyne CB, Zeh HJ, Lotze MT. PAMPs and DAMPs: signal 0s that spur autophagy and immunity. Immunological reviews. 2012;249(1):158-75..

Tang Y, Wu X, Lei W, Pang L, Wan C, Shi Z, et al. TGF-beta1-induced migration of bone mesenchymal stem cells couples bone resorption with formation. Nature medicine. 2009;15(7):757-65.

Thoma DS, Benic GI, Munoz F, Kohal R, Sanz Martin I, Cantalapiedra AG, et al. Marginal bone-level alterations of loaded zirconia and titanium dental implants: an experimental study in the dog mandible. Clinical oral implants research. 2016;27(4):412-20.

Trindade R, Albrektsson T, Wennerberg A. Current concepts for the biological basis of dental implants: foreign body equilibrium and osseointegration dynamics. Oral and maxillofacial surgery clinics of North America. 2015;27(2):175-83.

Trindade R, Albrektsson T, Tengvall P, Wennerberg A. Foreign Body Reaction to Biomaterials: On Mechanisms for Buildup and Breakdown of Osseointegration. Clinical implant dentistry and related research. 2016;18(1):192-203.

Thalji GN, Nares S, Cooper LF. Early molecular assessment of osseointegration in humans. Clinical oral implants research. 2014;25(11):1273-85.

Thalji G, Cooper LF. Molecular assessment of osseointegration in vivo: a review of the current literature. The International journal of oral & maxillofacial implants. 2013;28(6):e521-34.

Thalji G, Gretzer C, Cooper LF. Comparative molecular assessment of early osseointegration in implant-adherent cells. Bone. 2013;52(1):444-53

Williams DF. On the mechanisms of biocompatibility. Biomaterials. 2008 Jul;29(20):2941-53.

Willie BM, Yang X, Kelly NH, Merkow J, Gagne S, Ware R, et al. Osseointegration into a novel titanium foam implant in the distal femur of a rabbit. Journal of biomedical materials research Part B, Applied biomaterials. 2010;92(2):479-88.

Vandamme TF. Use of rodents as models of human diseases. Journal of pharmacy & bioallied sciences. 2014 Jan;6(1):2-9.

Variola F, Yi JH, Richert L, Wuest JD, Rosei F, Nanci A. Tailoring the surface properties of Ti6Al4V by controlled chemical oxidation. Biomaterials. 2008 Apr;29(10):1285-98.

Vieira AE, Repeke CE, Ferreira Junior Sde B, Colavite PM, Biguetti CC, Oliveira RC, et al. Intramembranous bone healing process subsequent to tooth extraction in mice: micro-computed tomography, histomorphometric and molecular characterization. PloS one. 2015;10(5):e0128021.

Vishwakarma A, Bhise NS, Evangelista MB, Rouwkema J, Dokmeci MR, Ghaemmaghami AM, et al. Engineering Immunomodulatory Biomaterials To Tune the Inflammatory Response. Trends in biotechnology. 2016;34(6):470-82.

Yang H, Wang H, Chavan SS, Andersson U. High Mobility Group Box Protein 1 (HMGB1): The Prototypical Endogenous Danger Molecule. Molecular medicine. 2015 27;21 Suppl 1:S6-S12.

Zhang J, He F, Zhang W, Zhang M, Yang H, Luo ZP. Mechanical force enhanced bony formation in defect implanted with calcium sulphate cement. Bone research. 2015;3:14048.

APPENDIXES

DECLARATION OF EXCLUSIVE USE OF THE ARTICLE IN THESIS

We hereby declare that we are aware of the article **Oral implant osseointegration model in C57Bl/6 mice: microtomographic, histological, histomorphometric and molecular characterization** will be included in the Thesis of the student Claudia Cristina Biguetti and was not used and may not be used in other works of Graduate Programs at the Bauru School of Dentistry, University of São Paulo.

Bauru, March 27, 2017

Claudia Cristina Biguetti
Author
Signature

Franco Cavalla
Author
Signature

Elcia Varize Silveira
Author
Signature

Angélica Cristina Fonseca
Author
Signature

Andreia Espindola Vieira
Author
Signature

Andre Petenuci Tabanez
Author
Signature

Danieli C Rodrigues
Author
Signature

Ana Paula Favaro Trombo
Author
Signature

Gustavo Pompermaier Garlet
Author
Signature

DECLARATION OF EXCLUSIVE USE OF THE ARTICLE IN THESIS

We hereby declare that we are aware of the article **Evidences of HGMB1 and RAGE contributions in the regenerative host response to Ti-based biomaterials** will be included in the Thesis of the student Claudia Cristina Biguetti and was not used and may not be used in other works of Graduate Programs at the Bauru School of Dentistry, University of São Paulo.

Bauru, March 27, 2017

Claudia Cristina Biguetti
Author
Signature

Franco Cavalla
Author
Signature

Angélica Cristina Fonseca
Author
Signature

Andreia Espindola Vieira
Author
Signature

Elcia Varize Silveira
Author
Signature

Ana Claudia Araujo Pires
Author
Signature

Renato Menezes Silva
Author
Signature

Gustavo Pompermaier Garlet
Author
Signature

DECLARATION OF EXCLUSIVE USE OF THE ARTICLE IN THESIS

We hereby declare that we are aware of the article **HGMB1 and RAGE mediates Ti oral osseointegration in C57Bl/6 mice** will be included in the Thesis of the student Claudia Cristina Biguetti and was not used and may not be used in other works of Graduate Programs at the Bauru School of Dentistry, University of São Paulo.

Bauru, March 27, 2017

Claudia Cristina Biguetti
Author
Signature

Franco Cavalla
Author
Signature

Elcia Varize Silveira
Author
Signature

Andre Petenuci Tabanez
Author
Signature

Danieli C Rodrigues
Author
Signature

Gustavo Pompermaier Garlet
Author
Signature

ANNEXES

ANNEX

Approval of Animal Ethical Committee

Universidade de São Paulo
Faculdade de Odontologia de Bauru

Comissão de Ética no Ensino e Pesquisa em Animais

CEEPA-Proc. Nº 012/2014

Bauru, 30 de junho de 2014.

Senhor Professor,

O projeto de pesquisa encaminhado a esta Comissão de Ética no Ensino e Pesquisa em Animais, denominado **Participação de DAMPs na modulação da resposta de macrófagos à implantação de um biomaterial clássico (Ti) e seu impacto no processo de reparo e osseointegração subsequentes,** de autoria de Cláudia Cristina Biguetti, sob sua orientação foi enviado ao relator para avaliação e considerado APROVADO em reunião desta Comissão realizada no dia 23 de junho de 2014.

Solicitamos que ao final da pesquisa seja enviado, para avaliação desta Comissão, um Relatório com os resultados obtidos para análise ética e emissão de parecer final, o qual poderá ser utilizado para fins de publicação científica.

Atenciosamente,

Prof. Dr. Luís Antônio de Assis Taveira
Vice-Presidente da Comissão de Ética no Ensino e Pesquisa em Animais

Prof. Dr. Gustavo Pompermaier Garlet
Docente do Departamento de Ciências Biológicas

Al. Dr. Octávio Pinheiro Brisolla, 9-75 – Bauru-SP – CEP 17012-101 – C.P. 73
e-mail: mferrari@fob.usp.br – Fone/FAX (0xx14) 3235-8356
http://www.fob.usp.br